

Doctoral theses at NTNU, 2023:124

Nicholas Trussell

Sprayed concrete – effect of accelerator, cracks and composition on compaction, porosity, strength and water transport properties

NTNU
Norwegian University of Science and Technology
Thesis for the Degree of
Philosophiae Doctor
Faculty of Engineering
Department of Structural Engineering



Norwegian University of
Science and Technology

Nicholas Trussell

Sprayed concrete – effect of accelerator, cracks and composition on compaction, porosity, strength and water transport properties

Thesis for the Degree of Philosophiae Doctor

Trondheim, April 2023

Norwegian University of Science and Technology
Faculty of Engineering
Department of Structural Engineering



Norwegian University of
Science and Technology

NTNU

Norwegian University of Science and Technology

Thesis for the Degree of Philosophiae Doctor

Faculty of Engineering

Department of Structural Engineering

© Nicholas Trussell

ISBN 978-82-326-5331-7 (printed ver.)

ISBN 978-82-326-6882-3 (electronic ver.)

ISSN 1503-8181 (printed ver.)

ISSN 2703-8084 (online ver.)

Doctoral theses at NTNU, 2023:124

Printed by NTNU Grafisk senter

Preface

This doctoral thesis was submitted to the Norwegian University of Science and Technology (NTNU) in Trondheim for the degree of Philosophiae Doctor.

This PhD thesis is a part of the research project “Sprayed sUstainable Permanent Robotized CONcrete tunnel lining (SUPERCON)” financed by the Research Council of Norway (project no. 294724), in cooperation with industrial partners AMV, BASF, Bever Control, Bekaert, Elkem, Entreprenørservice, NORCEM, SWECO Norge, Veidekke, Wacker Chemicals Norway and Unicon AS. Research partners in SUPERCON are NGI, NTNU and SINTEF. The following project owners support the project; Bane NOR, Nye Veier and the Norwegian Public Roads Administration.

Full-scale spraying experiments and field testing were carried out at four locations. The laboratory experiments were carried out in the concrete laboratory at the Department of Structural Engineering, Norwegian University of Science and Technology (NTNU), and the adjacent SINTEF concrete laboratory.

The main supervisor was Professor Stefan Jacobsen, with co-supervisor Adjunct Professor Rolands Cepuritis, both from NTNU.

Trondheim, Friday 10th February, 2023.

Nicholas Trussell

Summary

The research described in this PhD thesis investigated key aspects of sprayed concrete material, with an intention of gaining knowledge to enable greater use of sprayed concrete for permanent tunnel linings. The two unique attributes of sprayed concrete are the addition of set accelerator at the nozzle, which is essential to achieve adhesion to the substrate and high early strength development, and the relatively large, irregular macro pores from the spray application. Both these topics were investigated to increase understanding of sprayed concrete. The effect of cracks on water transport was also investigated. Improving sustainability of sprayed concrete linings by reducing cement content and improving durability by reducing water transport properties of the sprayed concrete material was investigated. These investigations are described in the six papers included in this thesis.

The first paper was a systematic literature review covering all aspects of sprayed concrete application, including proportioning, pumping, addition of set accelerator at the nozzle, propulsion of the concrete towards the substrate and the hardening and hardened properties. Proportioning principles based on the particle-matrix model were discussed and the term placed concrete composition was introduced. The effect of set accelerator and irregularly shaped macro pores were discussed. A definition of “sprayability” linking the production to the obtained quality of the placed sprayed concrete was offered.

The research in the second and third papers studies the effect of aluminium sulphate based set accelerators on the hardening and hardened properties of sprayed concrete. Investigations were on specimens produced by full scale spraying experiments (paper two) and laboratory cast specimens with the water/binder ratio kept constant (paper three). Higher doses of set accelerator were measured to give higher early strength development but reduce density, long term strength and increase suction porosity. Strength was measured to correlate well to both density and total porosity (suction porosity + macro porosity). The Powers’ equation quantifying the relationship between water/cement mass ratio, degree of hydration and porosity was demonstrated to be inapplicable for sprayed concrete with set accelerator added, due to the hydration products being different to those for conventional concrete.

The research in the fourth paper investigated the anisotropy of sprayed concrete due to the shape and orientation of macro pores, orientation of fibres and the presence of laminations. A trend of increasing macro porosity with increased set accelerator dose was found. Measurements of the macro pores confirmed them to be non-spherical, with 50 % of length/width ratios greater than 1.5. The orientation of both macro pores and steel fibres were measured to tend towards orientation parallel to the substrate. Three methods to measure macro porosity were compared: image analysis, PF (pore fraction) method and CT scanning. Macro porosity measurements by image analysis were higher than by PF method with only one exception among the data set. The measurements by CT scanning were closer to the measurements by image analysis. 80–94 % of the macro pores were measured to be closed by capillary suction and PF method. Furthermore, water penetration tests on specimens with the water pressure applied parallel and perpendicular to the direction of sprayed concrete application are described. Water penetration was measured to be very low parallel to the direction of application, but much higher perpendicular to the direction of application, due to macro porosity and laminations in this direction for specimens sprayed with 10 % set accelerator in a single, continuous application. The detection of laminations at higher accelerator doses and the effect on permeability demonstrated the importance of careful execution for wet spraying of concrete.

The fifth paper describes experiments undertaken on sprayed concrete discs to investigate the effect of cracking on capillary suction and permeation through sprayed concrete for tunnel linings. The specimens were cracked by tensile splitting, with the crack widths controlled and measured by digital image correlation. The use of CT scanning to measure cracks through the full thickness of specimens, compared with measurements at one surface of the disc only, was also explored. Both a standard sprayed concrete mix and a mix containing an EVA (ethylene-vinyl-acetate) based co-polymer

powder were tested, to determine the effect of this co-polymer on water transport. Cracks increased the rate of capillary suction compared to uncracked samples, due to rapid rise of water in the crack compared to the intact concrete and absorption occurring over the surface area of the crack in addition to the area of the base of the disc. Inclusion of the co-polymer reduced the rate of capillary suction – both the rise of water in the crack and the rate of absorption in the bulk concrete. Wider crack widths exhibited a higher rate of water permeation per area of crack. The theoretical rate of permeation in a perfectly smooth, ideal crack is proportional to the crack width cubed, but the flow rate coefficient (measured flow / theoretical viscous laminar flow) was found to also increase with crack width. This is likely due to the decreasing effect of crack surface roughness with increasing crack width, though narrower cracks are more likely to be less continuous through the thickness of the disc. Inclusion of the co-polymer reduced the rate of permeation for a given crack width compared to the standard mix. Self-healing both during water permeation and water storage of the cracked specimens was measured.

The sixth paper describes research to improve the sustainability of sprayed concrete tunnel linings by reducing the cement content and improving the water transport properties of the material. Reference mixes and innovative mixes were proportioned to investigate reducing the cement content in sprayed concrete tunnel linings, by either replacement of cement with supplementary cementitious materials or by reducing the matrix content of the concrete. Shrinkage and thermal contraction were studied, with the aim of reducing tensile strains, cracking and hence water transport. The investigations described in paper 5, where inclusion of the EVA (ethylene-vinyl-acetate) based co-polymer powder in the sprayed concrete was measured to reduce water transport both in cracks and in the capillary pore network, were applicable for this study. By reducing the water transport properties of the sprayed concrete material, improved durability over single shell linings or reduced material consumption over linings including a waterproofing membrane can be achieved.

While inclusion of the ethylene-vinyl-acetate (EVA) based dispersible co-polymer powder in the concrete significantly reduced water transport, it also reduced the rate of early strength development. Inclusion of the EVA based co-polymer would be beneficial for a secondary lining with reduced water transport properties, where sufficient early age strength development is needed only to achieve sufficient adhesion for the concrete to remain in place. But, depending on early age strength and thickness requirements, inclusion of the EVA based co-polymer may not be appropriate for primary linings applied for immediate ground support.

The experiments described in the sixth paper also included investigations of shrinkage and the risk of early age cracking, given the significance of cracks for water transport. The measured volume changes were due to both shrinkage and thermal contraction. Sprayed concrete experiences high early temperature development, due to the addition of set accelerator to give high early strength development, that may contribute to high risk of early age cracking during the subsequent cooling. It was determined that avoiding drying shrinkage in this period should be sufficient to reduce/eliminate the risk of cracking. This could be achieved by keeping the concrete wet at early ages, use of a curing membrane or inclusion of a shrinkage reducing agent in the mix.

Reducing the cement content by replacement with fly ash or limestone powder reduced the rate of early strength development due to the slower reaction rate of these supplementary cementitious materials, though they did increase long term strength and reduced suction porosity. The benefits of this are arguable – early strength is considered more critical than long term strength for sprayed concrete. On the other hand reducing the cement content by reducing the matrix volume gave promising results – the mix was successfully sprayed and the early age strength development was comparable with the reference mixes. Within the scope of the study, reduction of the matrix volume gives a more effective reduction of cement content than replacement of cement by supplementary cementitious materials.

Acknowledgements

I would like to thank Professor Stefan Jacobsen for his enthusiasm and support. Thanks to Adjunct Professor Rolands Cepuritis for additional support and advice.

I wish to thank all who have contributed to the experimental work covered in this PhD thesis. Thanks to Per Øystein Nordtug, Steinar Seehuus, Thomas Uhlving and Kåre Brottveit Olsby of NTNU and Jonny Tverdal and Erik Johansen of SINTEF for their help with laboratory investigations and preparing specimens. Thanks to Eivind Sjøbakk-Moe (NTNU), Olav Roset (NGI), Dirk van Oosterhout and Helene Strømsvik (SINTEF) for their contributions to the full scale spraying experiments.

Thanks to Karl Gunnar Holter for leading most of the full-scale sprayed concrete experiments and to Tor Arne Hammer, Ola Skjølsvold and Anja Klausen for their work on the shrinkage and thermal contraction.

Thanks to Trond Auestad, Per Øystein Nordtug and Martin Kristoffersen for their work on controlling and measuring crack widths by digital image correlation. Thanks to Pål Erik Endrerud and Iman Asadi for their work with the CT scanning and processing of the results.

Thanks to Magne Stangeland Hårr for his help preparing specimens for image analysis, and to Magne and Gaute Kjeka for their work on the computation and analysis of the image analysis results.

And thanks to all the professors at NTNU who have taught me about concrete.

Finally, I acknowledge the Research Council of Norway and all the industrial partners for their financial support and for their contributions to the project.

Table of Contents

Preface	2
Summary.....	3
Acknowledgements.....	5
1. Introduction.....	7
2. Methods.....	8
3. Results.....	10
3.1. Investigation of spraying mechanics.....	10
3.2. Effect of laminations.....	10
3.3. Particle tracking	11
4. Conclusions.....	12
5. Further Research	14
References.....	15
Status of papers and contribution of the candidate	16

1. Introduction

This thesis is a study into wet sprayed concrete, which is widely used for tunnel linings. Sprayed concrete linings act to provide immediate ground support, allowing access for excavation to proceed, and are increasingly considered to act as permanent linings [1]. However sprayed concrete may not necessarily comply with today's service life requirements for durability – typically in the range 60-150 years [2]. Improved material properties may be needed to improve the durability of sprayed concrete tunnel linings.

Furthermore the environmental impacts associated with concrete are mostly due to the CO₂ emissions from the production of cement [3] [4]. Cement contents have been reduced in conventional concretes by replacement with supplementary cementitious materials (SCMs) or filler. However the cement content of sprayed concrete remains relatively high given the requirement for high early strength in sprayed concrete tunnel linings, and given that replacement by high levels of cement replacement by SCMs reduce the rate of strength development [5]. Progress towards reducing the environmental impacts associated with sprayed concrete tunnel linings is required.

Some key previous studies of the fundamental properties of sprayed concrete were Opsahl's [6] and Beaupré's [7] and Holter's [8] PhD theses. Two recent PhD theses study the durability of existing sprayed concrete tunnel linings – Hagelia's thesis [9] focuses on deterioration mechanisms due to presence of sulphates and acids, while Manquehual's thesis [10] investigates the current condition of sprayed concrete linings constructed 20–25 years prior to the investigations. Furthermore the Norwegian Concrete Association have arranged a series of symposia (for example [10] & [11]) that, together with the Norwegian Concrete Association Publication on sprayed concrete [12], contain considerable knowledge and experience on wet sprayed concrete tunnel linings.

This PhD thesis attempts to build on the knowledge established in these sources – adding to, but not duplicating, the knowledge. This PhD thesis consists of six journal papers. The first paper is a literature review of sprayed concrete and identifies areas of interest for the rest of the study. For each topic studied in papers 2 – 6, the paper begins with a detailed literature review of the topic in each case. Each paper contains description of the methods, results and discussions of the findings along with conclusions.

Papers 2 – 4 focus on key properties of sprayed concrete – the effect of the set accelerator added at the nozzle and the large, irregularly shaped macro pores, both of which are unique to sprayed concrete compared with cast concrete.

Papers 5 and 6 investigate improvements in sprayed concrete that can be implemented. Paper 5 investigates improving durability by reducing water transport in the sprayed concrete material. Paper 6 investigates improving sustainability through reducing the cement content, while also focusing on the properties of the sprayed concrete that affect durability – cracking and water transport.

The experimental work for this thesis has been based on working with concrete sprayed at full-scale, both for field measurements on sprayed concrete and for obtaining specimens for laboratory testing, rather than investigating cast concrete with similar properties to sprayed concrete. This approach was taken as the mixing of set accelerator at the nozzle, spraying process and unique macro porosity are fundamental properties of sprayed concrete and are impossible to reproduce in cast concrete.

2. Methods

Four full scale spraying experiments were central for this PhD study, both for field measurements and for obtaining specimens for laboratory tests. These are summarised in Table 1.

Table 1 Summary of the full scale spraying experiments

Location	AMV premises, Flekkefjord, Norway	Outside the SINTEF concrete lab, Trondheim, Norway	Svorkmo hydroelectric power station access tunnel, near Orkanger, Norway	UDK 01 tunnel project site, Drammen, Norway
Experimental scope	Accelerator dose varied. Single concrete mix.	Accelerator dose varied – 1 concrete mix. Spraying mechanics varied – 1 concrete mix.	Concrete proportioning varied – 8 mixes	Concrete proportioning varied – 6 mixes
Dates	February 2020	June 2020	March 2021	April 2022
Spraying machine	AMV 7450 shotcrete robot	Normet Spraymec NorRunner 140 DVC shotcrete robot	Normet Spraymec NorRunner 140 DVC shotcrete robot	AMV 4200 H shotcrete robot
Concrete batching location and transportation	Trondheim 5 minutes drive to spraying location	Trondheim 10 minutes drive to spraying location	Trondheim 60 minutes drive to spraying location	Drammen 15 minutes drive to spraying location
Concrete flow rate	10 m ³ /hr	14 m ³ /hr	15 – 20 m ³ /hr	15 – 20 m ³ /hr
Accelerator type	Master Builders Masterroc SA 188	Master Builders Masterroc SA 168	Master Builders Masterroc SA 188	Master Builders Masterroc SA 168
Accelerator dose	0, 3, 6 and 10% of binder mass	0 (cast), 3.5 and 7% of binder mass	7 % of cement mass	8.5 % of cement mass
Distance nozzle to substrate and angle	2.0 m Perpendicular to the panel	1.5 m Perpendicular to the panel	1.5 – 2 m	1.5 – 2 m
Curing and coring	Wrapped in plastic before coring. Cored 13th March 2020 Ø 75 mm, h 150 mm for strength and density tests. Cured in water until compressive strength testing. Ø 100 mm for capillary suction, PF and image analysis tests. Cured in air before oven drying.	Wrapped in plastic before coring. 1st – 2nd July 2020 Ø 75 mm, h 150 mm for strength and density tests. Cured in water until compressive strength testing. Ø 100 mm for capillary suction, PF and image analysis tests. Cured in water before oven drying.	Panels stored in tunnel for 5 weeks. Then transported to laboratory for coring. Cores stored in water before laboratory tests.	Panels stored in tunnel for 20 weeks. Then transported to laboratory for coring. Cores stored in water before laboratory tests.

A summary of all the test methods – both field and laboratory tests – is given in Table 2. The methods are detailed in the relevant papers.

Table 2 Summary of field and laboratory testing

Test method	Property measured
Field tests	
Slump and slump-flow test	Workability of fresh concrete before spraying
Air content	Air content of fresh concrete before spraying
Temperature	Temperature of concrete (before and after spraying)
Penetrometer	Early strength
Hilti stud driving and pull-out	Early strength
Filming of sprayed concrete application by normal and high speed cameras.	Normal camera – video studied for pulsation. High speed camera – particle tracking.
Laboratory tests on hardened concrete	
Density	Density
Compressive strength	Compressive strength
Capillary suction	Rate of water absorption and suction porosity
PF test	Suction porosity, open macro porosity and closed macro porosity
Image analysis	Macro porosity and detection of laminations. Shape and orientation of macro pores.
CT (computed tomography) scanning	Macro porosity, and measurement of cracks. Fibre content and orientation.
Water penetration	Depth of water penetration and equivalent permeability (Valenta)
Water permeation through cracks	Permeation through cracks

3. Results

The main results from the research contained in thesis are contained within the six papers. Some other results are included below.

3.1. Investigation of spraying mechanics

Both normal cameras and a high speed camera were used to take video recordings of the spray application for the spraying experiments. We can use normal camera videos to observe a key phenomenon in sprayed concrete – pulsation of the spray from the nozzle. This is illustrated in Figure 1, which a two still pictures extracted from a video – the left image shows a consistent grey spray cone, while the image on the right shows a much lighter spray cone which consists only of accelerator. A momentary pause in the concrete flow has occurred in the picture on the right.

The accelerator is a liquid with (relatively) low viscosity and consistent flow rate of the accelerator can be achieved, whereas the concrete has a much higher viscosity and the flow rate can experience momentary pauses, in which case the flow from the nozzle becomes pure accelerator. The pure accelerator flow from the nozzle leads to a local overdose of accelerator in the concrete and may cause a lamination in the hardened material.

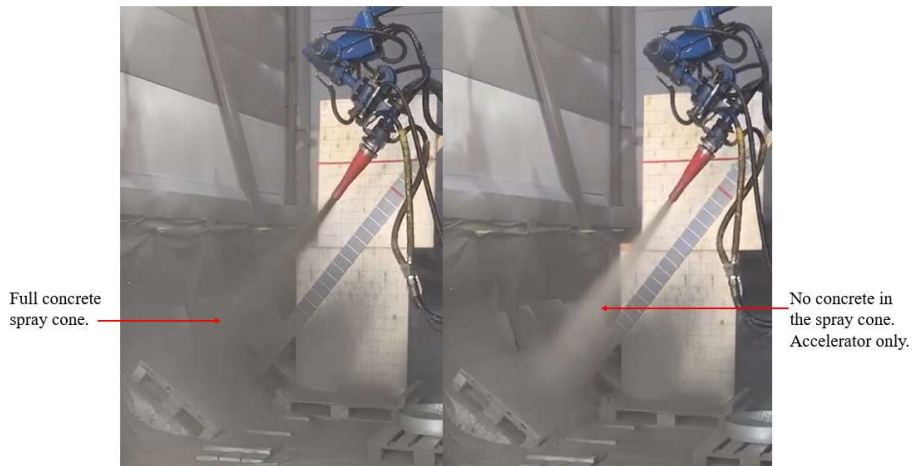


Figure 1 Photographs of the spraying experiments. Left: sprayed concrete application with a full concrete spray cone. Right: sprayed concrete application with a pause in concrete flow, so pure accelerator is propelled through the nozzle to the substrate. The mesh on the board behind the spraying is 100×100 mm.

3.2. Effect of laminations

The water penetration tests in paper 5 demonstrate that water transport along laminations (perpendicular to the direction of spray application) is much higher than that through the bulk concrete. Furthermore paper 6 contains compressive strength tests of cores containing laminations. These are identified in Figure 2, which is duplicated in paper 6. The measured compressive strength of the cores containing laminations was 60 % of the strength measured in comparable cores. So laminations cause reduced mechanical properties of, and increased water transport in, the hardened sprayed concrete. This demonstrates the importance of execution for wet spraying of concrete.



Figure 2 Identification of laminations in the cored specimens from the Drammen spraying experiments used for compressive strength tests

3.3. Particle tracking

The primary aim of using the high speed camera was to track particles in the spray cone and measure particle velocities. This was largely unsuccessful – particles in the spray cone could be distinguished by eye but the consistency of the particles compared to the surroundings was too variable from frame to frame to enable successful automated particle tracking. Manual particle tracking was possible but only at the periphery of the spray cone, where particle velocities are lower, and not representative of those towards the centre of the spray cone. An example frame from a high speed camera video taken at the Svorkmo spraying experiments is shown in Figure 3. The impact of the sprayed concrete with the substrate and rebound of particles can also be studied in the high speed videos – an example is shown in Figure 4.

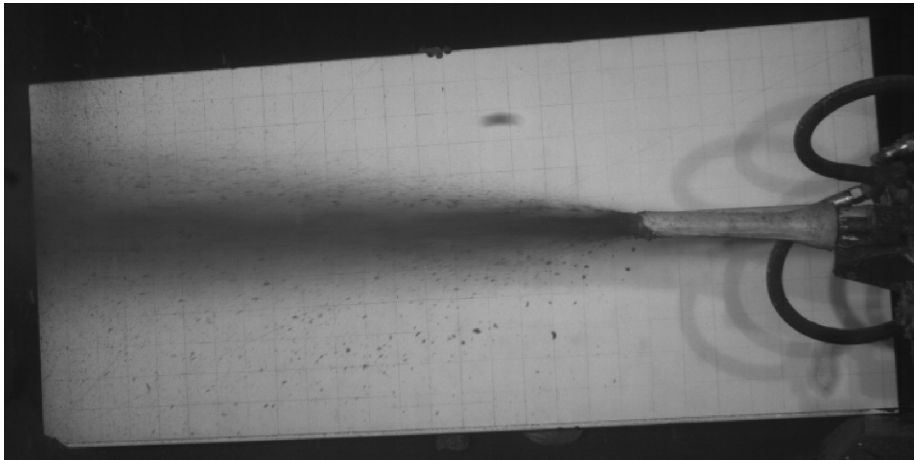


Figure 3 High speed camera image from the Svorkmo experiments, showing a consistent spray cone where individual particles cannot be distinguished, while individual particles can be identified at the periphery of the spray cone. The mesh on the board behind the spraying is 100×100 mm.

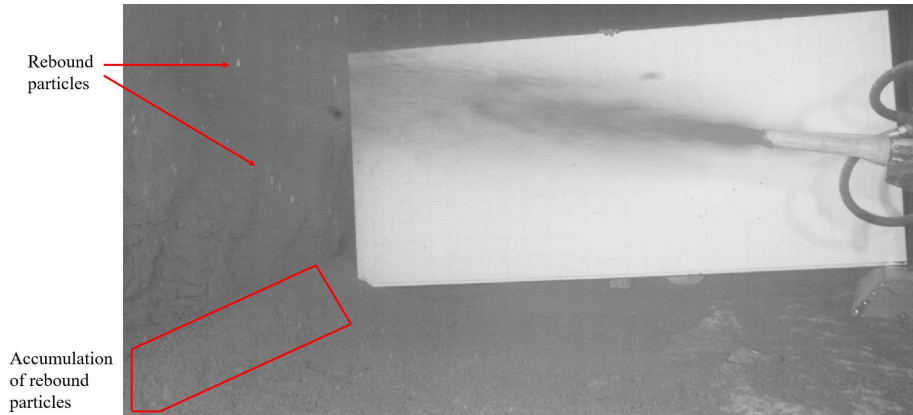


Figure 4 High speed camera image from the Svorkmo experiments, showing particles rebounding from the sprayed material and accumulating on the ground below. The mesh on the board behind the spraying is 100×100 mm.

4. Conclusions

The key conclusions that we can infer from the investigations and results contained in the six appended papers that constitute the main body of research in this PhD thesis are presented below.

- Addition of set accelerator at the nozzle increases the early age strength development but reduces density, reduces long-term strength and increases suction porosity of the sprayed concrete, both due to the water content of the set accelerator increasing the water/binder ratio, and due to the effect of the accelerator on the hydration products. This conclusion was demonstrated by tests on specimens produced by full-scale spraying experiments, and specimens produced in the laboratory where the accelerator doses were precisely controlled. The capillary suction curves (absorption in kg/m^2 against square root of time in seconds^{0.5}) show clear knee points after drying at 105°C in all the sprayed concrete specimens containing accelerator studied in papers 2 & 3, indicating percolated capillary pore systems.
- The presence of laminations in sprayed concrete increases the permeability of the material in the direction parallel to the lamination, i.e. perpendicular to the direction of spray application. Laminations reduce the compressive strength in the direction of the spray application, i.e. parallel to the substrate. Cylindrical specimens extracted from the lining by coring parallel to the direction of spray application and tested for compressive strength with the force applied in this same direction will give lower strength results if the cored cylinders contain laminations.
- Macro pores are ubiquitous in sprayed concrete and are non-spherical in shape. The spraying process causes the spherical entrained air bubbles due to use of an air entrainment agent to be lost. Like the orientation of fibres, the orientation of macro pores tends towards perpendicular to the direction of spray application. This tendency of the orientation of both fibres and macro pores, and the potential for laminations, demonstrates that sprayed concrete is an anisotropic material.
- The rate of water transport from both capillary suction and permeation is increased due to cracks in sprayed concrete. The higher rate of capillary suction is due to rapid rise of water in the crack, with the crack surface then providing additional area for absorption. The theoretical rate of permeation increases with crack width cubed following Poiseuille's Law [14], while the flow rate

coefficient also increases with crack width. So crack width is the major criterium for the rate of permeation through cracks. Describing a crack by the maximum crack width, rather than a mean value, gave clearer trends in the measured flow data, because most of the water flows through the wider parts of the crack.

- Inclusion of the EVA (ethylene-vinyl-acetate) based co-polymer admixture in sprayed concrete reduces water transport in sprayed concrete linings, both through the capillary pore network and through cracks. Inclusion of the EVA based co-polymer reduced the rate of capillary suction both in the cracks and in the bulk material. Inclusion of the EVA based co-polymer had no clear effect in cracks below 0.1 mm width but above this width, flow rate coefficient increased exponentially with increasing crack width in the standard sprayed concrete specimens, whereas the flow rate coefficient increased less with increasing crack width in the specimens with the EVA based co-polymer.

Inclusion of the EVA based co-polymer retarded the rate of early strength development in the sprayed concrete. Depending on early strength and thickness requirements for the primary sprayed concrete, applied directly onto the excavated surface, inclusion of the EVA based co-polymer may be unsuitable for this first layer given the slower rate of strength development.

The EVA based co-polymer can be included in sprayed concrete for secondary (inner) linings, where the requirement for early age strength is lower – strength need only be sufficient for adhesion to the previous layer. Inclusion of the EVA based co-polymer can reduce water transport in the linings to either:

- Give improved durability over single shell sprayed concrete linings, or
 - Enable omission of waterproofing membranes to achieve reduction in material consumption.
- Reducing the cement content of sprayed concrete reduces the CO₂ emissions associated with construction of sprayed concrete linings. A number of mixes with reduced cement content were studied. Replacement of cement content with fly ash increased the long term strength and reduced the rate of capillary suction but reduced the rate of early strength development. So, depending on early strength requirements, replacement of cement content by fly ash may be undesirable for sprayed concrete. Reduced cement content was achieved by reducing the matrix volume fraction, while maintaining the composition of the matrix. The sprayability of this mix was good – no major pulsation was observed when spraying compared to the reference mixes – and the rate of early strength development was comparable with the reference mixes.
 - Shrinkage and thermal contraction are difficult to measure in sprayed concrete. But it is desirable to minimise the cracking induced from these strains to reduce water transport through the linings, which is discussed in paper 5. A shrinkage reducing agent included in the mix was shown to reduce drying shrinkage in the Svorkmo experiments, as shown by results in paper 6. But other than this finding, atmospheric conditions were determined to be more significant than the mix composition for the magnitude of the volume changes. Avoiding early drying was determined to be particularly important.

5. Further Research

The following areas of sprayed concrete may be investigated further.

- Further investigation into compaction and macro porosity in sprayed concrete. Can the spraying process be improved to reduce/avoid the macro porosity of sprayed concrete?
- Study into the flow of sprayed concrete from the nozzle using a high speed camera. Analysis of particle velocities, impact with the substrate and rebound. Analysis of how to synchronise pump stroke rates and spraying process to avoid pulsation and momentary halts of concrete flow rate and hence avoid laminations in the hardened sprayed concrete.
- Can high performance or ultra-high-performance sprayed concrete be used to reduce the capillary porosity and improve strength and durability? Such concretes would likely give smoother capillary suction curves without such pronounced knee points seen in capillary suction tests of sprayed concrete. The use of ultra-high-performance concrete for sprayed concrete has been studied in [14] with a focus on the mechanical properties.
- Further investigation of self-healing in sprayed concrete. What are the critical crack widths for self-healing in sprayed concrete? What are the effects of mix composition and accelerator?
- Development of new accelerators compatible with supplementary cementitious materials. Current aluminium sulphate accelerators react with the Portland cement, and addition of supplementary cementitious materials retards this reaction, which reduces the early strength of sprayed concrete, which is so crucial for sprayed concrete.

References

- [1] W. Aldrian, A. Thomas, N. Chittenden and K. G. Holter, "ITA Report no. 24: Permanent sprayed concrete linings," ITA Working Group no. 12 and ITAtech, 2020.
- [2] The British Tunnelling Society and The Institution of Civil Engineers, "Tunnel lining design guide," Thomas Telford, London, 2004.
- [3] A. Thomas, "Achieving sustainability in underground construction through innovation," *Proceedings of the Institution of Civil Engineers – Civil Engineering*, vol. 173, no. 5, pp. 5-10, 2020.
- [4] L. Huang, P. D. Jakobsen, R. A. Bohne, Y. Liu, A. Bruland and C. J. Manquehual, "The environmental impact of rock support for road tunnels: the experience of Norway," *Science of the Total Environment*, vol. 712, pp. 1-13, 2020.
- [5] B. Lothenbach, K. Scrivener and R. D. Hooton, "Supplementary cementitious materials," *Cement and Concrete Research*, vol. 41, pp. 1244-1256, 2011.
- [6] O. A. Opsahl, A study of a wet-process shotcreting method, PhD thesis, Trondheim: The Norwegian Institute of Technology, 1985.
- [7] D. Beaupre, Rheology of high performance shotcrete, PhD thesis, Vancouver: University of British Columbia, 1994.
- [8] K. G. Holter, PhD thesis: Properties of waterproof sprayed concrete tunnel linings, Trondheim: Norwegian University of Science and Technology, 2015.
- [9] P. Hagelia, Deterioration mechanisms and durability of sprayed concrete for rock support in tunnels, Delft: Delft University of Technology, 2011.
- [10] C. J. Manquehual, Durability of rock support in Norwegian road tunnels, Trondheim: Norwegian University of Science and Technology, 2022.
- [11] "Proceedings - Seventh International Symposium on Sprayed Concrete - modern use of wet mix sprayed concrete for underground support," Sandefjord, 2014.
- [12] "Proceedings - Eight International Symposium on Sprayed Concrete - modern use of wet mix sprayed concrete for underground support," Trondheim, 2018.
- [13] Norwegian Concrete Association, "Publication no.7: Sprayed concrete for rock support," Oslo, 2011.
- [14] C. Edvardsen, "Water permeability and autogenous healing of cracks in concrete," *ACI Materials Journal*, Vols. 96-M56, no. July-August, pp. 448-454, 1999.
- [15] C. Larive, S. Bouteille, D. Chamoley, B. Petit, A. Huynh, F. Teply, S. Bernardi, L. Trucy, J. Derima and P. Marchand, "Spraying UHPFRC opens new application field for underground works," in *World Tunnel Congress*, 2018, 2018.

Status of papers and contribution of the candidate

Paper 1 – Review of Sprayability of Wet Sprayed Concrete

Status: Published

Contribution of the PhD candidate All

Paper 2 – Effect of Set Accelerator on Properties of Wet Sprayed Concrete

Status Published

Contribution of the PhD candidate: All

Paper 3 – Effect of Set Accelerator on Capillary Suction and Porosity of Concrete – Cast Samples with Constant Water/Binder Ratio

Status Published

Contribution of the PhD candidate All

Paper 4 – Anisotropy of sprayed concrete: macro porosity, layering and fibre orientation measured by image analysis, PF test, water penetration and CT scanning

Status Submitted and with editor

Contribution of the PhD candidate: All of the work except: Data analysis and plotting of graphs for macro porosity measured by black and white image analysis was done by Masters students Magne Stangeland Hårr and Gaute Kjecha, but this was done under guidance of the PhD candidate. CT scanning was done by Pål Erik Endrerud. Analysis of the CT scanning data was done by Iman Asadi.

Paper 5 – Water transport in cracks controlled by digital image correlation in wet sprayed concrete with and without an EVA based co-polymer admixture

Status Submitted and under review

Contribution of the PhD candidate: All of the work except: Crack width measurements by digital image correlation (DIC) were done by Per Øystein Nordtug and Nicholas Trussell, with guidance from Martin Kristoffersen. CT scanning was done by Pål Erik Endrerud. Analysis of the CT scanning data was done by Iman Asadi.



Paper 6 – More sustainable sprayed concrete tunnel linings: reducing cement content and improving water transport properties of sprayed concrete linings

Status: Submitted and with editor

Contributions: Introduction, discussion and conclusions were done by Nicholas Trussell with input from Karl Gunnar Holter and Tor Arne Hammer. Field measurements of early strength and laboratory measurements of density, strength and porosity were done by Nicholas Trussell. Concrete

proportioning was determined by Karl Gunnar Holter, Tor Arne Hammer and Rolands Cepuritis. Fresh concrete properties and field volume change measurements were done by Ola Skjølsvold. Analysis of shrinkage and temperature induced volume changes were by Tor Arne Hammer. The TSTM (Temperature-Stress Testing Machine) measurements on cast concrete and cracking computer simulations were done by Anja Birgitta Estensen Klausen.

Paper I

	
<p>© Article authors. This is an open access article distributed under the Creative Commons Attribution-NonCommercial-NoDerivs licens. (http://creativecommons.org/licenses/by-nc-nd/3.0/).</p>	<p>ISSN online 2545-2819 ISSN print 0800-6377</p>
<p>DOI: 10.2478/ncr-2020-0016</p>	<p>Received: Sept. 29, 2020 Rev. received: Dec. 7, 2020 Accepted: Dec. 14, 2020</p>

Review of Sprayability of Wet Sprayed Concrete



Nicholas Trussell
MEng, CPEng, MIEAust, PhD Student
Norwegian University of Science and Technology,
Department of Structural Engineering,
Richard Birkelands vei 1A, 7034 Trondheim, Norway
E-mail: nicholas.h.trussell@ntnu.no



Stefan Jacobsen
MSc, Dr.Ing, Professor
Norwegian University of Science and Technology,
Richard Birkelands vei 1A, 7034 Trondheim, Norway
E-mail: stefan.jacobsen@ntnu.no

ABSTRACT

Wet sprayed concrete quality is affected by more production factors than cast concrete, particularly due to the propulsion through the nozzle and the flash set caused by the set accelerator. Practitioners often use the term “sprayability” to describe these factors. We propose a definition of “sprayability” that relates the application to the final properties of the hardened sprayed concrete and review factors affecting it: concrete constituents, proportioning, and application mechanics. These factors affect the hardening and the structure of the hardened sprayed concrete – the porosity, permeability and durability. We consider improving sustainability through proportioning with increased share of supplementary cementitious materials, calculate the placed composition and focus on factors that affect water transport, and hence durability. Due to the spray application and flash-set, irregular compaction voids dominate the macro pore structure of sprayed concrete. Studies of permeability of sprayed concrete have shown that it is possible to obtain low permeabilities given adequate composition and curing. Presumably these samples have been well-cured, uncracked and with non-percolating macro voids. Given observations of cracks in sprayed concrete linings and the macro voids, important further studies will be on the effect of accelerator, compaction porosity and cracking on permeability.

Keywords: Sprayed concrete, sprayability, proportioning, accelerator, durability, porosity, permeability.

1. INTRODUCTION

Sprayed concrete is concrete that is applied by pumping through a nozzle and is consolidated by the impact of subsequent sprayed particles. Wet sprayed concrete means that a ready mixed concrete is pumped from a hopper to the nozzle where compressed air and accelerator are added so that the wet mix is sprayed and flash-set occurs as it hits the substrate. This is different to conventional concrete, which is applied manually or by pumping through a pipe, and consolidated under gravity and often mechanically by vibration or other forms of compaction. The placement method enables sprayed concrete to be placed in vertical or overhead locations, in irregular geometry, and with little or no formwork [1].

The sustainability of sprayed concrete tunnel linings (SCL) mainly depends on the concrete composition, the volume of concrete used and on the service life.

1.1 Sprayability

The term sprayability is frequently used to describe sprayed concrete properties. The term sprayability is a European term, whereas the term “shootability” is commonly encountered in North America.

We can refer to a definition for the pumpability of concrete, i.e. how easily concrete can be pumped. Jolin et al [2] defined concrete pumpability as the capacity of a concrete to be mobilised under pressure while maintaining its initial properties. We can develop this definition further: concrete pumpability is the capacity of a concrete to be pressed through pipes and hoses under pressure while maintaining its initial properties.

The properties of concrete are affected by the spray application process due to the addition of accelerator at the nozzle, which increases the early age strength. The final compressive strength of sprayed concrete can be lower than that for cast concrete [3] due to the effect of the set accelerator and the compaction porosity, see further discussion in Sections 4 and 5. So the above definition for sprayability is too simple and we propose the following definition:

Sprayability is the ability of a specific concrete mix to be sprayed and obtain satisfactory production and in-situ properties after pumping, addition of accelerator at the nozzle and spraying with a specific spraying set up and specific settings (pump speed, air pressure, accelerator dosage, spraying distance and angle, nozzle rotation etc).

Sprayability can be considered as a qualitative measurement, defined by a series of defined and measurable criteria:

- Mix composition
- Flow or slump
- Adhesion and cohesion
- Rebound
- Strength gain with time
- Compaction.

Sprayability is dependent on several processes through the process of producing and applying the sprayed concrete. This starts with the composition of the mix: the mix must be sufficiently flowable to be pumped and sprayed, but sufficiently “stiff” for the sprayed concrete to adhere to the substrate and not fail in cohesion. The sprayed concrete must achieve sufficient “set” to solidify and develop shear strength, and not fall or drip away from the surface as a liquid.

1.2 Dry or wet process

For a dry process of sprayed application of concrete, a dry cementitious mixture is transported through a hose to the nozzle, where water is added by the operator. The dry process relies on the skill level of the operator to determine and implement the mixing ratios of the dry mix and water at the nozzle. A schematic diagram showing the dry process for sprayed concrete is presented in Figure 1 [4].

For a wet process the fresh concrete mixture, excluding set accelerator, is fed into the hopper of the spraying machine. From there it is pumped to the nozzle, where compressed air and set accelerator are added. A schematic diagram depicting the wet process for spraying concrete is included in Figure 2. The water content of the fresh sprayed concrete is determined during batching rather than at the nozzle, so the nature and the quality of the final product is less dependent on the skill of the operator.

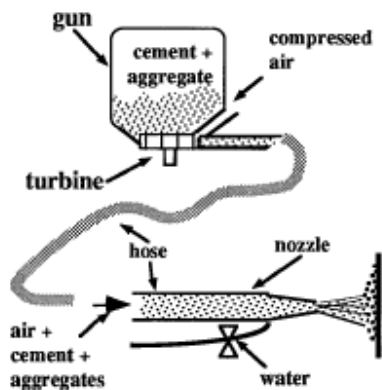


Figure 1 – Diagram of dry process for sprayed concrete [4]

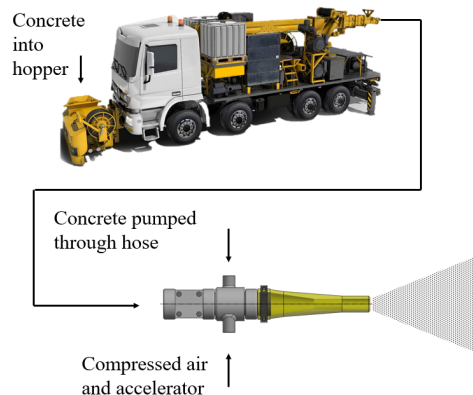


Figure 2 – Diagram of wet process for sprayed concrete

The wet process for sprayed concrete is more common than the dry one and is used for sprayed concrete tunnel linings. Dry process application would be used more for repair works or projects in remote locations, where supply of concrete from batching plant is impractical. As such this study only considers the wet process for sprayed concrete.

1.3 Scope

The scope of this paper is to investigate and describe the often-encountered term “sprayability” of concrete and the variables that affect this. Then we give an overview of constituent materials,

application and central properties of wet sprayed concrete that we believe are essential for the sprayability, with regard to productivity, economy, function, durability and sustainability.

This paper studies the mix composition, rheology, pumping, application, compaction of wet sprayed concrete. Physical properties of the in-situ properties that are related to the quality of application are considered – such as the presence of macro air voids.

Suggestions for investigations to understand sprayability and the essential material properties that affect SCL quality and sustainability are proposed. The outlook for the future of wet sprayed concrete is also discussed, for example ideas for improved durability and sustainability.

2. MATERIALS, PROPORTIONING AND RHEOLOGY

2.1 Constituent materials and proportioning

Proportioning and rheology of fresh concrete can be modelled by the two-phase particle matrix model (PMM) [5]. The matrix phase consists of water, additives, admixtures and the finest aggregate particles, whilst the particle phase consists of all particles larger than 0.125 mm.

The air voids can be considered as a part of the matrix since workability is assumed to be a function of quality and volume fraction of matrix. A rule of thumb could be that half a litre of air voids could be equivalent to a litre of matrix for workability, per metre volume of concrete. In practical calculation of the two phases the sum must be 1 so air voids can then be placed as part of the matrix, though reported separately in the proportioning:

$$V_{\text{matrix including air}} + V_{\text{particles}} = 1 \quad (1)$$

A typical sprayed concrete mix is detailed in Table 1. A set accelerator is added at the nozzle. In Table 1 we have presented the batched composition and then determined the placed composition due to increased water content from the accelerator and macro voids in the placed composition.

Table 1 – Typical sprayed concrete mix declared by ready mix producer and placed composition corrected for volume change by accelerator added at spraying and compaction porosity after spraying

Phase	Constituent	Mass (kg/m ³)	Volume (l/m ³)	Volume composition* (l/m ³)	Placed concrete composition* (kg per m ³ concrete after spraying)
Matrix phase	Standard fly ash cement	462	156		440
	Water	206	206		219
	Silica fume	19,2	8,7		18,3
	Super plasticiser	4,8	4,6		4,6
	Air entrainment agent	0,45	0,45	424	0,43
	Set accelerator (dry)	-	-		24,8
	0 – 8 mm aggregate (<0.125 mm)	21,8	8,3		20,8
	Air		40		65
Particle phase	0 – 8 mm aggregate (>0.125 mm)	1505,8	570,4	576	1435
	Steel fibres	45	5,6		42,9

* The placed concrete composition is calculated from the mass and volume in the first two columns in two steps:

- 1) Correct the mass of constituents to (kg/m^3) due to increased volume by 10 % accelerator of effective binder mass = +24 kg of water. The dissolved chemicals of the accelerator are assumed to have no volume.
- 2) Correct the mass of constituents to (kg/m^3) due to final, sprayed macro void content, for example 6.5 % macro voids, i.e. 2.5 % more air voids than declared by the ready-mix concrete producer at batching.

The purpose of the air entrainment agent is to improve the workability of the fresh concrete. This is thought to work by the ball bearing effect of air voids in the fresh concrete. These air voids are believed to be ejected upon impact of the sprayed concrete with the substrate, and the removal of this entrained air reduces the workability of the concrete. Air entraining agents are thus assumed to increase the workability to improve performance during pumping and spraying, whilst reducing the workability after impact with the substrate, improving stability during hardening [1].

A retarder may be added to delay set time and achieve a longer duration of full workability.

For sprayed concrete the maximum aggregate size is typically 6–8 mm. This aggregate size, smaller than for conventional concrete, improves the performance of the concrete under spraying and pumping. Furthermore smaller aggregate sizes reduce the amount of rebound compared with larger aggregate sizes [6].

Structural fibres are generally included in the sprayed concrete mix. The structural fibres give the concrete ductility and tensile strength and replace conventional reinforcement. Structural fibres can either be steel or macro-polymer fibres. Only steel fibres are considered for this review, because macro-polymer fibres are now banned for use in sprayed concrete linings for Norwegian road tunnels for environmental reasons, as described by Myren et al [7].

The particle matrix model will be useful to investigate how to:

- Increase the use of supplementary cementitious materials such as fly ash or limestone filler,
- Reduce cement content to make more environmentally friendly sprayed concrete mixes,
- Add fillers and other mineral additives whilst keeping matrix volume constant to maintain workability.

Table 2 – Example of sprayed concrete mix with reduction of cement content by use of fly ash and filler

Phase	Constituent	Mass per volume (kg/m ³)	Volume (litres per m ³)	Volume (litres per m ³)
Matrix phase	Standard fly ash cement 18% FA	384	130	
	Fly ash	43	20	
	Water	200	200	
	Silica fume	19.2	8.7	
	Super plasticiser	4.8	4.6	424
	Air entrainment agent	0.45	0.45	
	Hardening accelerator	14.0	12.3	
	0 – 8 mm aggregate (< 0.125 mm)	21.8	8.3	
	Air	-	40	
	Particle phase	0 – 8 mm aggregate (> 0.125 mm)	1505.8	570.4
Steel fibres		45	5.6	

Limestone powder and other fillers, for example from manufactured sand and crushed aggregate, would be good alternatives for filler to be investigated in sprayed concrete studies.

Table 2 provides details on proportioning for two variations of a standard sprayed concrete mix, based on the ready-mix proportions in Table 1. The cement content is reduced by adding fly ash. Hardening accelerator is added to compensate for the low early age strength development of high fly ash concrete [9].

2.2 Rheology

Rheology is defined as “the science of the deformation and flow of matter” [10]. But why is the rheology of the fresh concrete important? Clearly if concrete cannot be pumped from the hopper of the spraying machine to the nozzle, neither can it be sprayed. Kaplan et al [11] determined the range of fresh concrete properties across which concrete can be pumped through a pipe. The criteria that Kaplan determined included the slump of the fresh concrete, stability such as bleed tendency and aggregate size. Perhaps we can infer a similar range of properties at which concrete can be sprayed.

The rheology of concrete can be measured by using a viscometer, which consists of a cylindrical array of steel ribs that is placed into a cylinder that is filled with the concrete to be tested. As the cylinder filled with concrete rotates, the torque versus speed is recorded. This enables the shear stress vs the rate of shear to be plotted for the fresh concrete. The yield shear stress and plastic viscosity can then be derived. A diagram of a concrete viscometer is included in Figure 3.

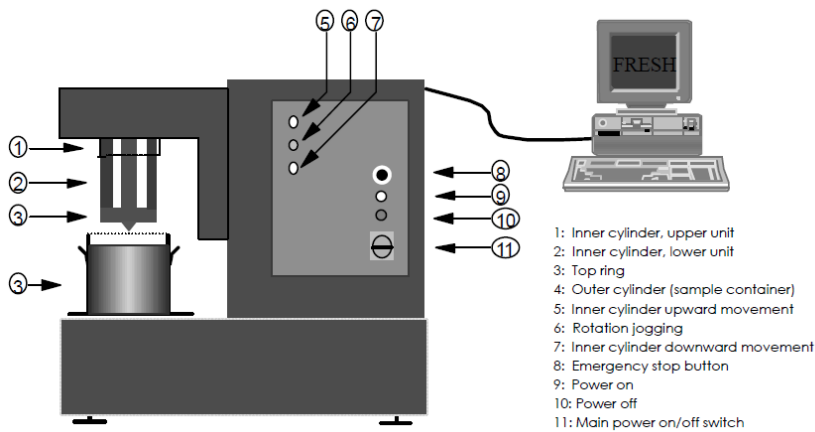


Figure 2 – Concrete viscometer [12]

According to the particle matrix model the rheology of the concrete is governed by:

- The properties of the particles,
- The properties of the matrix,
- The volume ratio of matrix phase/particle phase.

But is the rheology of the concrete important once the sprayed concrete has left the nozzle? Does the rheology of the sprayed concrete effect the adhesion to the application surface, or the cohesion of the freshly sprayed concrete?

Beaupré [4] measured build up thicknesses for different sprayed concrete mixes, measuring the thickness of sprayed concrete that was sprayed onto the application surface whilst keeping the nozzle stationary, before the in place sprayed concrete fell under its own weight. Beaupré determined a relationship between build up thickness and yield stress – the concrete was able to be built up in thicker layers with higher yield stress of the concrete [4]. He also calculated minimum yield stress to avoid fall out under shear stress caused due to self-weight of the sprayed concrete [4]. Note that Beaupré termed the yield stress “flow resistance of the fresh concrete”, though still following the Bingham flow model [10] for simple concrete viscometers:

$$T = g + hN \quad (2)$$

with T Torque (Nm),
 g initial yield (or yield stress x constant 1),
 h proportionality (or plastic viscosity x constant 2) and
 N rotational speed (rpm) of the viscometer impeller.

2.3 Workability

The workability of fresh concrete is a practical term used to describe the most important properties of fresh concrete: stability, ability to flow by gravity and ability to be compacted and let out encapsulated air.

Standard practice is to perform a flow test [13] or slump test [14] for each batch of sprayed concrete before application. Both tests are simple procedures and can be readily undertaken in a small area of a construction site or concrete mixing plant.

The purpose of either is to test the concrete is sufficiently flowable to be pumped and sprayed, but stiff enough to adhere to the application surface and not fail in cohesion. Stability can be assessed by looking at the edge of the pancake for bleeding and at the centre to look for segregation of the coarse particles.

Based on our preliminary observations of the spraying of a batch of concrete, which experienced a workability loss over a time of more than two hours while varying the accelerator from 0 to 10 % of the binder mass, we think accelerator variation has a greater effect on sprayability than varying workability.

2.4 Accelerator

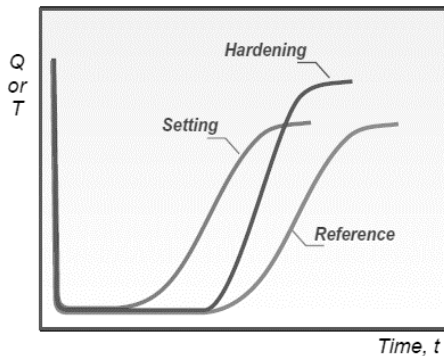


Figure 4 – The effects of setting and hardening accelerators on the rate of heat evolution [15]

Accelerators for concrete fall into two categories:

- Setting accelerators are applied at the nozzle and produce an earlier initiation of hydration of the cement.
- Hardening accelerators are incorporated into the mix and increase the rate of hydration of the cement, once the reaction has initiated.

The effect of these two types of accelerator is shown in Figure 4 [15].

2.4.1 Set accelerator

Set accelerator is normally added at the nozzle to reduce the set time of the sprayed concrete and enabling thickness of the sprayed concrete to build up on the application surface. Use of accelerator is particularly important when applying sprayed concrete to the sides and crown of tunnel sections, where the sprayed concrete would run off or fall from the substrate without accelerator. Set accelerator increases the rate of strength development of the sprayed concrete, which is described in Section 4.1.

The set accelerator dosage is controlled by the operator and typical dosages can range from 2 % to 10 % of binder mass. For example a low dosage may be selected when spraying onto the invert of a tunnel, whereas a higher dosage would be desirable when spraying onto the tunnel crown, enabling a faster strength development and hence reducing the likelihood of a fall of the sprayed concrete.

Due to the addition of the accelerator at the nozzle and the compaction porosity, the placed concrete has a different composition to the batched concrete. The additional water content Δw was calculated for the concrete proportioned in Table 1 after the addition of varying dosages of a set accelerator, with 48 % water content, at the nozzle.

$$\Delta w = \text{accelerator dosage} \times \text{accelerator water content} \times (m_c + k m_s)$$

$$\text{New } m_w / (m_c + k m_s) = (206 + \Delta w) / 500$$

6 % accelerator

$$\Delta w = 0.06 \times 0.48 \times (500) = 14.4 \text{ kg}$$

$$m_w / (m_c + k m_s) = (206 + \Delta w) / 500 = 0.441$$

0 % accelerator

$$m_w / (m_c + k m_s) = 206 / 500 = 0.412$$

10 % accelerator

$$\Delta w = 0.10 \times 0.48 \times (500) = 24.0 \text{ kg}$$

$$m_w / (m_c + k m_s) = (206 + \Delta w) / 500 = 0.460$$

3 % accelerator

$$\Delta w = 0.03 \times 0.48 \times (500) = 7.2 \text{ kg}$$

$$m_w / (m_c + k m_s) = (206 + \Delta w) / 500 = 0.426$$

where m_c mass of cement
 m_s mass of silica fume
 w mass of water
 k k factor for equivalent w/m_c ratio

2.4.2 Hardening accelerator

Hardening accelerator can be incorporated into the mix to compensate for the lower rate of strength development that occurs when fly ash is incorporated into the mix. Hardening accelerators are incorporated into the mix and increase the rate of hydration of the cement, without changing the initial reaction time (see Figure 4) [15]. Recently hardening accelerators been used in sprayed concrete with high volume of fly ash [9].

Incorporating fly ash into the concrete proportioning, whilst reducing the rate of early strength development, increases the final strength of concrete due to the pozzolanic reaction. The silica in the pozzolan reacts with the calcium hydroxide, which is a by-product of cement hydration, to produce more calcium silicate hydrate (CSH). This pozzolanic reaction, though increasing the amount of gel and hence gel porosity, reduces the capillary porosity, which reduces water transport through the concrete and hence improves durability. Long term strength is also increased due to the reduced capillary porosity and higher CSH content.

3. SPRAY APPLICATION

3.1 Pumping

When concrete is pumped from the hopper to the nozzle through pipes, coarser particles migrate towards the centre of the flow, whilst a layer of paste, formed from smaller particles, forms around the pipe wall. This paste can be referred to as a lubrication layer and a schematic picture is shown in Figure 5 [16].

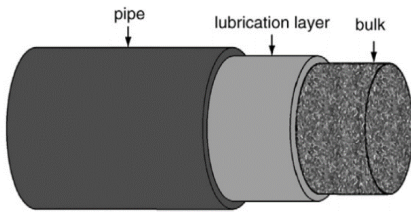


Figure 5 – Schematic of concrete flow in pipe, reproduced from Choi [16], showing lubrication layer during concrete pumping

Choi [16] measured the thickness of this layer as approximately 2 mm, for concrete flow through a plastic pipe of 125 mm diameter. For concrete spraying equipment, the concrete line to the nozzle is through a rubber hose. A rubber hose will have a rougher intrados than a smooth plastic pipe. It is therefore anticipated that the thickness of the lubrication layer would be greater for the flow of pumped concrete through the rubber hose, compared to the 2 mm thickness measured by Choi.

3.2 Mixing at the nozzle

Sprayed concrete is pumped to the nozzle, where it is mixed with pressurised air and accelerator, and discharged through the nozzle. A typical schematic of the interactions at the nozzle is presented in Figure 6. Blockages at the nozzle can occur. The cause of this is likely to be the concrete gaining cohesion during pumping and upon addition of accelerator, and hence clogging the nozzle.

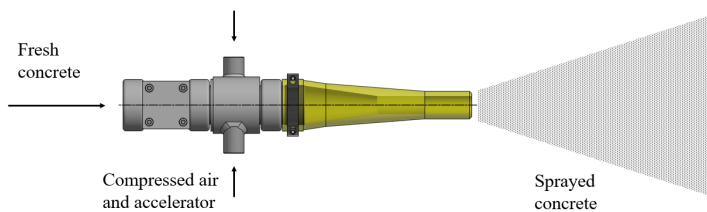


Figure 6 – Typical diagram showing interactions between pressurised air, accelerator and sprayed concrete

3.3 Application mechanics

The quality of sprayed concrete is, to a great extent, determined by the actions of the operator, who can affect the application parameters, notably distance and angle between spray and substrate, movement of the nozzle, ratio between concrete and air flow, and accelerator dosage. It has been demonstrated by Ginouse and Jolin [17] that there is a greater mass flux density at the centre of the spray cone than at the edges, as shown in Figure 7. Furthermore, there is a different material content throughout the spray cone – there is a migration of aggregate and larger particles towards the centre of the spray cone, whereas at the edge of the spray cone there is a higher proportion of concrete paste or matrix. This is perhaps an extension of the lubrication layer effect in the pipe flow, where the coarse particles migrate towards the centre of the pump line flow,

described Section 3.1. So the flow conditions of concrete in the hose before reaching the nozzle likely affect the composition and material distribution in the spray cone.

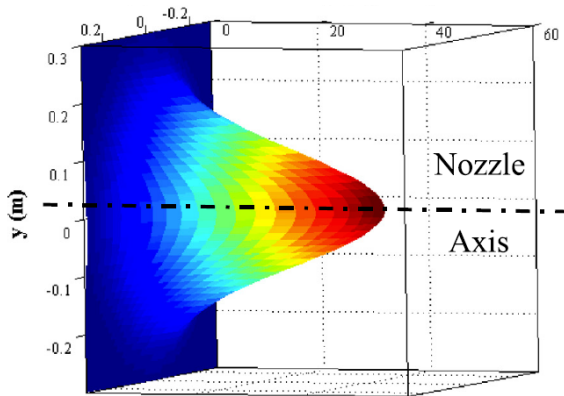


Figure 7 – Max flux density of spray cone [17]

To ensure consistent mass and particle distribution throughout the sprayed concrete, the operator often articulates the nozzle in small circular motions. Ginouse and Jolin [17] opined that the circular motions and particle distribution ensure that paste-rich material is always deposited immediately before larger particles and fibres hit the surface. The paste and fine particles provide better encapsulation for the larger particles and the fibres and enable better retention, hence reducing rebound from the spray application. The final effect of this on compaction is hard to judge in our opinion since little information exists on the sequence of events and movement through the different phases, impact, compaction and rate of set at impact.

The distance of the nozzle from the application surface is an important parameter. A study by Ginouse et al [17] measured the velocity of particles greater than 5 mm diameter and these were found to accelerate over distances 0.5 – 1.0 m from the nozzle. At smaller distances the spray area is narrower, due to the total cone angle of 24.5 degrees for wet spraying reported by Ginouse et al [18]. Ginouse et al [18] also measured an influence of gravity in the spray cone – for a horizontal application of sprayed concrete, they measured a slightly greater flux density below the horizontal axis.

Ginouse & Jolin [19] used a high-speed camera to observe speed of particles greater than 5 mm from a nozzle with 32 mm outlet diameter during wet spray. They measured 26 and 28 ms^{-1} in the centre of the spray cones at 0.5 and 1 m distance. The speed towards the edge of the cone dropped to around 20–22 ms^{-1} .

Opsahl [20] sprayed on a wheel arrangement 0.2 m in front of a 1½ inch nozzle and observed 32–35 ms^{-1} exit velocity. Though perhaps the wheel arrangement was affected by the compressed air itself as well as the impact of the particles.

Reinhold and Wetzig [21] conducted concrete spraying experiments and determined that the variations in the nozzle distance and air flow rate did not significantly affect the in-situ properties of sprayed concrete.

The nozzle should be perpendicular to the application surface, as specified by [22]. Perpendicular application is important to improve compaction and reduce rebound. Although the irregular surfaces of blasted tunnels have relatively large roughness, so perpendicular application is impossible in practice when combined with the rotational movement.

3.4 Rebound

Rebound is an unavoidable by-product of the sprayed application of concrete and occurs when spray-applied material fails to adhere to the substrate and instead falls to the ground. Reference [22] reports that rebound material for today's sprayed concrete technology is measured as 5 % or less.

The rebound material does not have the same particle distribution as the sprayed concrete mix – there is a larger percentage of aggregate and steel fibres. Kaufman et al [23] measured the amount of fibre (both steel and polymer fibres were measured) rebound as 25–44 % of the fibre content of the concrete mix. They also observed that coarse aggregate was over-represented in the rebound, though not as much as that of the fibres. Thus the placed fibre content of the sprayed concrete is significantly reduced compared to that of the mix composition.

3.5 Adhesion and cohesion

Sprayed concrete applied onto a substrate must achieve sufficient adhesion to the substrate to avoid falling, and sufficient cohesion to avoid falling or slumping under its own weight. The cohesion of sprayed concrete can be measured in terms of the build-up thickness, i.e. how much thickness can be applied before the sprayed concrete falls under self-weight. Austin et al [24] measured build up thicknesses of 130–320 mm for different mix designs in laboratory tests.

Adhesion is controlled by two factors:

- the nature of the substrate, and
- the shear strength of the sprayed concrete.

The surface onto which the sprayed concrete is to be applied should be clean, moist and free from dust and loose material prior to application. The methods for cleaning the surface are described in [22]. Cleaning by jet wash with water is the most common surface preparation measure.

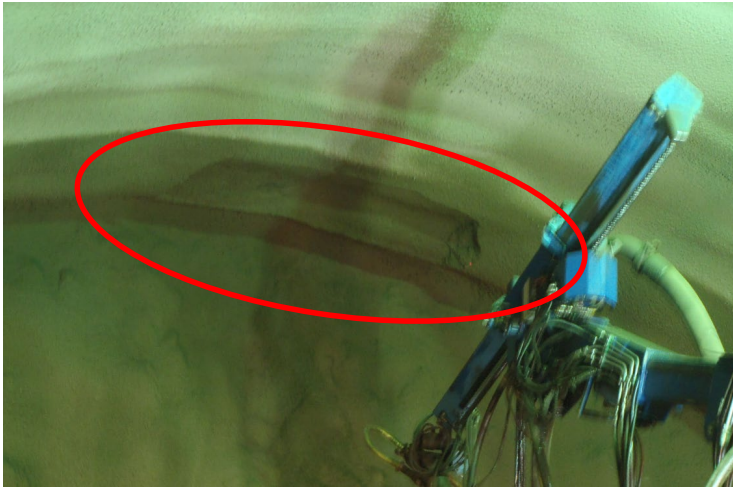


Figure 8 – Photograph showing area where sprayed concrete has fallen from tunnel crown, cause unknown but likely sprayed concrete failed under own self-weight (photograph Nicholas Trussell)

4. HARDENING

4.1 Strength development

Early age strength of sprayed concrete is the main quality criterion for immediate rock support. It allows the necessary progress, safety and quality during construction of sprayed concrete tunnels and reduces the likelihood of falls of loose rock or sprayed concrete during, or immediately after, application. In [25] the requirements to strength over time are given as classes, see Figure 9. The J is from the German word *jung*, meaning young, and A, B and C are the boundaries between the J_1 , J_2 and J_3 strength classes.

Early age strength is tested by penetrometer for strengths typically up to one or two hours. At higher strengths (from 3 hours to 24 hours) the Hilti stud driving test is used. 28 day and longer-term strength is tested by laboratory crushing of core samples.

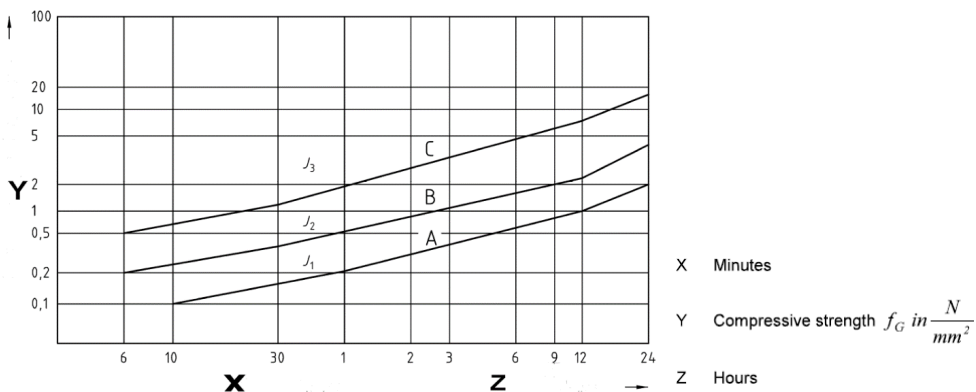


Figure 9 – Early age strength curves for sprayed concrete [25]

The high early strength gain is due to the effect of the set accelerator. However higher early age strength can reduce long term compressive strength in a similar way to high temperature early curing. A balance between early age and long-term strength should be achieved.

Neville [26] reported that higher temperature during and following the initial contact between cement and water reduces the length of the dormant period and leads to a coarser structure of the CSH gel with a higher porosity. A higher porosity leads to a lower long-term strength, as discussed in Section 5.1. Given that the set accelerator reduces the dormant period (as shown in Figure 10) for hydration, we suspect that this yields a coarser structure of the CSH gel (and/or perhaps capillary) porosity in the same way.

Opsahl [20] reported strength loss up to 50 % with a 12 % dosage of alkaline accelerator. Usually there are limits to the recommended dosage beyond which the accelerator can have a detrimental effect on the long-term strength.

4.2 Temperature development

The hydration of Portland cement generates approximately 500 kJ/kg [27] for complete hydration. Figure 10 shows how 3 % by cement mass of alkaline accelerator and 7 % by cement mass of alkali-free accelerator paste affect isothermal calorimeter curves for hydration of 100 g of cement [28]. Figure 10 shows how the dormant period was far briefer and the acceleration period of cement hydration occurred much sooner for the accelerated cement pastes.

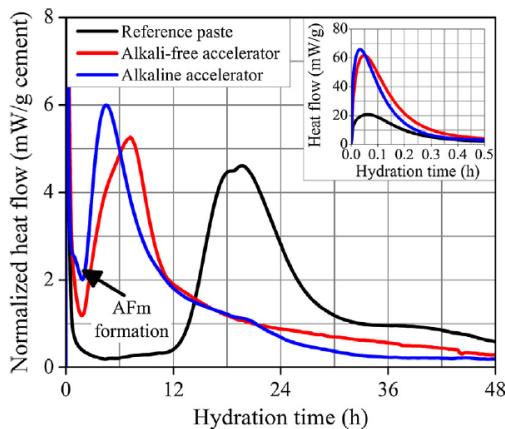


Figure 10 – Heat flow curves of hydration of cement pastes and effect of sprayed concrete accelerators [28]

Beck [29] measured early age strength gain whilst varying the ambient temperature and temperature of the fresh sprayed concrete. It was found that the initial temperature of the sprayed concrete and initial ambient temperature affect the rate of hydration of the cement in the same way as for conventional concrete.

Cepuritis [30] developed a test method for mixing cement paste with accelerator to test the set time of the paste. The test involves manually mixing cement paste with accelerator in a small container. The set time is then determined using the Vicat apparatus [31]. The needle is lowered into contact with the cement and then allowed to fall freely. The cement is considered set once

the Vicat needle is withdrawn and is clean from cement. This test is applicable to give an indication of the early age strength development of sprayed concrete.

4.3 Shrinkage and cracking in-situ

Concrete experiences volume changes during early age and curing. There is plastic shrinkage due to evaporation of water from fresh concrete, autogenous shrinkage due to hydration, temperature variations and chemical shrinkage, and drying shrinkage due to loss of water from the hardened phase. Internal tensile stresses develop which are resisted by the bond to the substrate. If shrinkage is great enough, the sprayed concrete will crack or debond [32].

Shrinkage of concrete, ε_c , is a function of volume of paste, $V_p = (1 - V_t)$ where V_t = volume fraction of aggregate and ε_p = shrinkage of the paste. So a high volume fraction of cement paste ($1 - V_t$) will lead to higher shrinkage.

$$\begin{aligned} \varepsilon_c &= \varepsilon_p (1 - V_t)^n & (3) \\ \text{with } n &= 1.2 - 1.7 & [26] \end{aligned}$$

The term “plastic shrinkage” does perhaps not apply to sprayed concrete because, due to the flash set of cement caused by addition of the set accelerator at the nozzle, the concrete is not in the plastic state after application. To our knowledge there is little information about the evolution of shrinkage stresses in sprayed concrete, especially at early age.

Opshal [20] measured free drying shrinkage at 50 % relative humidity on beams cut from sprayed panels at 6 days, then measured from 7 days to 360 days. He observed shrinkage up to 0.7×10^{-3} for sprayed concrete samples with 450 kg/m^3 cement content and water/cement ratio of 0.44. He hence concluded that sprayed concrete behaves in a normal way with respect to drying shrinkage in that period. He found that the presence of steel fibres in the sprayed concrete did not affect the shrinkage.

Holter [33] measured crack widths and spacings in the lining of the Gevingås rail tunnel. The lining was sprayed directly onto the rock and his observations were made a year after spraying. Holter [33] mapped approximately 210 cracks and determined most common crack spacing of 0.7–1.0 m with most crack widths between 0.05 to 0.5 mm. Distributing the crack widths over the spacing corresponds to strains in the order of 0.05×10^{-3} to 0.5×10^{-3} . Holter [33] observed typically 6 °C variation of the temperature of the lining over the year. Compared to a thermal expansion coefficient of approximately $10^{-5} \text{ }^\circ\text{C}^{-1}$ this 6°C decrease of temperature corresponds to a free deformation of 0.06×10^{-3} . When compared to a tensile fracture strain of concrete of 0.1×10^{-3} to 0.2×10^{-3} it appears likely that shrinkage is the most important cause of the cracking.

In the literature there are a few studies on shrinkage of sprayed concrete but few/none of these concern direct measurements of shrinkage of wet sprayed concrete tunnel linings. Bryne et al [34] studied restrained shrinkage by casting sprayable concrete into a ring test, on an instrumented granite slab and by modelling. They studied early age shrinkage up to a few weeks and found that glass fibres could be used to reduce cracking. Menu et al [35] also compared modelling with measurements of shrinkage up to some weeks. Further investigation is therefore needed into shrinkage of sprayed concrete.

5. POROSITY, PERMEABILITY AND DURABILITY

5.1 Porosity

Current sprayed concrete methods produce a less compacted and less consistent concrete than cast concrete – hardened sprayed concrete contains many small and larger air voids, or macro pores. A photograph of an example core from sprayed concrete is shown in Figure 11 where macro pores larger than 1 mm can be seen on the core surface.

Holter [33] used the capillary suction method [36] and the PF (pore ratio) method [37] to measure porosity of sprayed concrete samples from the Harangen road tunnel. Holter determined suction porosity as around 20 %, mean open macro porosity of 0.5 % and closed macro porosity of 4.2 %. The open macro porosity was defined as the increase in water uptake from the end point of the one-sided capillary suction curve to a constant mass after subsequent submersion at atmospheric pressure of the same concrete specimens, whereas the closed macro porosity is measured by pressure saturation in the PF test after submersion at atmospheric pressure. In Holter's experiments the open macro porosity made up 11 % of the total macro porosity $0.5/(0.5 + 4.2)$.



Figure 11 – Photograph showing typical core taken from sprayed concrete lining (photograph Nicholas Trussell)

Holter [33] also used an image analysis (IMA) method [38] to measure the macro porosity and compared it to the closed macro porosity measured with the PF method. This comparison was done on a larger set of specimens from four different tunnel linings. Macro pore volumes were measured to be 4.0–6.0 % from 27 samples, with a mean of 4.5 % measured with the PF method. The image analysis method determined macro pore volume on comparable specimens of 5.7 %. If we now define open macroporosity as the difference between macroporosity measured with IMA and with PF we find that the open macro porosity makes up 21 % of the total macroporosity $(5.7 - 4.5)/5.7$ of those specimens. Hence open macro porosity, depending on the test method, is in the order of 11–21 % of the total porosity.

Opsahl [20] used microscopic analysis following [39] with an automated camera procedure on a total of 21 different mixes sprayed in full scale on both tunnel linings and test panels. He measured 3.6 to 6.5 % air void content of which most were irregularly shaped compaction voids larger than 300 microns as determined by image analysis.

Macro pores can be greater than 10 mm in size for cores of a “good” quality [33]. Cores of poorer quality may have far larger macro pores. A high content of irregular macro pores is likely to increase the permeability of the sprayed concrete due to the increased probability the pores percolate.

From percolation theory we know that the critical volume fraction for percolation, p_c , of monospheres is 28 % of volume according to Garboczi et al [40]. Elongated pore shape reduces p_c . Ellipsoids of length/width ratio of 20/1 percolate at 4 % of volume. At length width ratio of 50/1, p_c is 1.5 % of volume and at ratio 100/1 it is only 0.6 % of volume.

Sprayed concrete permeability can be affected by percolation in two ways. Firstly, the shape of the macro pores seen in sprayed concrete is very angular so they are likely to percolate. Secondly, the interfacial transition zone (ITZ) is known to be more permeable than bulk concrete permeability. Therefore 0.6 % of volume as fibres with length/width ratio of 100/1 can increase the permeability. Both factors could lead to a reduction in the durability of the sprayed concrete. This is especially important for tunnel linings, where a high permeability enables groundwater, which may be aggressive to the concrete, to flow through the lining. Though a recent study of air voids in an asphalt concrete material using CT scanning [41] was used to determine interconnectivity between air voids, showing that not all interconnective air voids are valid for permeability.

Furthermore, strength depends on the porosity of the concrete. A 2 % increase in void ratio can decrease the compressive strength by 10 % [26].

An interesting comparison is that the features of the porosity in cold sprayed metals [42] are very similar to the macropore structure in sprayed concrete. Perhaps the relative size of the pores scales to the relative size of the particles in the two different materials.

5.2 Permeability

Opsahl [20] performed hydraulic conductivity tests on sprayed concrete specimens with water pressure of 4–8 MPa. Whilst permeability was found to vary largely, the lowest values measured were $2 \times 10^{-14} \text{ ms}^{-1}$ on concrete drilled from panels sprayed with $w/c = 0.35$ with fibres but without accelerator. With accelerator, fibre and higher $w/c = 0.47$ as low values as $4 \times 10^{-14} \text{ ms}^{-1}$ were reported. For some other specimens much higher values were measured. Poor curing and fibres were mentioned as possible explanations for the variation. Opsahl [20] also used the water penetration method to test permeability. He measured water penetration depths of maximum 7 mm for specimens from tunnel linings, subjected to pressure of 0.5 MPa on one side over 14 days. For specimens from test panels, subjected to pressure of 0.8 MPa on one side for 24 hours he measured water penetration depths in the range of 10–70 mm.

Holter [33] performed hydraulic conductivity measurements with 0.5 MPa water pressure on sprayed concrete without imperfections (i.e. cracks). He measured water permeability of 35 sprayed concrete specimens from three different tunnels. He measured water permeabilities between 3.3×10^{-11} and $9.6 \times 10^{-12} \text{ ms}^{-1}$ in four of the specimens, whilst measuring zero water flow through the remaining specimens. With the sensitivity of the equipment being $5 \times 10^{-14} \text{ ms}^{-1}$ he concluded that crack free and well compacted sprayed concrete can have a very low water permeability of less than $5 \times 10^{-14} \text{ ms}^{-1}$.

Based on this it seems that if one can avoid too high w/c ratio, too much variation in compaction, cracking and poor curing it is possible to produce low permeable tunnel linings with conventional wet sprayed concrete.

5.3 Durability

The durability of concrete is a large subject and is only covered briefly here. Whilst durability of sprayed concrete depends on the type of environment that the concrete is exposed to, it also depends on water transport in the sprayed concrete, which is discussed in Sections 5.1 and 5.2.

Accelerated freeze-thaw testing of sprayed concrete has been reported by several, for example by Opsahl [20], Shrader and Kaden [32] and Holter [33]. These studies showed that entrained air voids of the right size and/or very high strength can work to protect sprayed concrete against frost deterioration in severe testing. It was also shown that, as for conventional concrete, the critical dilation test can be used to assess whether a given capillary saturated state will cause internal frost damage. The principle of both type of environment (load: frost, saturation, salt, etc) and material (resistance: strength, air voids, permeability, etc) determine durability.

Hagelia [43] studied chemical degradation of sprayed concrete cores sampled from tunnel linings up to age of about 25 years with variable degrees of deterioration. He found that a w/b ratio of 0.4 and a low capillary porosity, less than 20 %, are good properties for the durability of sprayed concrete. He found that capillary porosities of 18 to 20 % seemed to largely prevent the diffusion of saline waters and corrosion of the specimens. The main deterioration mechanisms were found to be chemical and biological degradation of the cement paste in thin (less than 80 mm thickness) sprayed concrete linings with poor adhesion to the substrate rock.

6. CONCLUSIONS

- We propose a definition of “sprayability” that relates the application to the development and the final properties of the hardened sprayed concrete. “Sprayability” is governed by the concrete constituents, proportioning and application mechanics.
- The rheology of concrete is important to enable pumping of fresh concrete. If the concrete cannot be pumped, then it cannot be sprayed.
- The addition of set accelerator at the nozzle is essential to reduce the set time of the sprayed concrete and enables thickness of the sprayed concrete to build up on the substrate. The reaction of the set accelerator with the cement paste gives high early age strength but is detrimental to long term strength.
- Incorporating fly ash into the paste improves long term strength due to the pozzolanic reaction between the silica in the fly ash and calcium hydroxide to produce more calcium silicate hydrate (CSH). Inclusion of fly ash reduces the rate of strength development. This has been compensated for using a hardening accelerator. It has recently been proven possible to spray high fly ash concrete by the wet process (fly ash content up to 33 % of the cement content by mass).

- There is greater mass density at the centre of the spray cone. Furthermore there is a greater concentration of aggregate at the centre of the spray cone, with a higher proportion of paste at the edge. The nozzle operator should therefore manipulate the nozzle in small, circular movements to ensure even distribution and consistency of sprayed concrete. It is not fully understood how spraying mechanics affect the compaction of the sprayed concrete.
- There is a higher proportion of aggregate, and particularly fibres, in sprayed concrete rebound.
- Very few shrinkage measurements of in-situ sprayed concrete exist. From observed cracks in tunnel linings sprayed directly onto the rock, shrinkage seems to be the main cause of cracking. Whether the observed shrinkage cracking is due to plastic, early age or drying shrinkage is still under investigation.
- Measurements of macro porosity show that 10 to 20 % of the macro pores are open.
- Low permeabilities of less than $2 \times 10^{-14} \text{ ms}^{-1}$ are possible to achieve in uncracked sprayed concrete. Cracks and compaction voids cause higher permeabilities of sprayed concrete.

ACKNOWLEDGMENT

This paper/presentation is a part of the research project “Sprayed sUstainable PERmanent Robotized CONcrete tunnel lining (SUPERCON)” financed by the Research Council of Norway (project no. 294724), in cooperation with industrial partners Andersen Mek. Verksted, BASF, Bever Control, Bekaert, Elkem, Entreprenørservice, NORCEM, SWECO Norge, Veidekke, Wacker Chemicals Norway. Research partners in SUPERCON are NGI, NTNU and SINTEF. The following project owners support the project; Bane NOR, Nye Veier and the Norwegian Public Roads Administration.



REFERENCES

1. Jolin M, Melo F & Bissonnette B: “Concrete durability applied to sprayed concrete mixture design”. *Proceedings*, 7th International Symposium on Sprayed Concrete, Sandefjord, Norway, June 2014, pp. 233-244.
2. Jolin M, Burns D, Bissonnette B, Gagnon F & Bolduc L-S: “Understanding the pumpability of concrete”. *Proceedings*, Shotcrete for underground support XI, Davos, Switzerland, June 2009.
3. Bantia N, Trottier J-F & Beaupré D: “Steel fibre reinforced wet-mix shotcrete: comparisons with cast concrete”. *Journal of Materials in Civil Engineering*, Vol. 6, No. 3, 1994, pp. 430-437.
4. Beaupré N: “Rheology of high performance shotcrete”. PhD thesis, University of British Columbia, Department of Civil Engineering, Vancouver, Canada, 1994, 265 pp.
5. Mørtzell E: “The effect of the constituent materials on the rheology of fresh concrete”. PhD thesis, Norwegian University of Science and Technology, Department of Structural Engineering, Trondheim, Norway, 1996, 301 pp. (In Norwegian).

6. Banthia N: “Sprayed concrete (shotcrete)”, Chapter 4, “Developments in the Formulation and Reinforcement of Concrete” (edited by Mindess S), Woodhead Publishing Limited, Cambridge, UK, 2008, pp. 98-113.
7. Myren S, Hagelia P & Bjøntegaard Ø: “The ban of polymer fibre in FRSC in Norwegian road tunnels”. *Proceedings*, 8th International Symposium on Sprayed Concrete, Trondheim, Norway, June 2018, pp. 257-260.
8. Standard: EN 206, “Concrete – Specification, performance, production and conformity”, 2013.
9. “Bukte lavkarbon sprøyte-betong på bybaneprojekt” (Use of low-carbon sprayed concrete on an urban railway project). *Byggeindustrien* magazine, NR. 19 – 2019, p 96. (In Norwegian).
10. Tattersall & Banfill: “The Rheology of Fresh Concrete”, Pitman Books Ltd, London, UK, 1983.
11. Kaplan D, de Larrard F & Sedran T: “Avoidance of Blockages in Concrete Pumping Process”. *ACI Materials Journal*, May-June 2005, 102-M21, pp. 183-191.
12. Bartos P, Sonebi M & Tamimi A K: “Workability and rheology of fresh concrete: compendium of tests”, Report of RILEM technical committee TC145 WSM, RILEM Publications, 2002.
13. Standard: EN 12350-5, “Testing of fresh concrete – Part 5: Flow table test”, 2019.
14. Standard: EN 12350-2, “Testing of fresh concrete – Part 2: Slump test”, 2019.
15. Myrdal R: “Accelerating admixtures for concrete – state of the art”, SINTEF report, Trondheim, Norway, 2007.
16. Choi M, Roussel N, Kim Y & Kim J: “Lubrication layer properties during concrete pumping”. *Cement and Concrete Research*, Vol. 45, 2013, pp. 69-78.
17. Ginouse N & Jolin M: “Investigation of spray pattern in shotcrete applications”. *Construction and Building Materials*, Vol. 93, 2015, pp. 966-972.
18. Ginouse N, Jolin M & Bissonnette B: “Effect of equipment on spray velocity distribution in shotcrete applications”. *Construction and Building Materials*, Vol. 70, 2014, pp. 362-369.
19. Ginouse N & Jolin M: “Characterization of placement phenomenon in wet sprayed concrete”. *Proceedings*, 7th International Symposium on Sprayed Concrete, Sandefjord, Norway, June 2014, pp. 173-183.
20. Opsahl O A: “A study of a wet-process shotcreting method – Volume I”. Report BML 85.101, PhD thesis, Norwegian Institute of Technology, University of Trondheim, Division of Building Materials, Trondheim, Norway, 226 pp.
21. Reinhold M & Wetzig V: “Influence of air-flow at nozzle-distance on sprayed concrete properties”. *Proceedings*, 7th International Symposium on Sprayed Concrete, Sandefjord, Norway, June 2014, pp. 320-329.
22. Publication no. 7: “Sprayed Concrete for Rock Support”. Norwegian Concrete Association, Oslo, Norway, 2011.
23. Kauffman J, Frech K, Schuetz P & Münch: “Rebound and orientation of fibers in wet sprayed concrete applications”. *Construction and Building Materials*, Vol. 49, 2013, pp. 15-22.
24. Austin S, Goodier C & Robins P: “Low-volume wet-process sprayed concrete: pumping and spraying”. *Materials and Structures*, Vol- 38, 2005, pp. 229-237.
25. Standard: EN 14487-1, “Sprayed concrete – Part 1: Definitions, specifications and conformity”, 2012.
26. Neville AM: “Properties of Concrete”, 4th Edition, Longman Group Limited, Harlow, England, 1995.
27. Taylor H: “Cement Chemistry”, 2nd Edition, Thomas Telford Publishing, London, UK, 459 pp.

28. Salvador R, Cavalaro S, Segura I, Figueiredo A & Pérez J: “Early age hydration of cement pastes with alkaline and alkali-free accelerators for sprayed concrete”. *Construction and Building Materials*, Vol. 111, 2016, pp. 386–398.
29. Beck T: “Effect of fresh concrete temperature and temperature in surroundings on compressive strength development in sprayed concrete”. *Proceedings*, 7th International Symposium on Sprayed Concrete, Sandefjord, Norway, June 2014, pp. 50-55.
30. Cepuritis R: “Norbetong standard test method: determination of setting time for sprayed concrete containing accelerating admixture”, unpublished, 2009.
31. Standard: EN 196-1, “Methods of testing cement – Determination of strength”, 2016.
32. Shrader E & Kaden R: “Durability of shotcrete”. *Proceedings*, Concrete Durability International Conference, Volume 2, American Concrete Institute, Detroit, USA, 1987, pp. 1071-1101.
33. Holter: “Properties of waterproof sprayed concrete tunnel linings”. 197, PhD thesis, Norwegian University of Science and Technology, Department of Geology and Mineral Resources Engineering, Trondheim, Norway, 2015, 167 pp.
34. Bryne L E, Ansell A & Holmgren J: “Investigation of restrained shrinkage cracking in partially fixed shotcrete linings”. *Tunnelling and Underground Space Technology*, 42, 2014, pp. 136-143.
35. Menu B, Jolin M, Bissonnette B & Molez L: “Évaluation de la sensibilité à la fissuration des bétons projetés au jeune âge” (Assessment of the sensitivity to cracking of sprayed concrete at a young age). *Proceedings*, Conférence Internationale Francophone NoMaD 2018.
36. Punkki J & Sellevold E J: “Capillary suction in concrete: effects of drying procedure”. *Nordic Concrete Research*, Vol. 15, 1994, pp. 59-74.
37. Sellevold E J & Farstad T: “The PF-method – a simple way to estimate the w/c-ratio and air content of hardened concrete”. *Proceedings*, Construction materials: performance, innovations and structural implications, Vancouver, Canada, 2005, 10 pp.
38. Fonseca P C & Scherer G W: “An image analysis procedure to quantify the air void system of mortar and concrete”. *Materials and Structures*, Vol. 48, 2015, pp. 3087-3098.
39. ASTM Standard C457.C457M–11: Standard test method microscopical determination of parameters of the air-void system in hardened concrete, ASTM International, West Conshohocken, PA, 2003.
40. Garboczi E J, Snyder K A, Douglas J F & Thorpe M F: “Geometrical percolation threshold of overlapping ellipsoids”. *Physical Review E*, Vol. 52, No. 1, 1995, pp. 819-828.
41. Zhao Y, Wang X, Jiang J & Zhou L: “Characterisation of interconnectivity, size distribution and uniformity of air voids in porous asphalt concrete using X-ray CT scanning images”. *Construction and Building Materials*, Vol. 213, 2019, pp. 182-193.
42. Hodder K J, Izadi H, McDonald A G & Gerlich AP: “Fabrication of aluminium-alumina metal matrix composites via cold gas dynamic spraying at low pressure followed by friction stir processing”. *Materials Science & Engineering*, A 556, 2012, pp. 114-121.
43. Hagelia P: “Durability of sprayed concrete for rock support – a tale from the tunnels. *Proceedings*”. 8th International Symposium on Sprayed Concrete, Trondheim, Norway, June 2018, pp. 172-187.

Paper II

	
<p>© Article authors. This is an open access article distributed under the Creative Commons Attribution-NonCommercial-NoDerivs licens. (http://creativecommons.org/licenses/by-nc-nd/3.0/).</p>	<p>ISSN online 2545-2819 ISSN print 0800-6377</p>
<p>DOI: 10.2478/ncr-2022-0005</p>	<p>Received: April 7, 2022 Revision received: May 26, 2022 Accepted: May 30, 2022</p>

Effect of Set Accelerator on Properties of Wet Sprayed Concrete



Nicholas Trussell
MEng, CPEng, MIEAust, PhD Student
Norwegian University of Science and Technology,
Department of Structural Engineering,
Richard Birkelands vei 1A, 7034 Trondheim, Norway
E-mail: nicholas.h.trussell@ntnu.no



Rolands Cepuritis
Adjunct Associate Professor, PhD
Norwegian University of Science and Technology,
Department of Structural Engineering,
Richard Birkelands vei 1A, 7034 Trondheim, Norway
E-mail: rolands.cepuritis@ntnu.no



Stefan Jacobsen
Professor, PhD
Norwegian University of Science and Technology,
Department of Structural Engineering,
Richard Birkelands vei 1A, 7034 Trondheim, Norway
E-mail: stefan.jacobsen@ntnu.no

ABSTRACT

This paper describes sprayed concrete experiments varying the set accelerator dose. Literature on the hydration of cement with modern alkali-free set accelerators is reviewed and two full scale wet spraying experiments have been conducted, varying the dose of set accelerator in each. The effects on the properties of the hardening and hardened sprayed concrete were investigated by field and laboratory testing. Increasing the set accelerator dose was found to increase the rate of early age strength development but reduce density, long term strength and increase suction porosity of hardened sprayed concrete.

Key words: Sprayed concrete, shotcrete, accelerator, porosity.

1 INTRODUCTION

1.1. Background

Set accelerators are added to sprayed concrete at the nozzle immediately before spraying and increase the early age strength development of sprayed concrete. Studies [1–4] state that alkali-free sprayed concrete set accelerators increase the rate of the early-age strength development due to formation of hydrous calcium aluminium sulphates (mainly ettringite), which causes rapid increase in stiffness of the matrix (setting). The addition of set accelerator at the nozzle is essential for sprayed concrete used for tunnel linings as the rapid early age strength development allows concrete sprayed onto sidewalls and overhead to remain in place, rather than falling or flowing from the substrate. The set accelerator reduces the dormant period after the initial reaction during hydration [1].

Several authors [1,5,6,7,8] have reported that modern alkali-free set accelerators are mainly aluminium sulphate water solutions or slurries. Myrdal [5] reviewed well-known commercial alkali-free sprayed concrete accelerators on the market in Europe and North America, based on their Material Safety Data Sheets (MSDS), and demonstrated that modern, commercial, alkali-free set accelerators contain aluminium salts and almost all (probably all) contain aluminium sulphate. Although Myrdal [5] stated that the actual chemical composition of the commercial alkali-free accelerators are closely guarded trade secrets and therefore the precise chemical compositions are not published. Wang [8] reported that alkali-free accelerators can also contain fluoride salts, such as hydrogen or sodium fluoride, which increase the solubility of aluminium sulphate, as well as accelerate the setting of Portland cement. Furthermore Wang [8] reported that almost all alkali-free liquid accelerators contain alkanolamines, especially diethanolamine and triethanolamine, which both accelerate the hydration of Portland cement and increase the solubility of aluminium sulphate.

Many of the latest studies [1–4] on the effect of alkali-free accelerators on the hardening and hardened cementitious matrixes used accelerators that were composed of aluminium hydrosulphate solutions (aluminium sulphate solutions with different additions of aluminium hydroxide) with an addition of inorganic silicate or organic acid as the stabilisers. These admixtures had a pH of around 3.0 and an $\text{Al}_2\text{O}_3/\text{SO}_4^{2-}$ molar ratio of 0.33–0.74.

Higher alkali-free shotcrete accelerator doses are in the range of 6–8 % of the mass of cement or equivalent binder (further simply stated as dose %), or even exceeding 10 % [5,7]. The actual dose is varied depending on the concrete and binder composition, ambient environment [7] and geometry of the substrate. The dose can be varied to compensate for the changes in any of these conditions. However, the actual effect of the accelerator dose on the hardening and hardened properties of concrete has not been thoroughly explored and only a few papers on this subject have been published over the last few years. Furthermore, almost no publications are available that have also attempted to consider the actual full-scale spraying mechanisms in combination with the set accelerator dose.

Previous studies [1,2,3,4,6,8,9] have shown that the use of the alkali-free accelerators increases the rate of the early-age strength development due to formation of hydrous calcium aluminium sulphates (mainly ettringite), which causes rapid increase in stiffness of the matrix (setting). Each mole of ettringite contains 32 moles of water [10]. Ettringite formation and chemical binding of water thus increase the solid/liquid ratio and the viscosity of the cement paste, leading to setting of the cement. Wang [8] reported that the needle-like ettringite crystals connect to form a reticular

structure, which also causes setting. Tan [11] mixed C_3S pastes with aluminium sulphate and found that CSH and ettringite coexist at ages 2 hours to 28 days.

It has also been demonstrated [1,2,3,4,6] that the compatibility between the cement type and the alkali-free accelerator plays a major role in the hydration kinetics and mechanical strength evolution. This is mainly with respect to the final C_3A/SO_3 molar ratio that is calculated considering the sulphate remaining after the accelerator reaction and the initial C_3A content of a cement. The initial strength and setting determined by needle penetration resistance testing (up to 3–4 hours of sprayed concrete age) will mainly depend on the accelerator reactivity. A high Al^{3+} content incorporated into cement matrices will result in exothermic ettringite formation, providing fast setting and elevated early strength gain. The strength gain after 3–4 hours (typically measured by the stud driving or pin penetration testing) will not depend solely on the porosity of the obtained matrix, but also on the final C_3A/SO_3 molar ratio. This is because when the system is under-sulphated (high final C_3A/SO_3 molar ratio), accelerated C_3A reactions occur before or during the acceleration period of the silicate reactions, filling the pores of the matrix and reducing solubility of the main cement phases. Consequently the accelerator decreases the extent and rate of alite hydration and leads to lower degrees of hydration and strength gain at lower ages. This explains a lower strength development after the initial 4 hours when high (about 8–10 %) alkali-free accelerator doses are used.

A low dose (typically at around 2 %) is known from practice to cause retardation of the sprayed concrete [7]. This has been explained experimentally by [9], who showed that a low dose, a small extra amount of Al^{3+} and SO_4^{2-} are supplied to the pore solution, leading to a further thin layer of ettringite forming on the surface of the cement particles. This thin layer can slow the hydration of cement pastes, causing a retarded setting compared to samples without accelerator.

The above mechanisms also suggest that the availability of the sulphate ions in the solution of the fresh cementitious matrix is important. This has been verified by [1,9], who demonstrated that these mechanisms of alkali-free accelerator effect in a cementitious matrix depend on the type of set regulator in a cement. It has been found [1,9] that calcium sulphate hemihydrate saturates the mixing water faster with calcium and sulphate ions (as it has a higher solubility than gypsum) and thus leads to a faster sulphate ion reactivity and faster precipitation of the hydrous aluminium sulphates.

The addition of set accelerators changes the microstructure of the concrete [8]. When large ettringite amounts are formed, the matrix stiffens quickly due to increase in solid/liquid ratio leading to improper consolidating and air entrapment [4]. Salvador [4] reported that the “water accessible porosity”, which we interpret as the suction porosity, increases in accelerated matrices and the compressive strength reduces. Han [12] reported that a 6 % dose of aluminium sulphate decreased the volume of 5–30 nm pores but increased the volume of 30–100 nm pores at 24 hour age, indicating a coarser capillary pore structure, with a similar conclusion at 28 days.

It has been demonstrated by [4] that from a certain time the accelerated mix compressive strength is always lower than that of a reference mix without alkali-free set accelerator. The faster the setting time (more reactive accelerator or higher dose), the lower the compressive strength from 1 day on.

Salvador [3] investigated the influence of the spraying process on the hydration of cement pastes with alkali-free accelerators and demonstrated that the mixing procedure significantly influences the microstructure of the matrix. They determined that the aluminate hydrates are more evenly

distributed throughout the whole matrix in sprayed pastes. Furthermore, ettringite is found in a disarranged microstructure and is composed by shorter, irregular, and dispersed needle-like crystals. Salvador [3] accordingly recommended preparing pastes by spraying in contrast to simple hand-mixing in order to obtain a more representative microstructure of the resulting hardened cementitious matrix.

The suction porosity of hardened wet sprayed concrete in tunnel linings was investigated by Holter [13] by systematic measurements on 234 slices sawn from drilled cores taken from four different tunnels after 150–1100 days. Suction porosity measurements on the concretes with $w/b = 0.45$, 0.44, 0.46 and 0.47 were compared to theoretical values calculated with Power's model [14]. Holter [13] stated that mix designs, including w/b ratio, were corrected for water content of the set accelerator. The comparison to Power's model indicated degrees of hydration of 65 %.

Myren & Bjøntegaard [15] measured the suction porosity of sprayed concrete samples with w/b ratio of 0.42 and set accelerator dose of 6 % of binder mass. The sprayed panels were cured in air then cores were taken, which were cured in water and tested at 400 days age. Again, Power's model [14] was used to calculate theoretical values of suction porosity, and an assumed 80 % degree of hydration gave similar suction porosity values to those measured by capillary suction and PF (pore fraction) tests.

1.2 Scope

This paper attempts to connect the previous detailed laboratory studies, which have been mainly done on paste and mortar samples with the actual sprayed concrete process by describing two full scale wet spraying experiments and presenting results from these experiments. The set accelerator dose added at the nozzle was varied in both spraying experiments. The properties of the hardening and hardened sprayed concrete from full scale wet spraying experiments that are investigated are early age strength development, density, compressive strength, porosity and capillary absorption.

2 EXPERIMENTAL WORK

2.1 Spraying experiments

Two full scale wet spraying experiments were carried out at separate locations with different equipment, teams and ready mixed concrete suppliers. The details of the two full scale wet spraying experiments are given in Table 1.

Table 1 – Details of two full scale wet spraying experiments

Location	AMV, Flekkefjord	NTNU, Trondheim
Dates	18 th February 2020	16 th June 2020
Spraying machine	AMV 7450 shotcrete robot	Normet Spraymec NorRunner 140 DVC shotcrete robot
Concrete pump	Olin pump	Normet pump
Hose diameter	75 mm	75 mm
Nozzle diameter	40 mm	40 mm
Concrete flow rate	10 m ³ /hr	14 m ³ /hr
Accelerator type	Master Builders Masterroc SA 188	Master Builders Masterroc SA 168
Accelerator dose	Varied 0, 3, 6 and 10% of binder mass	Varied 3.5 and 7% of binder mass
Distance nozzle to substrate and angle	2.0 m Perpendicular to the panel	1.5 m Perpendicular to the panel
Curing and coring	Wrapped in plastic before coring. Cored 13 th March 2020 Ø 75 mm, h 150 mm for strength and density tests. Cured in water until compressive strength testing. Ø 100 mm for capillary suction, PF and image analysis tests. Cured in air before oven drying.	Wrapped in plastic before coring. 1 st – 2 nd July 2020 Ø 75 mm, h 150 mm for strength and density tests. Cured in water until compressive strength testing. Ø 100 mm for capillary suction, PF and image analysis tests. Cured in water before oven drying.

Concrete constituents, proportioning and placed concrete composition

The concrete proportioning for the Flekkefjord spraying experiment is shown in Table 2. This mix represents a typical sprayed concrete mix currently used for sprayed concrete tunnel linings in Norway. The slump test immediately after batching was 220 mm. The placed concrete composition was corrected for the addition of set accelerator (at the nozzle) and equating compaction voids, measured by image analysis, to air content following [16].

Table 2 – Fresh concrete composition and placed concrete composition (for sample with 10 % accelerator added) from set accelerator spraying experiment in Flekkefjord

Phase	Constituent	Mass [kg/m ³]	Volume [l/m ³]	Volume [l/m ³]	Placed concrete composition* [kg per m ³ concrete after spraying] for 10 % set accelerator dose
Matrix phase	Standard fly ash cement	462	156		444
	Water	206	206		221
	Silica fume	19.2	8,7		18.5
	Super plasticiser	4.8	4,6		4.6
	Air entrainment agent	0.45	0,45	424	0.43
	Set accelerator (dry)	-	-		25.0
	0 – 8 mm aggregate (< 0.125 mm)	21.8	8,3		21.0
	Air		40*		Volume = 55.5 litres **
Particle phase	0 – 8 mm aggregate (> 0.125 mm)	1505,8	570,4	576	1448
	Steel fibres	45	5,6		43.3
SUM		2304.8			2225.1

* Assumed air content for batching.

** Typical measured value for macro porosity of hardened specimens, see Table 6.

The binder was standard fly ash cement, with density 2990 kg/m³, and microsilica with density 2200 kg/m³. The aggregate was granitic sand (crushed) with a particle density of 2645 kg/m³ and a water absorption of 0.46 % by mass. The effective water/binder ratio of the mix was 0.42. But with set accelerator added to the mix at the nozzle the water/binder ratio of the placed concrete

changed. The additional water content Δw was calculated for the concrete proportioned in Table 2 after addition of the varying doses of set accelerator. The set accelerator used had a water content of 0.48 and solids content of 0.52 by mass [17]. A placed concrete composition, which is calculated for the 10 % set accelerator and corrected for compaction porosity, is shown in the column on the right of Table 2.

Table 3 – Particle size distribution and density of aggregate of the Flekkeford mix

Sieve size (mm)	32	16	11.2	8	4	2	1	0.5	0.25	0.125	0.063
% passing	100	100	100	98	82	72	53	25	8	2	1

$$\Delta w = \text{accelerator dose} \times \text{accelerator water content} \times (m_c + k m_s)$$

$$\text{New } m_w / (m_c + k m_s) = (206 + \Delta w) / 500$$

0 % accelerator

$$m_w / (m_c + k m_s) = 206 / 500 = 0.419$$

3 % accelerator

$$\Delta w = 0.03 \times 0.48 \times (500) = 7.2 \text{ kg}$$

$$m_w / (m_c + k m_s) = (206 + \Delta w) / 500 = 0.434$$

6 % accelerator

$$\Delta w = 0.06 \times 0.48 \times (500) = 14.4 \text{ kg}$$

$$m_w / (m_c + k m_s) = (206 + \Delta w) / 500 = 0.448$$

10 % accelerator

$$\Delta w = 0.10 \times 0.48 \times (500) = 24.0 \text{ kg}$$

$$m_w / (m_c + k m_s) = (206 + \Delta w) / 500 = 0.467$$

where m_c mass of cement
 m_s mass of silica fume
 w mass of water
 k k factor for equivalent w/m_c ratio

The concrete proportioning for the Trondheim set accelerator experiment is detailed in Table 4. Again this mix was intended to represent a typical mix for sprayed concrete, but in this case steel fibres were omitted from the mix. The slump test before spraying was 220 mm. The placed concrete composition for the addition of 7 % set accelerator by binder mass and corrected for compaction porosity is shown in the right column of Table 4.

Table 4 – Fresh concrete composition and placed concrete composition (with 7 % accelerator added) from set accelerator spraying experiment in Trondheim

Phase	Constituent	Mass [kg/m ³]	Volume [l/m ³]	Volume [l/m ³]	Placed concrete composition* [kg per m ³ concrete after spraying]
Matrix phase	Standard fly ash cement	433	145		424
	Water	214	214		226
	Microsilica	43	19.5		42.0
	Retarder	0.4	0.36		0.4
	Super plasticiser	3.7	3.5		3.6
	Air entrainment agent	0.6	0.6		0.6
	Set accelerator (dry)	-	-	477	21.5
	0 – 4 mm aggregate (<0.125 mm)	22	7.2		21.2
	0 – 8 mm aggregate (<0.125 mm)	129	47.3		126
Air		40*		Volume = 45.5 litres **	
Particle phase	0 – 4 mm aggregate	153	50.5		150
	0 – 8 mm aggregate	1284	472	523	1256
	Steel fibres	-	-		-
SUM		2282.7			2268.9

* Assumed air content for batching.

** Typical measured value for macro porosity of hardened specimens, see Table 6.

Table 5 – Particle size distribution of aggregate of the Trondheim mix

Sieve size, mm	32	16	11.2	8	4	2	1	0.5	0.25	0.125	0.063
0/8 aggregate % passing	100	100	100	98.2	84.5	70.6	55.2	39.2	22.3	9.1	2.3
0/4 aggregate % passing	100	100	100	99.8	89.2	58.9	38.4	26.2	18.0	12.4	8.1

The binder was standard fly ash cement, with density 2990 kg/m³, and microsilica with density 2200 kg/m³. The sand 0/4 mm was crushed gabbro rock with a particle density of 3030 kg/m³ and a water absorption of 0.5 % by mass. The 0/8 mm sand was natural fluvial glacial deposits with mainly granitic gneiss and some sandstone and mafic rock with a particle density of 2720 kg/m³ and 0.7 % water absorption by mass. The effective water/binder ratio of this mix was 0.42. The additional water content Δw was calculated for the concrete proportioned in Table 4 after additional of the varying doses of set accelerator. The accelerator used had a water content of 0.425 and solids content of 0.575 [18].

$$\Delta w = \text{accelerator dose} \times \text{accelerator water content} \times (m_c + k.m_s)$$

$$\text{New } m_w/(m_c+k.m_s) = (214 + \Delta w)/519.1$$

0 % accelerator

$$m_w/(m_c+k.m_s) = 214/519.1 = 0.418$$

$$m_w/(m_c+k.m_s) = (214 + \Delta w)/519.1 = 0.433$$

7 % accelerator

$$\Delta w = 0.07 \times 0.48 \times (519.1) = 15.44 \text{ kg}$$

$$m_w/(m_c+k.m_s) = (214 + \Delta w)/500 = 0.448$$

3.5 % accelerator

$$\Delta w = 0.035 \times 0.48 \times (519.1) = 7.72 \text{ kg}$$

One batch of concrete was used for each of the Flekkefjord and the Trondheim experiments.

Set accelerator

In the Flekkefjord spraying experiments the accelerator dose by effective binder mass was varied, and the different doses were 0, 3, 6 and 10 %. Concrete mixes with all four doses were sprayed. However the concrete intended to be sprayed with 6% accelerator did not behave as expected and likely contained zero accelerator – a blockage was discovered in the accelerator line immediately after spraying. This panel showed early strength development equal to the panel sprayed with 0 % accelerator and this result is marked with * in each case.

In the Trondheim spraying experiments the accelerator dose by effective binder mass was varied, and the different doses were 0, 3.5 and 7 %. Concrete was sprayed with 3.5 % and 7 % set accelerator, whilst the concrete with zero accelerator was cast by pumping the concrete through the nozzle, adding neither compressed air nor set accelerator.

Spray application

For the experiments in Flekkefjord concrete was sprayed into 600 mm diameter and 100 mm deep moulds with a plywood base and steel sides. The moulds were placed horizontally on the floor so that the unaccelerated sprayed concrete would not flow during/after spraying. The nozzle was perpendicular to the mould and 2 m away when spraying, as shown in Figure 1.

For the experiments in Trondheim concrete was sprayed in 1 m × 1 m wooden panels of 150 mm depth and slanted sides in accordance with EN 14488-1 [19]. The panels were placed at 60° from

the horizontal. The concrete was sprayed with the nozzle at 1.5 m distance and perpendicular to the mould, as shown in Figure 2.

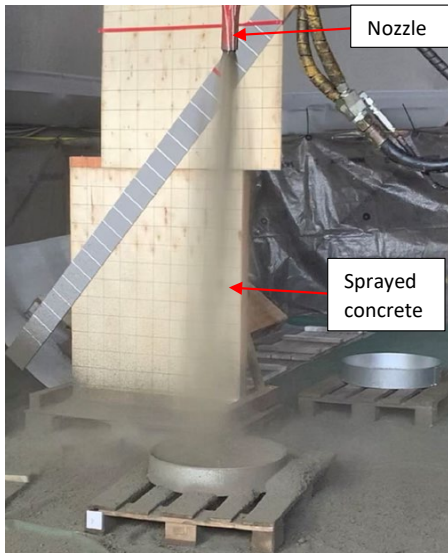


Figure 1 – Spraying set up for Flekkefjord spraying experiments.

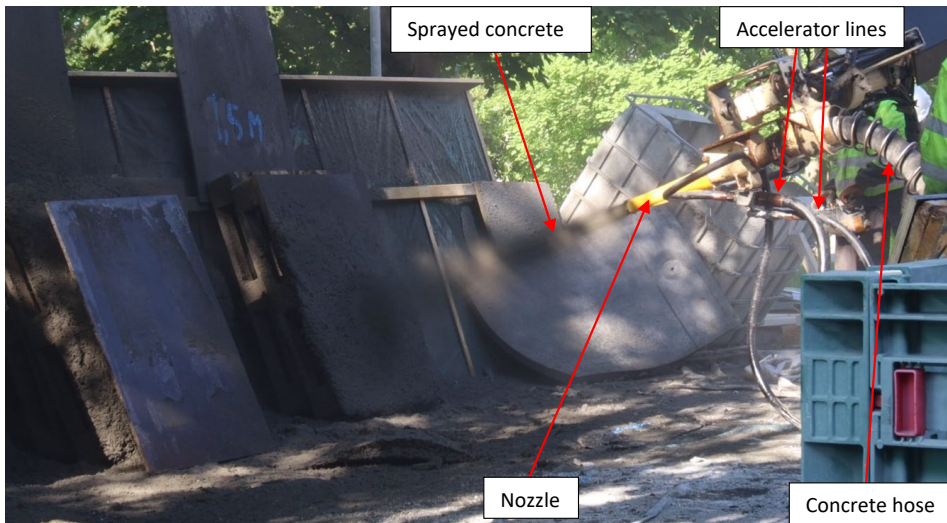


Figure 2 – Spraying set up for Trondheim spraying experiments.

2.2 Laboratory testing

Strength

The early age strength development of the sprayed concrete was tested in accordance with EN 14487-1 [20] and EN 14488-2 [21]. The penetration needle was used up to a compressive strength of 1 MPa and above that the stud driving method was used until 24 hours after spraying. The

penetrometer needle method measures the force required to drive a needle of 3 mm diameter into the concrete to a depth of 15 mm [21]. For the stud driving method a stud is percussively fired into the concrete and the penetration depth measured. The stud is then extracted and the pull-out force measured. The ratio of pull-out force to penetration depth is used to determine the compressive strength [21].

Three parallel cores of 75 mm diameter and height 150 mm were drilled through the full thickness of the panels and tested for compressive strength in accordance with EN 12390-3 [22] at 28 days after spraying. The panels were wrapped in plastic before coring. The cores for density and compressive strength were cured in water before testing. The Flekkefjord cores for capillary suction and PF test were cured in air before oven drying, while the Trondheim cores for these tests were cured in water before oven drying.

Density

Cores were weighed in air and then in water to determine the density immediately before compression strength testing. Furthermore the PF test (Section 2.2.4) also gives density results for individual discs.

Capillary suction

The capillary suction test was undertaken on the sprayed concrete samples following [23] and [24]. Discs of 100 mm diameter and 25 mm thickness were cut and dried at 105 °C for 48 hours before testing. The mass of each sample after drying was recorded as w_1 .

The discs were then placed on a perforated metal tray with a depth of 1 mm of the disc immersed in the water. The capillary suction causes water to be drawn into the concrete and there is an increase of mass from this absorbed water. The relationship between mass increase and square route of time is normally linear [24] and the capillary number of the concrete is determined by the gradient of the mass increase against square route of time. After immersion in 1 mm of water the samples were weighed at regular intervals over the first four days. The experiment determines the capillary and resistance numbers.

$$K_{\text{cap}} = \frac{G(t)}{\sqrt{t}} \quad (1)$$

where K_{cap} is the capillary number, and $G(t)$ is absorption (kg/m^2) at time t (seconds)

The resistance number m is given by t_{cap} , which is the time for the water front rising in the specimen to reach the top of the specimen of thickness h . t_{cap} is the point of inflection on the absorption vs square route of time plot.

$$m = \frac{t_{\text{cap}}}{h^2} \quad (2)$$

A lid was placed over the samples to reduce evaporation. The mass after four days of capillary suction and before submersion is recorded as $w_{1.5}$. The sum of gel and capillary porosity, equal to the suction porosity, is calculated as:

$$\varepsilon_{\text{suction}} = \frac{w_{1.5} - w_1}{v} \quad (3)$$

where v is volume measured by weighing in air and in water. $\varepsilon_{\text{suction}}$ can then be used for comparison with total porosity (equal to capillary plus gel porosity) in Power's model after correction for paste volume fraction in the concrete [14].

PF (pore fraction) test

Following the capillary suction test the same samples were submerged completely under water at atmospheric pressure for four days. The additional uptake from unilateral to complete submersion is considered to fill the open macro pores. The mass after atmospheric (unpressurised) submersion is recorded as w_2 . The samples were then submerged under a pressure of 5 MPa for 48 hours to fill the closed macro pores. The mass after pressurised submersion is recorded as w_3 [14].

The total porosity is calculated by:

$$\varepsilon_{\text{total}} = \frac{w_3 - w_1}{v} \quad (4)$$

The open macro porosity is calculated by:

$$\varepsilon_{\text{open macro}} = \frac{w_2 - w_{1.5}}{v} \quad (5)$$

And the closed macro porosity, or air voids, is calculated by:

$$\varepsilon_{\text{closed macro}} = \frac{w_3 - w_2}{v} \quad (6)$$

Image analysis

The macro porosity was measured by black and white image analysis [25]. A core from each sprayed panel was cut in half lengthways to make two samples and the flat surface of each sample was polished. A Tegamin 30 apparatus was used and the samples were polished using resin bonded, diamond surfaced discs of:

1. Vickers hardness 220, grain size 75 μm ,
2. Vickers hardness 600, grain size 30 μm ,
3. Vickers hardness 1200, grain size 15 μm .

The polished surface was then coloured black using marker pen, and then the macro pores were filled with white sulphate nitrate powder of particle size 1–4 μm . An example is shown in Figure 3(a). The samples were then scanned at a resolution of 2400 pixels per inch. A Matlab script was used to calculate the ratio of white and hence the macro porosity of each specimen.

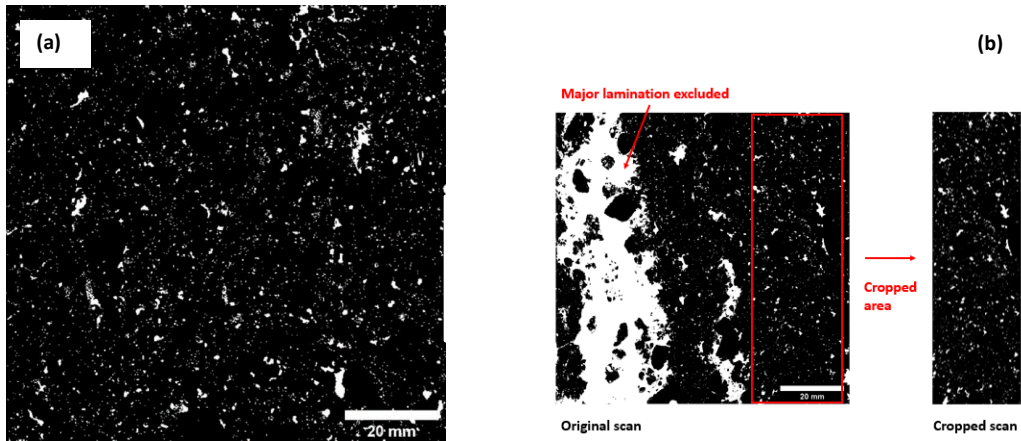


Figure 3 – Scanned black and white image of sample sprayed with: (a) 7 % set accelerator (Trondheim series); (b) 10 % set accelerator (Flekkefjord series), with major lamination was considered not representative of the bulk material and was removed by cropping.

Major imperfections were cropped out of the image analysis. For example the concrete sprayed with 10 % set accelerator in Flekkefjord contained a major lamination normal to the spraying direction, several tens of millimetres wide, due to pulsation of the flow at the nozzle where accelerator was added at a steady flow, and this is omitted from the image analysis, as shown in Figure 3(b).

3 RESULTS AND DISCUSSION

3.1 Early age strength development

The early age strength development of the Trondheim set accelerator experiments is shown in Figure 4, which shows the higher set accelerator dose with a faster strength development. The J1, J2 and J3 curves in Figure 4 are standard strength development curves that are defined in [20] and these define the strength class of the sprayed concrete.

Furthermore Figure 4 also gives a comparison of three different measurement methods of early age strength: penetrometer, stud driving and compressive testing of drilled cores. Both the penetrometer and stud driving method measurements were taken at 2.5 hours for the concrete sprayed with 7 % set accelerator, with a difference of 0.5 MPa between the readings. For the same specimen the stud driving method was used at 9 hours, with a result of 9.3 MPa, and a core was tested in compression at 8.5 hours after spraying, with the strength measured at 12 MPa. Furthermore a core was tested in compression at 30.5 hours after spraying with the strength measured at 20 MPa, and this can be compared to a compressive strength of 17.6 MPa measured at 26 hours after spraying with the stud driving method. The penetrometer and stud driving methods indicate a clear acceleration of strength the first 6 hours and then the stud driving method and the compressive strength of cores indicate same strength class after 9 hours.

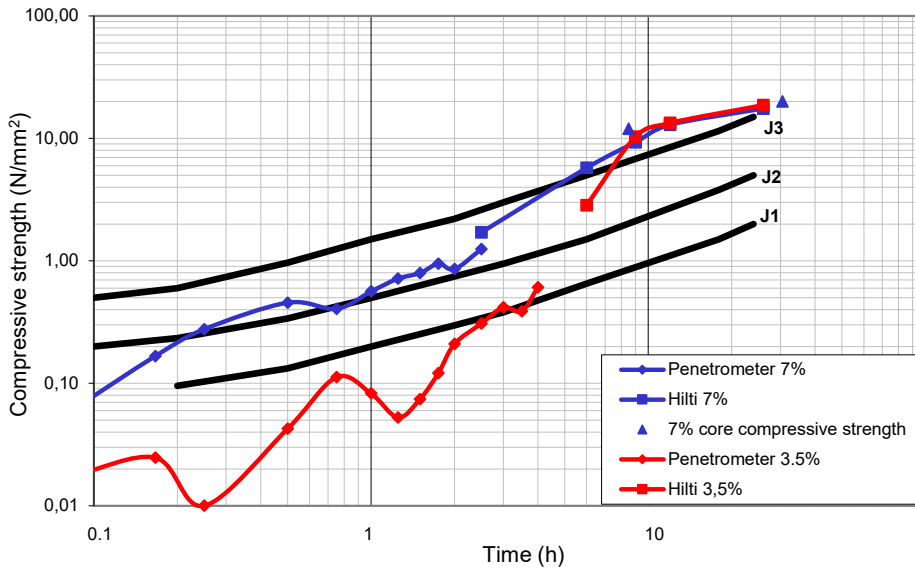


Figure 4 – Early age strength development of samples sprayed in set accelerator experiment in Trondheim.

3.2 Density and strength

The relationship between density and compressive strength for individual specimens from both the Flekkefjord and Trondheim series is plotted in Figure 5. This graph shows that there is a clear relationship between bulk density and compressive strength – higher density causes higher compressive strength. This is as we would expect since bulk density, ρ_{bulk} , scales linearly to total porosity ε_{tot} as $\varepsilon_{\text{tot}} = 1 - (\rho_{\text{bulk}} / \rho_{\text{solid}})$ where ρ_{solid} is the density of pore free concrete material and porosity is the key to concrete strength. Furthermore Figure 5 shows that higher doses of set accelerator give a lower density of sprayed concrete, and hence a lower compressive strength.

The measured density values for the cast Trondheim samples are in fairly good agreement with the sum of mass calculated in Table 4 (2283 kg/m³) and after correction for the addition of 7 % accelerator given that the moisture content of the cylinders for strength measurements had first dropped during air curing of the panels and then increased after coring and 3 days water storage before testing.

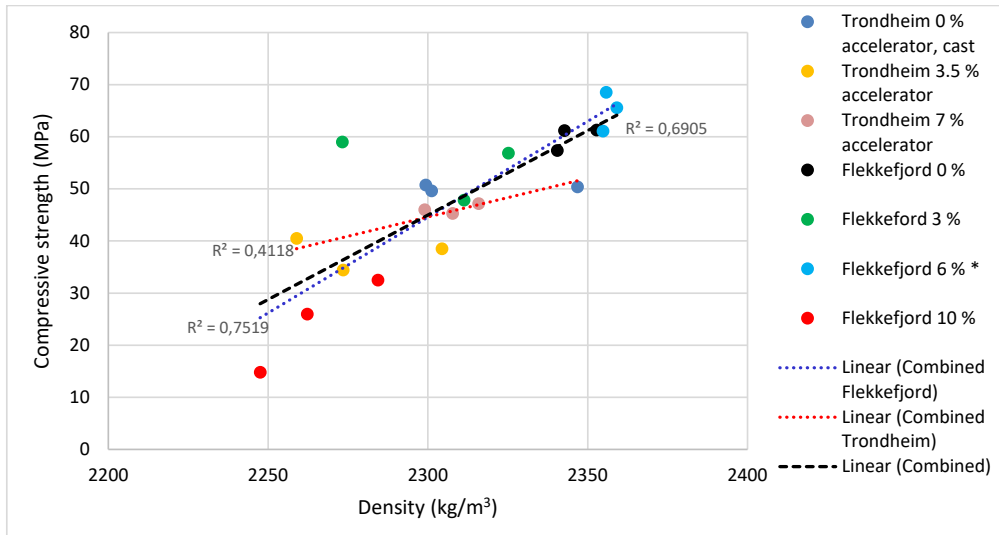


Figure 5 – Combined plot of compressive strength at 28 days against density results from Flekkefjord and Trondheim (individual cylindrical specimens).

3.3 Porosity

The porosity of the samples measured by the PF test are shown in Table 6. There is a higher suction porosity values of the samples with higher doses of set accelerator. The capillary numbers in Table 6 are calculated as the gradient capillary absorption graphs during the initial phase of absorption [24], as defined by Eq. 1, and these are calculated from the capillary suction graphs included in Figures 7 and 8. The results show increasing capillary numbers and higher total volume of water absorption for the higher accelerator doses.

The capillary number is sensitive to the paste volume fraction of the concrete, which can vary in sprayed concrete due to rebound of the particle phase [26], whereas the resistance number, defined by Eq. 2, does not depend on the paste volume.

A graph of compressive strength against total porosity for samples from all the spraying experiments is presented in Figure 6(a). This shows a notable relationship, with decreasing compressive strength with increasing total porosity. Figure 6(b) shows a graph of compressive strength against macro porosity, but no relationship is evident. Figure 6(c) shows a graph of compressive strength against suction porosity, which shows the trend of decreasing compressive strength with increasing suction porosity, although with slightly weaker correlation than for total porosity vs strength. A graph of compressive strength against capillary number is shown in Figure 6(d), and no relationship is evident.

The relationship of decreasing strength with increasing total porosity is as we would expect – Neville [27] reported that a 2 % increase in void ratio (i.e. macro porosity) can decrease the compressive strength by 10 %. It is interesting that the relationship of decreasing strength is with the suction porosity, and even stronger with total porosity, rather than the macro porosity of the sprayed concrete, and this warrants further studies of the suction and microporosity of sprayed concrete. Perhaps the nature of the macro pores and the suction pores in sprayed concrete are

different from those of conventionally cast concrete in terms of the size and type of pores that fill under suction and under pressure saturation in the PF test.

Table 6 – Capillary numbers, resistance numbers and porosity results from capillary suction and PF tests (individual specimens) and macro porosity from image analysis

Sample	Capillary suction and PF test						Image analysis
	K_{cap} Eq.(1) Capillary number ($kg/m^2 \cdot s^{0.5}$)	m Eq.(2) Resistance number (s/m^2)	Total porosity Volume %	Suction porosity Volume %	Open macro porosity Volume %	Closed macro porosity Volume %	Macro porosity Volume %
Flekkefjord	0.012	1.30×10^8	18.4	14.6	0.4	3.7	4.4
0%	0.012	1.21×10^8	18.3	14.5	0.4	3.7	5.3
Flekkefjord	0.018	7.74×10^7	20.5	16.4	0.7	4.1	4.7
3%	0.018	7.06×10^7	20.4	15.8	0.5	4.7	4.5
Flekkefjord	0.015	10.8×10^7	19.2	15.4	0.4	3.8	4.4
6% *	0.015	9.60×10^7	18.1	14.7	0.3	3.4	4.0
Flekkefjord	0.055	2.88×10^7	26.5	22.7	0.6	3.8	5.3
10%	0.046	3.46×10^7	25.8	22.1	0.7	3.7	5.8
Trondheim	0.011	2.76×10^7	22.3	17.9	0.3	4.3	6.3
zero	0.013		22.7	18.2	0.3	4.5	6.1
accelerator – cast		2.76×10^7					
Trondheim	0.013	2.76×10^7	21.8	18.1	0.5	3.7	3.1
3.5%	0.009		22.5	17.7	0.6	4.9	4.7
accelerator		4.15×10^7					
Trondheim	0.017	2.76×10^7	24.5	20.5	0.5	4.0	4.4
7%	0.016		23.8	20.1	0.6	3.8	4.7
accelerator		2.76×10^7					

* actually zero percent accelerator.

Furthermore, with the increasing suction porosity with accelerator dose (Table 6) there is a trend of decreasing strength with increasing set accelerator dose. This is apparent in the density against strength plot Figure 5, with higher porosity (and hence lower density) from higher set accelerator dose resulting in lower strength. This is as we would expect, for instance Opsahl [28] reported strength loss up to 50 % with a 12 % dose of (alkaline) accelerator. The mechanisms could perhaps be a mixture of increased w/c , different hydration products and how the macro-pores are formed during the spraying process.

As discussed with Figure 4, a higher dose of set accelerator increases the rate of early strength development of sprayed concrete. This agrees with the early strength gain found by [1,2,3,4,6,9] discussed in Section 1. But an excessive dose of set accelerator can have a detrimental effect on long term strength. Figure 4 shows that the early age strength development of the concrete with 3.5% set accelerator dose overtakes that with 7% dose at around 10–12 hours after spraying.

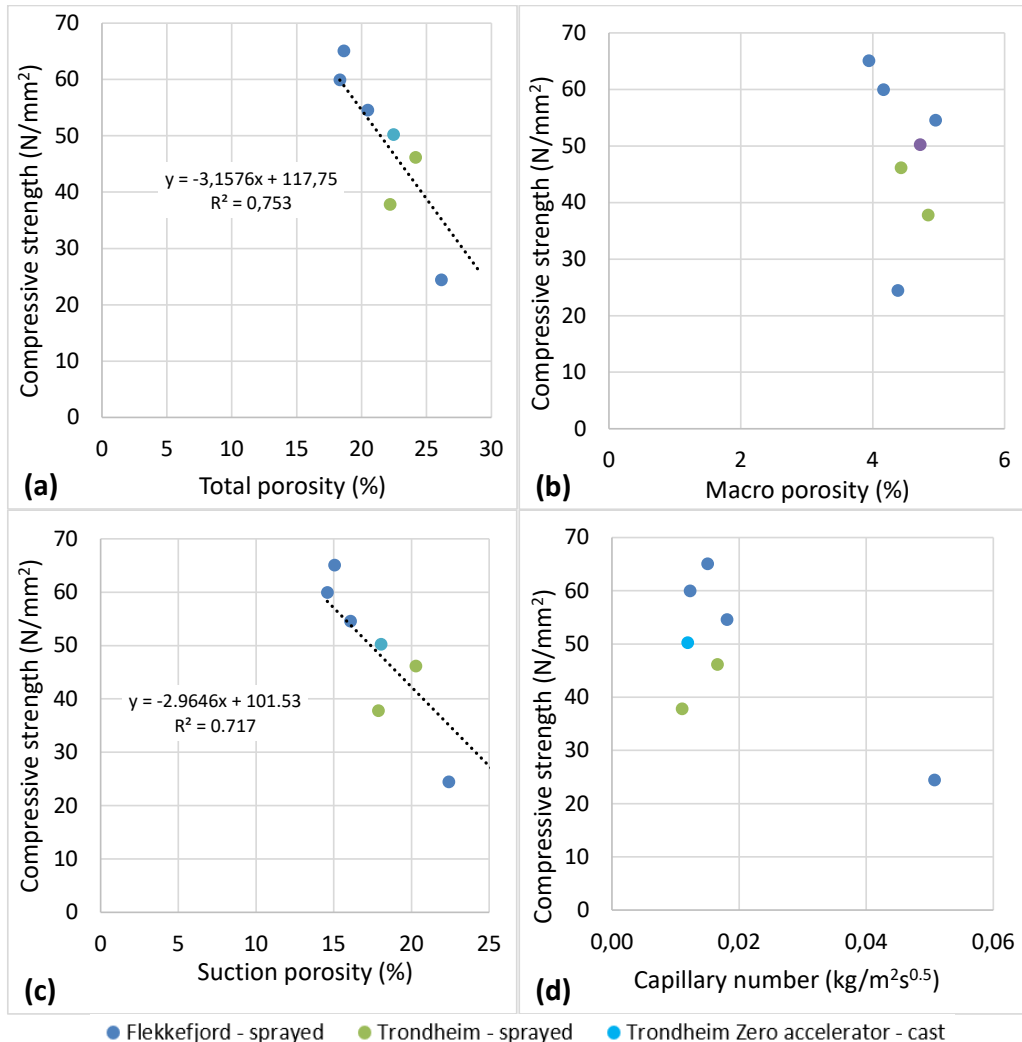


Figure 6 – Compressive strength (mean value for cores from each panel) against: (a) total porosity (mean value for cores from each panel); (b) macro porosity (mean value for cores from each panel); (c) suction porosity (mean value for cores from each panel); (d) capillary number (mean value for cores from each panel).

The samples of higher accelerator doses exhibited a higher total porosity than the zero and lower accelerator doses, as shown in Table 6. The values for macro porosity are similar, albeit with a degree of scatter. The difference between the higher accelerator doses and the lower and zero doses is the effect on suction porosity. The difference in suction porosity could be for two reasons:

- The set accelerator has a water content of 0.4–0.5 so adding set accelerator at the nozzle increases the water/binder ratio of the placed concrete as discussed in Section 2.1.1.
- The effect on hydration of the set accelerator is “freezing” the hydration at a low degree and/or altering the hydration products, in line with Salvador [1–4].

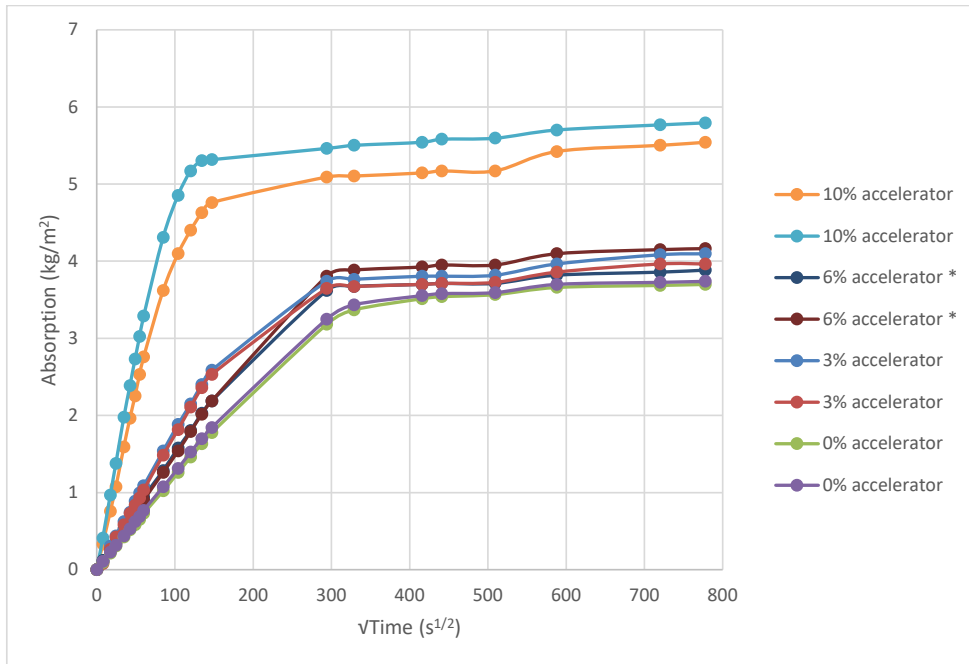


Figure 7 – Capillary suction curves for samples from Flekkefjord spraying experiments.

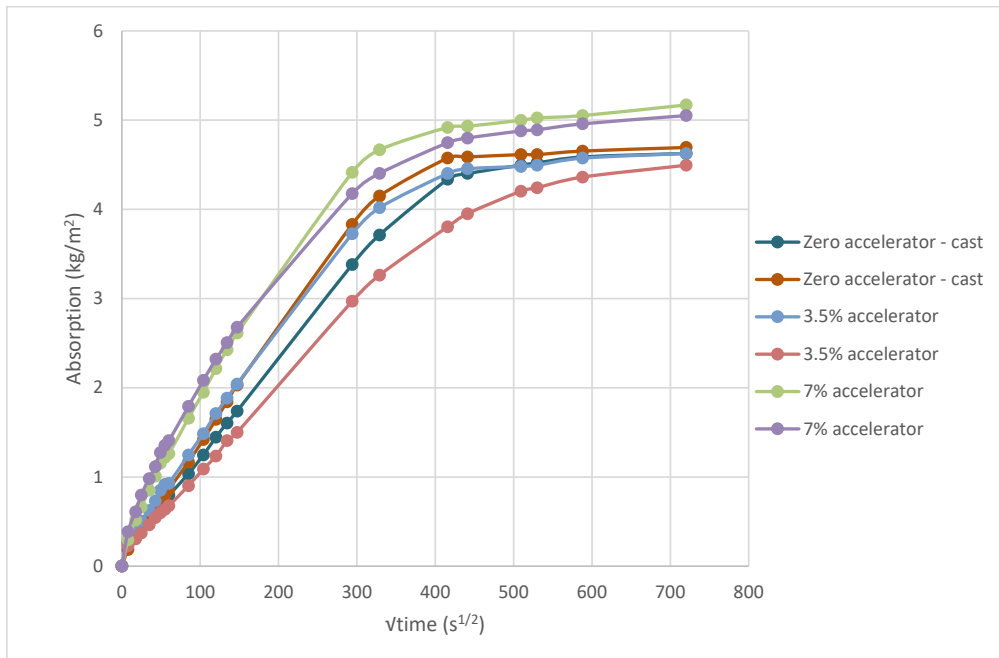


Figure 8 – Capillary suction curves for samples from Trondheim spraying experiments.

We can use Power’s equation linking suction porosity, w/b ratio and degree of hydration to calculate the expected increase of suction porosity due to the increased w/b ratio only. Eq. 7 is a modified Power’s equation [14,29].

$$\varepsilon_{\text{suction}} = \frac{\frac{w}{c} - 0.172\alpha + 0.116\frac{s}{c}\alpha_s}{\frac{w}{c} + 0.333 + \frac{1}{2.2c}} V_p \quad (7)$$

where	$\varepsilon_{\text{suction}}$	suction porosity
	w/c	mass of water / mass of cement
	α	degree of hydration of cement
	s/c	mass of microsilica / mass of cement
	α_s	degree of hydration of microsilica
	V_p	volume fraction of paste.

Calculating $\Delta\varepsilon_{\text{suction}}$ using the w/b ratios of the sprayed concrete with 7 % set accelerator by equivalent binder mass versus that with zero set accelerator, the theoretical $\Delta\varepsilon_{\text{suction}}$ is 1 %. Whereas there is a measured difference of 2.3 % between suction porosity of the Trondheim samples with 7 % set accelerator and those with zero set accelerator. Likewise there is a measured difference of 7.8 % between suction porosity of the Flekkefjord samples with 10 % set accelerator and those with zero set accelerator, whereas there is a theoretical $\Delta\varepsilon_{\text{suction}}$ of 1.2 % between these samples.

Therefore the increased suction porosity is not only due the increased water content from the set accelerator added at the nozzle. There must be a “freezing effect” of the set accelerator on the hydration as well. This is consistent with [5], who used the notion that the water accessible porosity of the mortars increases in accelerated matrices and compressive strength reduces. This could be due to the matrix stiffening quickly due to the increase in solid/liquid ratio when large amounts of ettringite form, leading to improper consolidating and air entrapment [5].

Eq. 7 can be rearranged to solve for degree of cement hydration, giving Eq. 8. Calculated degree of hydration values are shown in Table 7, using calculated w/c from the concrete compositions in Section 2.1.1. The degree of hydration of the microsilica, α_s , is assumed to be 1.0.

$$\alpha = \frac{1}{0.172} \frac{w}{c} + \frac{0.116\alpha_s s}{0.172 c} - \frac{\varepsilon_{\text{suction}}}{0.172 V_p} \left(0.333 + \frac{w}{c} + \frac{1}{2.2} \frac{s}{c}\right) \quad (8)$$

The calculated degrees of hydration shown in Table 7 for the Flekkefjord samples with zero or low accelerator doses (remember the concrete supposedly sprayed with 6 % set accelerator actually contained zero accelerator) are from 0.681 to 0.984. These seem reasonable degrees of hydration given the age of these samples was 125 days at the start of the capillary suction test. However, calculated degrees of hydration for the samples sprayed with the accelerator dose of 10 % are 0.285 to 0.326, which are low. It appears that addition of accelerator has affected the usefulness of the equation and it appears that the modified Power’s equation is not applicable for concrete with set accelerator added, presumably because the hydration products no longer have the usual fractions of CSH.

Table 7 – Suction porosity and solving for degree of hydration using modified Powers equation

Sample	Suction porosity ϵ_{suc}	w/c	s/c	Paste volume V_p Volume of cement + silica fume + water + water from accelerator	Degree of hydration α Calculated with Equation 8
Flekkefjord 0%	14.6	0.446	0.0416	0.367	0.775
Flekkefjord 0%	14.5	0.446	0.0416	0.367	0.788
Flekkefjord 3%	16.4	0.478	0.0416	0.372	0.681
Flekkefjord 3%	15.8	0.478	0.0416	0.372	0.759
Flekkefjord 6% *	15.4	0.511	0.0416	0.376	0.944
Flekkefjord 6% *	15.1	0.511	0.0416	0.376	0.984
Flekkefjord 10%	21.5	0.554	0.0416	0.382	0.285
Flekkefjord 10%	21.2	0.554	0.0416	0.382	0.326
Trondheim zero accelerator – cast	17.9	0.494	0.099	0.377	0.532
Trondheim zero accelerator – cast	18.2	0.494	0.099	0.377	0.492
Trondheim 3.5% accelerator	18.1	0.536	0.099	0.382	0.666
Trondheim 3.5% accelerator	17.7	0.536	0.099	0.382	0.721
Trondheim 7% accelerator	20.5	0.578	0.099	0.387	0.483
Trondheim 7% accelerator	20.1	0.578	0.099	0.387	0.541

* Actually zero set accelerator.

All the concrete mixes for these experiments contained an air entrainment agent, which forms spherical air bubbles in the fresh concrete. Beaupré [30] reported that, for mixes with a high air content due to inclusion of an air entrainment agent, most of the air content can be lost during spraying and/or impact with the substrate, leaving an air content of, for example, 5 %. Table 6 shows that while this effect has expelled most of the entrained air from the sprayed samples, for the cast samples the high air content of the fresh concrete was retained. This high air content accounts for the higher suction porosity values recorded in Table 6 for the unaccelerated cast samples (Trondheim series), and hence lower calculated average degree of hydration values (Table 7), compared with the unaccelerated sprayed samples (Flekkefjord series). For the Trondheim samples with 3.5 % set accelerator the results are comparable to the Flekkefjord samples with 3 % set accelerator, while the samples with 7 % set accelerator show a reduction in calculated degree of hydration, but less than the samples with 10 % set accelerator from Flekkefjord.

Table 7 shows that when calculating cement paste volume fraction and then using it to calculate degree of hydration based on the modified Power’s equation (Eq. 8), the accelerator reduced the degree of hydration for the Flekkefjord series, and possibly also for the Trondheim series. Though Eq. 8 is sensitive to the volume fraction of paste.

Concerning the low calculated degree of hydration values, it is likely that a high dose of set accelerator has led to an excess of aluminium-based ions and sulphate ions and that these have altered the hydration products – firstly due to the needle-like structure of the excess ettringite formed, which is likely to give a higher suction porosity. Secondly the composition of the CSH gel is likely to be altered. Gartner [31] reported that sulphates, alumina and other impurities are

found in the CSH, and that up to 50 % of the total sulphates and alumina are found in the CSH gel, rather than in the ettringite or monosulphate phases that are generally considered to contain these species. Therefore it is likely that such a high dose of set accelerator has led to an excess of aluminium based ions and sulphate ions and that these have altered the composition of the CSH gel, giving different CSH gel porosity in the samples with lower or zero set accelerator doses. The altered hydration products renders the modified Power's equation inapplicable given that it is based primarily on the hydration products of the standard Portland cement reactions. The latter reaction has its chemical shrinkage, gel and capillary formation from mainly CSH and calcium hydroxide- and not so much from aluminate-sulphate phase reactions.

Due to the extra water added with the accelerator the capillary number is possibly affected by both accelerator and variations in w/c . Smeplass [23] indicated that for silica fume concrete with w/c increasing from 0.41 to 0.46, the capillary number could increase from 0.010 to almost 0.015. And that for concrete with w/c variation in the range 0.41–0.46, resistance number could vary in the range $9 - 11 \times 10^7$ (s/m²). Comparing these findings from [23] with the observed effects of accelerator on capillary and resistance numbers in Table 6, the variations for Flekkefjord 3 % mixes are within this scatter. However there is a probable effect of accelerator when comparing the 3 % to the 0 % mix, and there is a clear effect on capillary and resistance numbers for 10 % accelerator. For Trondheim there is a probable/clear effect on capillary and resistance numbers from the 0 % to the 7 % mix.

To definitively determine whether the increase in suction porosity in sprayed concrete with higher set accelerator doses, further work is planned: laboratory casting of concrete with varying doses of set accelerator, but with water also added to samples to give a constant w/b ratio in the samples. Capillary suction and PF test would then be carried out to measure suction porosity. Given constant w/b , any change in the suction porosity would be solely due to the effect of the accelerator on the hydration products.

4 CONCLUSIONS

- A higher set accelerator dose gives a higher early age strength development in sprayed concrete but reduces density and long-term strength of the sprayed concrete.
- There is a clear trend between the density of the hardened sprayed concrete and its compressive strength – samples with a higher density have a higher compressive strength.
- The methods of measuring early age strength – the penetrometer, the stud driving method and compression testing of cores – give relatively close results.
- A higher set accelerator dose causes a lower density and a higher suction porosity in the hardened sprayed concrete. The higher suction porosity also causes an increased rate of capillary absorption in the hardened sprayed concrete.
- The capillary porosity increases with higher doses of set accelerator. This is due to the matrix stiffening quickly when large amounts of needle-like ettringite are formed in the early stages of hydration.
- With increasing doses of set accelerator the hydration products are altered and renders the modified Power's suction porosity equation inapplicable.
- The macro pore content of sprayed concrete is different from that of conventional air entrained concrete and image analysis seems to give the largest measurement of macro pore content.

- A further experiment to cast samples with varying set accelerator doses, with water added to give a constant w/b ratio in the samples, is proposed. Given constant w/b , any change in the suction porosity would be solely due to the effect of the accelerator on the hydration products.

5 ACKNOWLEDGEMENTS

This paper/presentation is a part of the research project “Sprayed sUstainable PERmanent Robotized CONcrete tunnel lining (SUPERCON)” financed by the Research Council of Norway (project no. 294724), in cooperation with industrial partners Andersen Mek. Verksted, BASF, Bever Control, Bekaert, Elkem, Entreprenørservice, NORCEM, SWECO Norge, Veidekke, Wacker Chemicals Norway. Research partners in SUPERCON are NGL, NTNU and SINTEF. The following project owners support the project; Bane NOR, Nye Veier and the Norwegian Public Roads Administration.



Thanks to Karl Gunnar Holter for leading the Trondheim spraying experiments, and to Erik Johansen from SINTEF and to Per Øystein Nordtug from NTNU for assistance with laboratory experiments.

6 REFERENCES

1. Salvador R, Cavalaro S, Segura I, Figueiredo A & Pérez J: “Early age hydration of cement pastes with alkaline and alkali-free accelerators for sprayed concrete”. *Construction and Building Materials*, Vol. 111, 2016, pp. 386–398.
2. Salvador R P, Cavalaro S H P, Cano M, de Figueiredo A D: “Influence of spraying on the early hydration of accelerated cement pastes”, *Cement and Concrete Research*, Vol. 88, 2016, pp. 7-19.
3. Salvador R P, Cavalaro S H P, Cincotto M A, de Figueiredo A D: “Parameters controlling early age hydration of cement pastes containing accelerators for sprayed concrete”, *Cement and Concrete Research*, Vol. 89, 2016, pp. 230-248.
4. Salvador R P, Cavalaro S H P, Monte R, de Figueiredo A D: “Relation between chemical processes and mechanical properties of sprayed cementitious matrices containing accelerators”. *Cement and Concrete Composites*, Vol. 79, 2017, pp. 117-132.
5. Myrdal R, “Accelerating admixtures for concrete – state of the art”, SINTEF report, Trondheim, Norway, 2007.
6. Maltese C, Pistolesi C, Bravo A, Cella F, Cerulli T, Salvioni D, Dal Negro E: “Effects of alkali metal hydroxides on alkali-free accelerators”. *Advances in Cement Research*, Vol. 23 Issue 6, 2011, pp. 277-288.
7. Norwegian Concrete Association Publication no. 7: “Sprayed Concrete for Rock Support”. Oslo, Norway, 2011.
8. Wang Y, Shi C, Yihan M, Xiao Y, Liu Y: “Accelerators for shotcrete – chemical composition and their effects on hydration, microstructure and properties of cement-based materials”. *Construction and Building Materials*, Vol. 281, 2021, 122557.
9. Maltese C, Pistolesi C, Bravo A, Cella F, Cerulli T, Salvioni D: “A case history: Effect of moisture on the setting behaviour of a Portland cement reacting with an alkali-free accelerator”, *Cement and Concrete Research*, Vol. 37, 2007, pp. 856-865.
10. Taylor H F W: “Cement Chemistry”, 2nd edition, Thomas Telford, London, UK, 1997.

11. Tan H, Li M, Ren J, Deng X, Zhang X, Nie K, Zhang J & Yu Z: “Effect of aluminium sulfate on the hydration of tricalcium silicate”. *Construction & Building Materials*, Vol. 205, 2019, pp. 414-424.
12. Han J, Wang K, Wang Y & Shi J: “Study of aluminium sulfate and anhydrite on cement hydration process”. *Materials and Structures*, Vol. 49, 2016, pp. 1105-1114.
13. Holter K G: “Properties of waterproof sprayed concrete tunnel linings. A study of EVA-based based sprayed membranes for waterproofing of rail and road tunnels in hard rock and cold climate”, PhD 2015:197, Norwegian University of Science and Technology, Trondheim, Norway.
14. Sellevold E J & Farstad T: “The PF-method – a simple way to estimate the w/c-ratio and air content of hardened concrete”. *Proceedings*, Construction materials: performance, innovations and structural implications, Vancouver, Canada, 2005, 10 pp.
15. Myren S A & Bjøntegaard Ø: “Fibre reinforced sprayed concrete (FRCS): mechanical properties and pore structure characteristics”, *Proceedings*, 7th International Symposium on Sprayed Concrete, Sandefjord, Norway, June 2014, pp. 305-313.
16. Trussell N & Jacobsen S: “Review of Sprayability of Wet Sprayed Concrete”. *Nordic Concrete Research*, Vol. 63, 2/2020, article 2, pp. 21-42.
17. Product data sheet for Master Builders Solutions MasterRoc SA 188.
18. Product data sheet for Master Builders Solutions MasterRoc SA 168.
19. Standard: EN 14488-1, “Testing sprayed concrete – Part 1: Sampling fresh and hardened concrete”, 2005.
20. Standard: EN 14487-1, “Sprayed concrete – Part 1: Definitions, specifications and conformity”, 2012.
21. Standard: EN 14488-2, “Testing sprayed concrete – Part 2: Compressive strength of young concrete”, 2006.
22. Standard: EN 12390-3, “Testing hardened concrete – Part 3: Compressive strength of test specimens”, 2019.
23. Smeplass S, “Capillary absorption as a quality criterion”, SINTEF report, Trondheim, Norway, 1988 (in Norwegian).
24. Punkki J & Sellevold E J: “Capillary suction in concrete: effects of drying procedure”. *Nordic Concrete Research*, Vol. 15, 1994, pp. 59-74.
25. Fonseca P C & Scherer G W: “An image analysis procedure to quantify the air void system of mortar and concrete”. *Materials and Structures*, Vol. 48, 2015, pp. 3087-3098.
26. Kauffman J, Frech K, Schuetz P & Münch: “Rebound and orientation of fibers in wet sprayed concrete applications”. *Construction and Building Materials*, Vol. 49, 2013, pp. 15-22.
27. Neville AM: “Properties of Concrete”, 4th Edition, Longman Group Limited, Harlow, England, 1995.
28. Opsahl, 1985, A study of a wet-process shotcreting method – Volume I, PhD thesis, Norwegian Institute of Technology, University of Trondheim, Trondheim, Norway.
29. Sellevold E J, Bager D H, Klitgaard Jensen E & Knudsen T: “Silica fume – cement pastes: hydration and pore structure”. Condensed silica fume in concrete, Report BML 82.610, The Norwegian Institute of Technology, The University of Trondheim, Norway, 1982.
30. Beaupré N: “Rheology of high performance shotcrete”. PhD thesis, University of British Columbia, Department of Civil Engineering, Vancouver, Canada, 1994, 265 pp.
31. Gartner E M, Young J F, Damidot D A, Jawed I: “Hydration of Portland cement” in Bensted J, Barnes P (editors), *Structure and Performance of Cements*, Abingdon: Taylor & Francis, 2002, pp. 57-113.

Paper III

	
<p>© Article authors. This is an open access article distributed under the Creative Commons Attribution-NonCommercial-NoDerivs licens. (http://creativecommons.org/licenses/by-nc-nd/3.0/).</p>	<p>ISSN online 2545-2819 ISSN print 0800-6377</p>
<p>DOI: 10.2478/ncr-2022-0011</p>	<p>Received: Sept. 13, 2022 Revision received: Nov. 28, 2022 Accepted: Dec. 15, 2022</p>

Effect of Set Accelerator on Capillary Suction and Porosity of Concrete – Cast Samples with Constant Water/Binder Ratio



Nicholas Trussell
MEng, CPEng, MIEAust, PhD Student
Norwegian University of Science and Technology,
Department of Structural Engineering,
Richard Birkelands vei 1A, 7034 Trondheim, Norway
E-mail: nicholas.h.trussell@ntnu.no



Rolands Cepuritis
Adjunct Associate Professor, PhD
Norwegian University of Science and Technology,
Department of Structural Engineering,
Richard Birkelands vei 1A, 7034 Trondheim, Norway
E-mail: rolands.cepuritis@ntnu.no



Stefan Jacobsen
Professor, PhD
Norwegian University of Science and Technology,
Department of Structural Engineering,
Richard Birkelands vei 1A, 7034 Trondheim, Norway
E-mail: stefan.jacobsen@ntnu.no

ABSTRACT

Alkali-free set accelerators are added at the nozzle to ensure rapid set of wet sprayed concrete. The accelerator affects the strength development, porosity and transport properties, and hence the durability, of the sprayed concrete. We developed a method to cast samples with varying set accelerator doses to measure the effect of the accelerator on porosity, but with a constant effective water/binder ratio of 0.45 for each accelerator dose. Six cylinders of concrete were cast with set accelerator doses of 0, 2, 4, 6, 8 and 10 % of effective binder mass. High workability was achieved to enable mixing before rapid stiffening occurred, though this high workability led to some aggregate settlement in the cylinders. Porosity was measured by capillary suction on dried specimens of hardened concrete and subsequent pressure saturation of macro pores (PF test). The samples cast with higher doses of set accelerator had higher suction porosities and higher rates of

capillary suction. Using a modified Powers equation gave very low calculated degree of hydration values for concrete with set accelerator, indicating that the equation is not applicable for concrete with set accelerators, due to the higher suction porosity in accelerated matrices, caused by different hydration products.

Key words: Sprayed concrete, shotcrete, accelerator, porosity, tunnel, durability.

1. INTRODUCTION

Wet-sprayed concrete is increasingly used in large quantities for tunnel linings in infrastructure. The functions of sprayed concrete tunnel linings are to provide immediate ground support to enable excavation to proceed and provide safety during construction, and to provide long-term support of the tunnel. Due to its composition and production method sprayed concrete is not covered by usual standards for structural concrete such as EN 206 [1]. The production method consists of pulsed concrete flow from a piston pump to a nozzle where a steady flow of accelerator is added together with compressed air, propelling the concrete through the nozzle to the substrate while rapidly setting. Compared to the fresh concrete in the hopper of the pump, the final product is altered by addition of the accelerator, increased water/binder mass ratio due to the water content of the accelerator and the effects of the spraying. The spraying process causes variable composition over the spray cone [2], rebound [3], irregular compaction porosity [4, 5] and anisotropy of the hardened concrete [6].

We address porosity of sprayed concrete because the limiting water/binder mass ratios prescribed for the 18 exposure classes defined in EN 206 [1] are based on the limiting water transport by limiting capillary porosity. For cast concrete the suction porosity depends on the water/binder mass ratio, binder type, degree of hydration and the paste volume fraction [7]. The water/binder mass ratios defined in standard EN 206 [1] to achieve desired suction porosities govern durability, given that water transport underlines most degradation phenomena in concrete [8] and that water transport occurs, in intact concrete, through the capillary pore network. This is also where deleterious substances collect. Power's classic model [7, 8] quantifies the relationship between water/cement mass ratio, degree of hydration and porosity. The two classes of cement paste porosity are nanoscopic gel pores, where there is little transport of substance, and microscopic capillary pores, where transport can take place. Volume fraction, size and degree of interconnectivity of capillary pores depend on the water/cement mass ratio and degree of hydration. Powers' model was developed several decades ago for hydration of Portland cement [7]. The effect of microsilica, particularly the increased chemical shrinkage and increased CSH gel produced, was investigated later and the model adjusted accordingly [9]. Later investigations found the model to give good quantification of degree of hydration [10]. More recently the model was even adapted to cement replacement by limestone [11]. Knowledge of porosity is abundant for cast concrete with standardised constituents and captured by EN 206 [1], but scarce data exists for sprayed concrete.

However EN 206 does not cover sprayed concrete for tunnel linings [1]. The accelerator changes the hydration products, which in turn changes the porosity [12]. Durability classes for Norwegian sprayed concrete for tunnel linings can be found in Norwegian Concrete Association publication No. 7, "Sprayed concrete for rock support" [13]. These classes specify M40 concrete with water/binder ratio of 0.40 for most exposure classes for rock support in subsea tunnels, and M45 with water/binder ratio of 0.45 for most exposure classes for rock support where the lining is exposed to freshwater. Norwegian Concrete Association publication No. 7 [13] does stress that

the water content of the accelerator must be considered in the water/binder mass ratio. These classes are stricter than the equivalent classes for cast concrete, specified in the Norwegian national annex to EN 206 [1].

1.1 Effect of set accelerators

Modern, alkali-free set accelerators for wet sprayed concrete are mainly aluminium sulphate based solutions [13, 14, 15, 16]. They cause rapid set and increase the rate of early strength development due to the formation of hydrous aluminium sulphates (mainly ettringite). Given that each mole of ettringite binds 32 moles of water [17], ettringite formation increases the solid/liquid ratio and leads to stiffening of the matrix.

Addition of set accelerator affects the porosity of sprayed concrete. Firstly the set accelerator contains water, which increases the effective water/binder ratio when added to the fresh concrete and increases the suction porosity [18]. We can designate this the additional water effect. Furthermore Salvador et al. [16] described an increase in water accessible porosity, which we interpret as suction porosity, in matrices containing set accelerators, which we can designate as the accelerator effect. These effects on the suction porosity are separate to the typical 4–6 % macro porosity in sprayed concrete caused by the spraying process [4, 5].

Trussell et al. [19] varied set accelerator doses in full-scale sprayed concrete experiments and measured increased suction porosity with increased set accelerator dose. They found that Powers' equation linking suction porosity, water/binder ratio and degree of hydration in hardened cement paste [7] gives very low values for degree of hydration for concrete with high doses of set accelerator and concluded that Powers' model is inapplicable for sprayed concrete containing set accelerator.

Due the uncertainty of the placed concrete composition for concrete sprayed at full scale (uncertainty over the precise set accelerator dose added at nozzle, and the effect of rebound and dust) the laboratory experiment described in this manuscript, where the proportions could be controlled more precisely, was performed to verify the findings of Trussell et al [19]. This will give further understanding of the effect of set accelerators on concrete properties and is important for research and development on the use of sprayed concrete for permanent tunnel linings. Furthermore the water/binder ratio is kept constant in this study, to ensure that the difference in measured porosity between the samples is due to set accelerator effect only, and not due to the additional water effect.

Whilst set accelerators are essential for use in sprayed concrete to enable build-up of concrete thickness, the rapid stiffening of accelerated concrete makes it impractical to mix set accelerator into fresh concrete for casting – the rapid stiffening occurs before the accelerator can be mixed evenly into the concrete. Hence it is difficult to investigate the effect of set accelerator on concrete cast under controlled laboratory conditions.

1.2 Effect on durability

Experience on long-term durability of sprayed concrete is increasing, for example Hagelia [20] concluded that the main durability issue is chemical attack on the cement paste fraction, while Galan et al. [21] identified a wide range of causes and connections.

The sulphate content of modern, alkali-free set accelerators may affect the durability. Sulphates in concrete present durability issues [22]. Sulphate ions can react to form gypsum and/or ettringite, leading to expansion, cracking and/or spalling. Sulphate ions can also react to form thaumasite, leading to strength loss, which is covered in EN 206 by limiting the use of limestone filler where external sulphate attack may occur [1]. Degradation of tunnel linings due to sulphate in the groundwater has been recorded [20, 21, 23]. Small scale studies indicate that sulphate-containing accelerators increase the expansion of mortar exposed to external sulphate attack compared to mortar specimens without accelerator [24].

Recently research by Manquehual et al [25] on the effect of both old-fashioned water glass and modern alkali-free accelerators provide information about performance of alkali free accelerators in sprayed concrete with the (to our knowledge) longest service life so far – greater than 20 years at the time of writing. The tunnel linings studied in their paper were the first use of sprayed concrete linings with aluminium sulphate based set accelerators in Norwegian road tunnels [25]. Higher suction porosity, lower density and lower strength were measured in concrete sprayed with aluminium sulphate based set accelerator compared to that sprayed with traditional sodium silicate (water glass) based accelerator. Ettringite enrichment was measured in the sprayed concrete with aluminium sulphate based set accelerator, especially between layers of sprayed concrete application. Corrosion of the steel fibres was only observed in the carbonation zone at the intrados of the linings. Given the uncertainties about concrete composition and variations over the 6.8 km long tunnel, the study indicates no clear negative long-term durability of concerns of sprayed concrete with alkali free accelerators compared to water glass accelerators [25].

1.3 Scope

The manuscript investigates set accelerators for sprayed concrete and their effect on concrete properties. The effect of aluminium sulphate based set accelerators has been well covered at small scale level in cement samples, which we have referred to and discussed, but not at larger scale in concrete samples. In this work we maintain a constant water/binder ratio of the concrete for the different doses of set accelerator to remove the effect of this variable on the porosity, and thus isolate the effect of the set accelerator on concrete porosity. Thus we can definitively determine the effect of set accelerator on concrete porosity.

We developed the method for mixing the set accelerator into fresh concrete and casting this concrete. We carried out an experiment adding a range of set accelerator doses: 0, 2, 4, 6, 8 and 10 % of effective binder mass (mass of cement + 2 × mass of microsilica, following k factors specified in EN 206 [1]). The method involved adding water to the set accelerator to dilute it, giving more time before rapid stiffening occurred, and to achieve constant water/binder ratio between all the set accelerator doses. The capillary suction rates and porosity of the hardened concrete were investigated to verify that the effects on porosity and capillary suction measured by Trussell et al. [19] were due to the effect of set accelerator on porosity, and not merely a result of water/binder variations due to the additional water content with higher doses of set accelerator. We compared measured porosities to a modified Powers model to assess the effect of accelerator on the hydration products.

2. METHOD

2.1 Development and trials

A typical Norwegian sprayed concrete mix can have a water/binder ratio of 0.42 and matrix volume (total concrete volume – volume of aggregate greater than 0.125 mm) of 42 volume % before addition of the set accelerator [5]. With addition of, for example, 6 or 7 % set accelerator the water/binder ratio increases to around 0.45 [5]. To trial the method, a base mix was batched with a water/binder ratio of 0.42 and matrix volume of 0.42 to replicate a typical sprayed concrete mix. Two litres of concrete were placed in 150 mm diameter cylinders and doses of 6 and 10 % set accelerator by binder mass were added. The concrete was mixed for 15 seconds with a hand mixer and vibrated for 30 seconds. The hand mixer, cylinder and vibration table are shown in Figure 1. With these set accelerator doses the concrete stiffened rapidly and was not able to be mixed properly. The cylinders cast during these earlier trials are shown on the left of Figure 2, which shows that good compaction was not unachieved due to the rapid stiffening.



Figure 1 – Hand mixer, 150 mm diameter steel cylinder and vibration table used to mix and cast concrete with set accelerator.

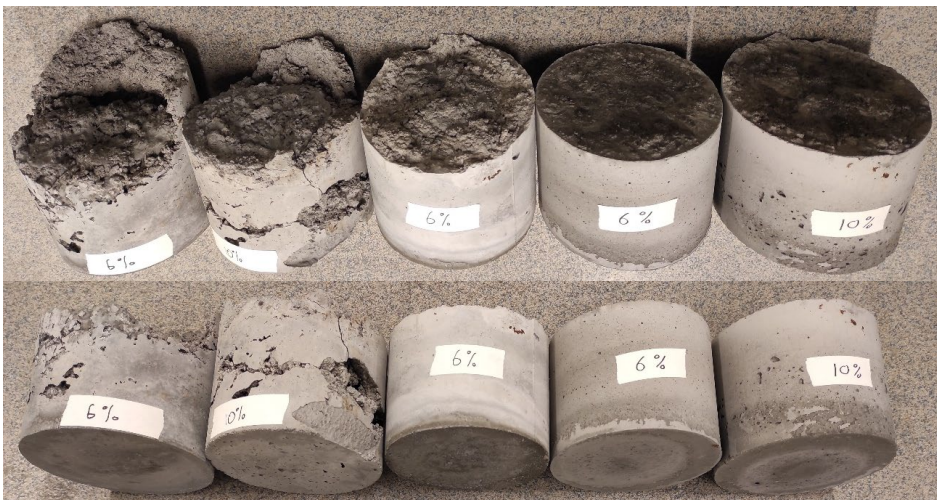


Figure 2 – Cylinders cast during method development – cylinders from early trials are to the left and those from later trials to the right of the photographs.

To reduce the rapid stiffening effect, the set accelerator was diluted with water. To compensate for this additional water added with the set accelerator, water was removed from the base mix, keeping the water/binder ratio at 0.45 after addition of the set accelerator solution. Diluting the set accelerator, whilst reducing the water in the base mix to achieve water/binder of 0.45 after adding the accelerator solution, delayed rapid stiffening long enough for mixing with doses of 6 and 10 % by binder mass. The trial cylinders cast with this method are the two cylinders on the right of Figure 2 and show much better compaction compared to the previous trials on the left.

2.3 Proportioning

For the actual experiments the base mix was proportioned as detailed in Table 1. The set accelerator doses added are detailed in Table 2. The set accelerator used was Masterroc SA 168, which has a solids mass fraction of 0.575 [26]. Hence the water content of the set accelerator is 0.425. Water doses were added to dilute the set accelerator and to achieve constant water/binder ratio for all the set accelerator doses.

Table 1 – Proportioning of base mix per litre (before addition of accelerator and water mixtures detailed in Table 2)

Constituent	Mass (kg)	Density (kg/m ³)	Volume (litres)
Standard fly ash cement	468	2990	156
Microsilica	46.3	2200	21.1
Water	175	1000	175
Superplasticiser (water content 0.79 by mass)	4.88	1050	4.64
Air (assumed)	0	0	25
Årdal 0-8 mm aggregate < 0.125 mm	129	2670	48.2
Årdal 0-8 mm aggregate > 0.125 mm	1522	2670	570
SUM	2357 kg		1000

Water / cement ratio of base mix = 0.382
 Effective water / binder ratio of base mix = 0.319

Table 2 – Set accelerator doses and water dilution per m³ of base mix concrete

Set accelerator dose (% of binder mass)	Mass of accelerator (kg)	Mass of water in the accelerator (kg)	Mass of water added to accelerator (kg)	Total water added (kg)
0	0	0	75	75
2	11	5	70	75
4	22	10	65	75
6	34	14	61	75
8	45	19	56	75
10	56	24	51	75

Water/cement ratio after addition of accelerator/water solutions = 0.542
 Effective water/binder ratio after addition of accelerator/water solutions = 0.453

2.4 Mixing and casting

The mixing procedure was as follows.

1. 40 litres of the base mix were batched.
2. Slump, density and air content of the fresh base mix concrete were measured following EN 12350 parts 1, 2, 6 and 7 respectively [27, 28, 29, 30].
3. For each specimen two litres of concrete were measured and placed in a cylindrical metal mould.
4. The set accelerator and water solution was added.
5. The concrete was mixed for 10 seconds in the cylinder with a hand mixer (shown in Figure 1) and vibrated using the vibration table for 45 seconds (from the time of set accelerator solution addition).

The moulds were 150 mm diameter cylinders. This diameter was selected to enable a 120 mm impeller to mix the concrete in the moulds. Three 100 x 100 x 100 mm cubes were cast with the base mix only, without addition of set accelerator nor additional water. So these cubes were cast with an effective water/binder ratio of 0.319. The cylinders were stripped after 48 hours and were stored in water. The density of the cubes (without accelerator) and cylinders (with different doses of accelerator added) after storage in water for 87 days was measured by weighing them in air and water.

2.5 Capillary suction

The capillary suction test was undertaken on the sprayed concrete samples following Punkki & Sellevold [31] and Smeplass [32]. Three 25 mm thick discs were cut from each cylinder and dried at 105°C for 72 hours before testing. The mass of each sample after drying was recorded as w_1 .

The discs were placed on perforated metal trays with a depth of 1 mm of the disc immersed in water. The suction face of the top and middle discs from each cylinder were sawn, while the suction face for the bottom disc had been cast against the steel mould.

Capillary suction leads to an increase of the mass of each disc. After immersion in 1 mm of water the samples were weighed at regular intervals up to a time of 5 days. The mass after 5 days of capillary suction was recorded as $w_{1.5}$. The graph plotted is mass increase/absorption area against $\sqrt{\text{time}}$ [18] and the capillary number of the concrete is determined by the gradient of the mass increase against $\sqrt{\text{time}}$, shown in Equation 1.

$$K_{\text{cap}} = \frac{G(t)}{\sqrt{t}} \quad (1)$$

Where K_{cap} capillary number
 $G(t)$ absorption (kg/m^2) at time t (seconds).

The resistance number is calculated by Equation 2.

$$m = \frac{t_{\text{cap}}}{h^2} \quad (2)$$

Where m resistance number
 t_{cap} the time for the rising water front in the specimen to reach the top of the specimen. This is the point of inflection on the capillary suction plot of water absorption against $\sqrt{\text{time}}$
 h height of the disc.

2.6 PF test

The PF (pore fraction) test was carried out following the capillary suction test on the same samples. These samples were submerged in water at atmospheric pressure for 5 days. The samples were then weighed in air and water to determine the mass after atmospheric (unpressurised) submersion, w_2 , and the volume, v . The density after submersion in water was calculated.

The samples were then submerged under a pressure of 5 MPa for 48 hours to fill the closed macro pores. The mass after pressurised submersion is recorded as w_3 [18]. The total porosity is calculated according to Equation 3:

$$\varepsilon_{\text{total}} = \frac{w_3 - w_1}{v} \quad (3)$$

The gel porosity plus the capillary porosity, equal to the suction porosity, is calculated by Equation 4:

$$\varepsilon_{\text{suction}} = \frac{w_{1.5} - w_1}{v} \quad (4)$$

The open macro porosity is calculated by Equation 5:

$$\varepsilon_{\text{open macro}} = \frac{w_2 - w_{1.5}}{v} \quad (5)$$

And the closed macro porosity, or air voids content, is calculated by Equation 6:

$$\varepsilon_{\text{closed macro}} = \frac{w_3 - w_2}{v} \quad (6)$$

The solid density, ρ_{solid} , was calculated by the mass after drying at 105 °C over the volume multiplied by 1 minus the total porosity, as detailed in Equation 7.

$$\rho_{\text{solid}} = \frac{\rho_{\text{bulk dry}}}{1 - \varepsilon_{\text{total}}} \quad (7)$$

3. RESULTS AND DISCUSSION

3.1 Fresh concrete properties of the base mix

The measurements of the fresh concrete base mix were:

Slump	270 mm
Density	2307.5 kg/m ³
Air content	0.8 %

No separation of water was observed at the edge of the slump test.

3.2 Casting and inspection of cylinders

For the cylinders with set accelerator doses of 6 % and higher, the increase in stiffness of the concrete occurred rapidly. Nevertheless the hand mixer was successfully used and extracted and each cylinder was vibrated for 45 seconds. Bleeding was observed at the top of the cylinder mixed with 0 % accelerator, whereas no separation had been observed at the edge of the slump test, so the addition of 150 g of water to the 2 litres of base mix before vibrating for 45 seconds led to this bleeding.



Figure 3 – Cast cylinders with different set accelerator doses

The cast cylinders are shown in Figure 3. Whilst the cylinders are all even and free of major voids, there is increasing layering visible in the cylinders with higher set accelerator doses. There is just a minor evidence of bleeding at the top of the cylinder cast with 0 % set accelerator.

3.2 Density

The density of the cylinders after water storage at 89 days age is shown in Figure 4. The graph shows reducing density with increasing dose of set accelerator, albeit with similar densities for 6, 8 and 10 % set accelerator doses. The cylinders for doses of 6, 8 and 10 % set accelerator have a decrease in density of 1.7–1.9 %.

The density of cubes cast from the base mix, with addition of neither set accelerator nor water, is also included in the graph. The density of the base mix (effective water/binder = 0.319) is higher than the cylinder cast with zero set accelerator but 150 g of water added (effective water/binder =

0.453) to the 2 litres of base mix, which is as we would expect. The higher water content results in a higher capillary porosity content after hydration [18].

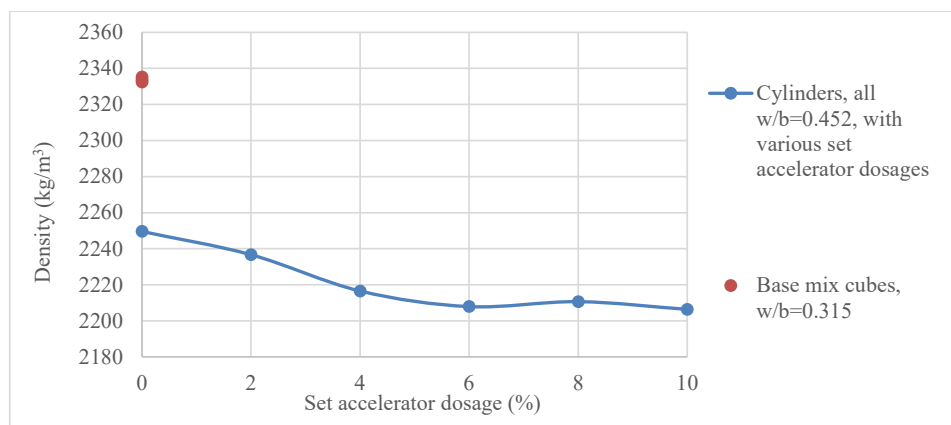


Figure 4 – Density against set accelerator dosage for the cast cylinders and cubes cast from the base mix at 89 days age after storage in water

Table 3 – Capillary numbers, resistance numbers, total porosity and suction porosity from capillary suction and PF tests

Sample	Capillary number kg/m ² .s ^{0.5}	Resistance number s/m ²	Total porosity (calculated by Eq. 3) Volume %	Suction porosity (calculated by Eq. 4) Volume %	Macro porosity (calculated by Eq. 6) Volume %	Solid density (calculated by Eq. 7) kg/m ³
0 % top	0.0261	8.1×10^7	25.1	23.4	1.6	2683
0 % middle	0.0206	8.5×10^7	21.2	19.6	1.4	2680
0 % bottom	0.0126	2.1×10^8	19.7	17.7	1.1	2673
2 % top	0.0294	6.1×10^7	26.5	24.0	2.1	2691
2 % middle	0.0273	6.4×10^7	25.2	22.7	2.1	2693
2 % bottom	0.0213	1.1×10^8	25.5	22.6	1.9	2690
4 % top	0.0331	5.2×10^7	28.2	25.1	2.4	2693
4 % middle	0.0314	5.5×10^7	27.1	23.8	2.7	2694
4 % bottom	0.0273	7.4×10^7	24.5	21.6	2.4	2687
6 % top	0.0377	4.6×10^7	29.8	26.6	2.4	2698
6 % middle	0.0332	4.6×10^7	27.6	24.4	2.6	2695
6 % bottom	0.0218	9.6×10^7	24.4	21.4	2.5	2689
8 % top	0.0374	4.6×10^7	29.6	26.5	2.5	2704
8 % middle	0.0348	4.9×10^7	27.8	24.9	2.3	2700
8 % bottom	0.0352	3.6×10^7	24.5	21.8	2.4	2692
10 % top	0.0470	3.4×10^7	29.6	26.4	2.8	2699
10 % middle	0.0371	4.1×10^7	28.6	25.3	2.8	2699
10 % bottom	0.0252	6.4×10^7	23.8	20.7	2.6	2689

3.2 Capillary suction and PF test

The capillary suction curves are shown in Figures 6 and 7. The capillary numbers and resistance numbers from the capillary suction curves, as well as total porosity and suction porosity calculated from the PF test, are included in Table 3. The capillary numbers against set accelerator dose are plotted in Figure 5.

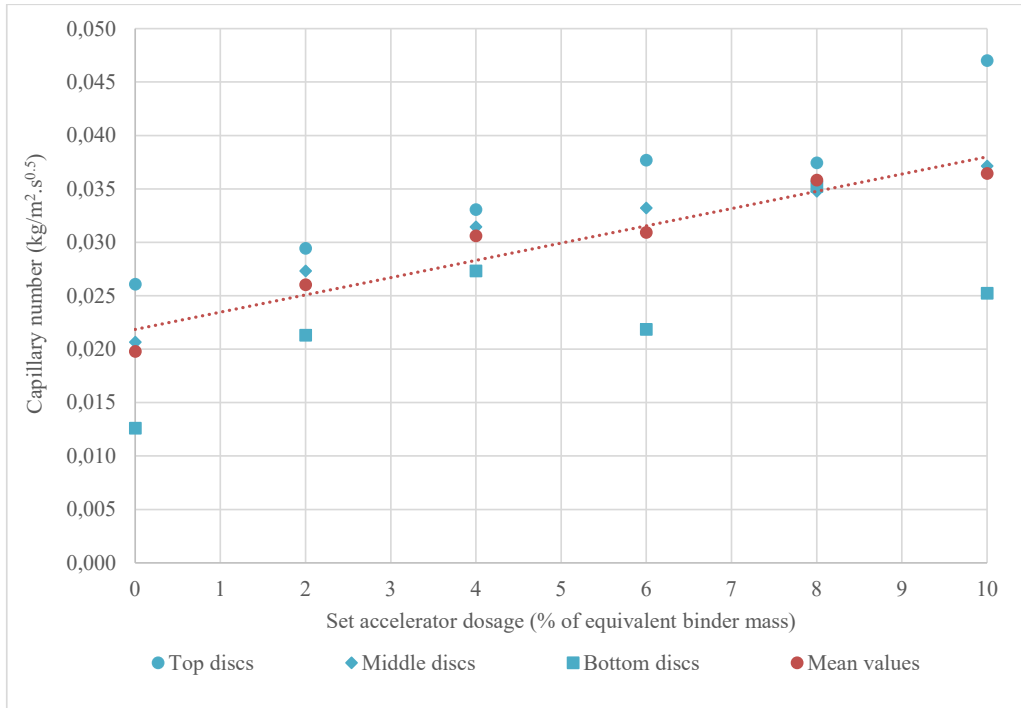


Figure 5 – Capillary number against set accelerator dose

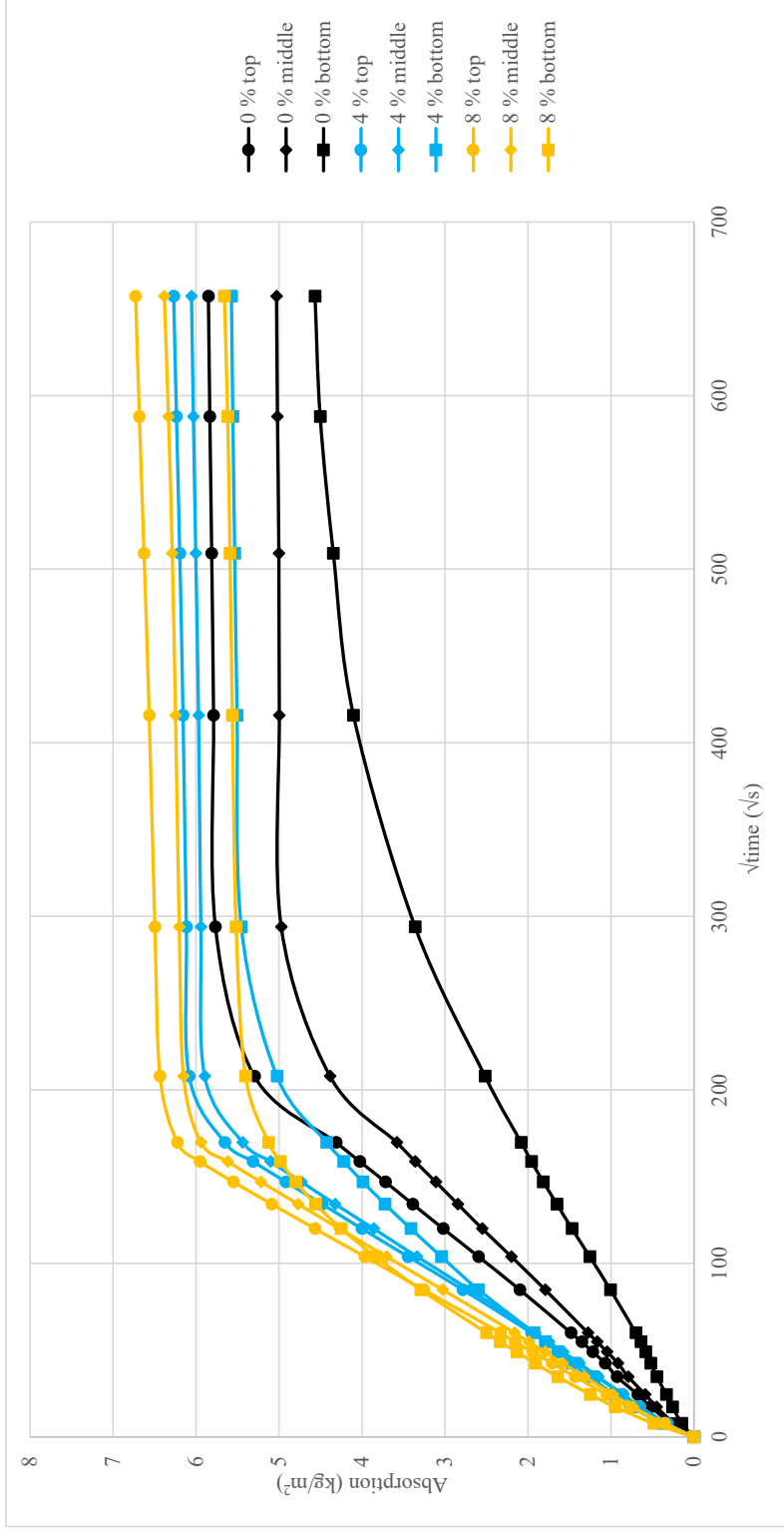


Figure 6 – Capillary suction curves with the set accelerator dosage varied (graph 1 of 2)

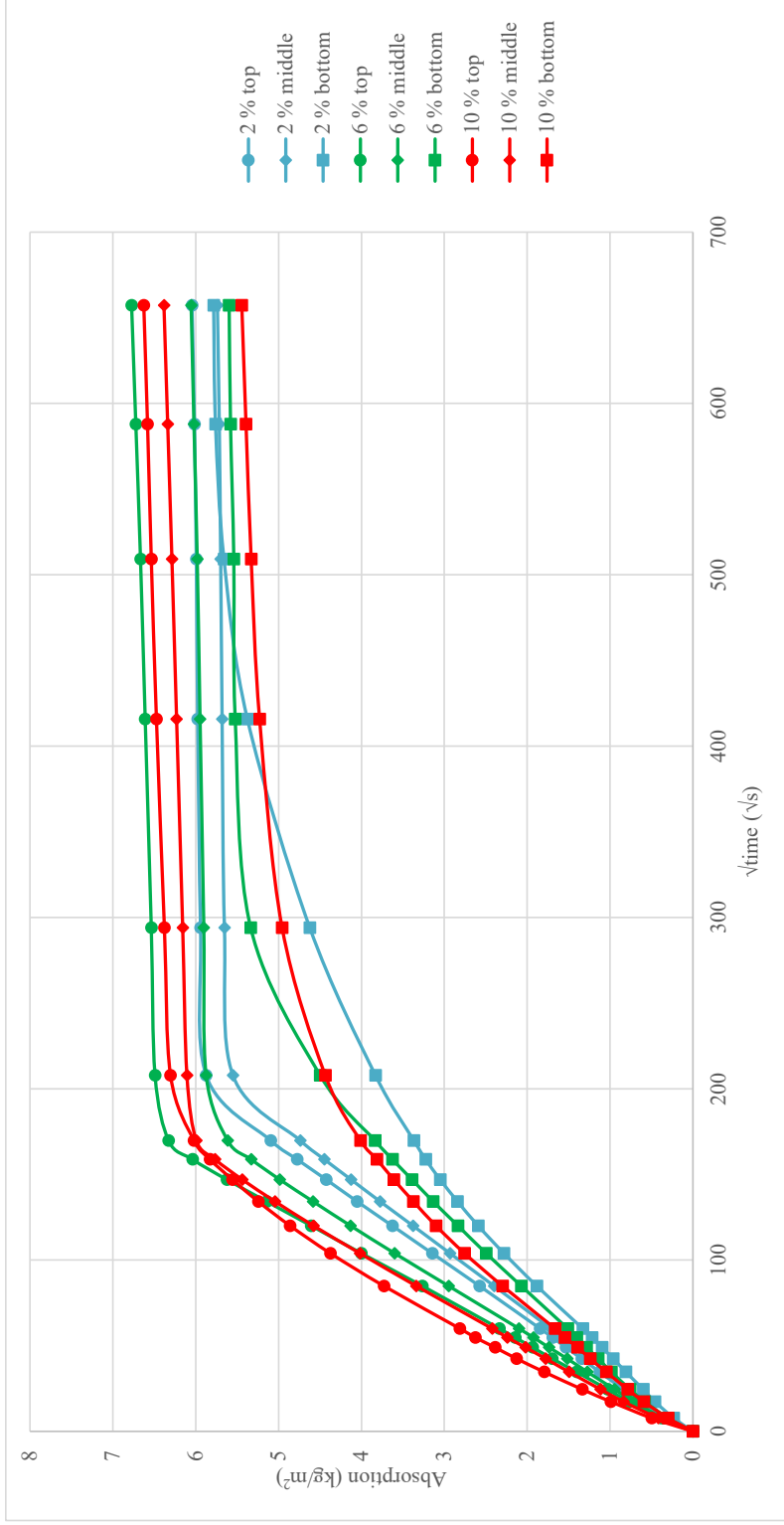


Figure 7 – Capillary suction curves with the set accelerator dosage varied (graph 2 of 2)

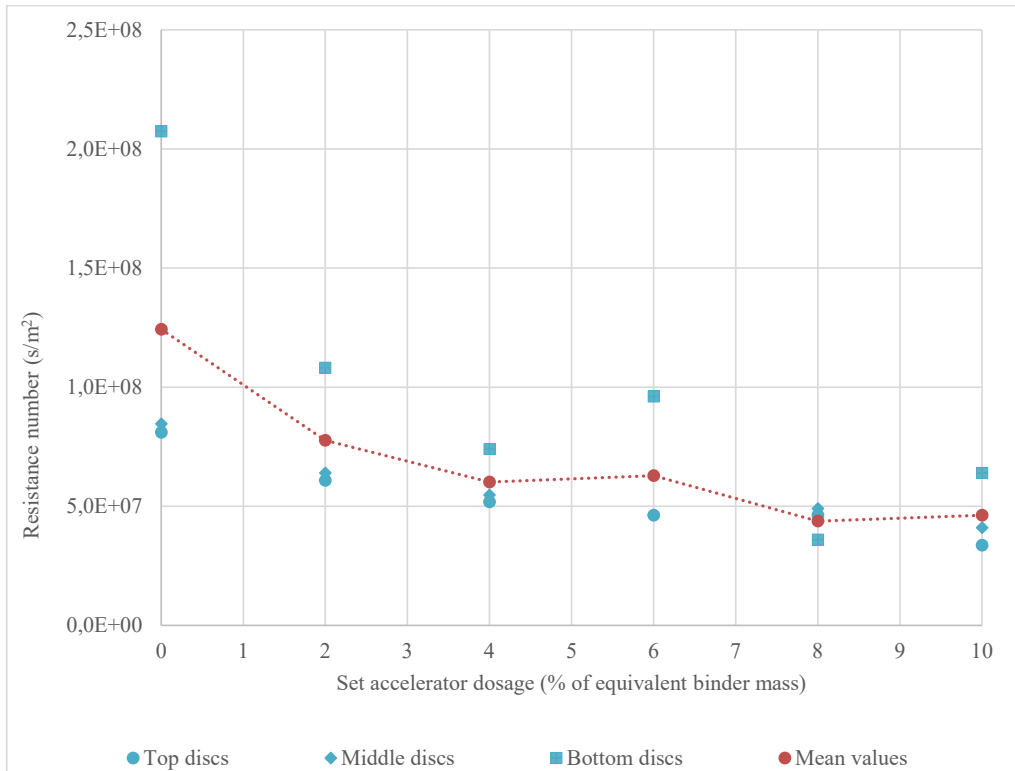


Figure 8 – Resistance number against set accelerator dose

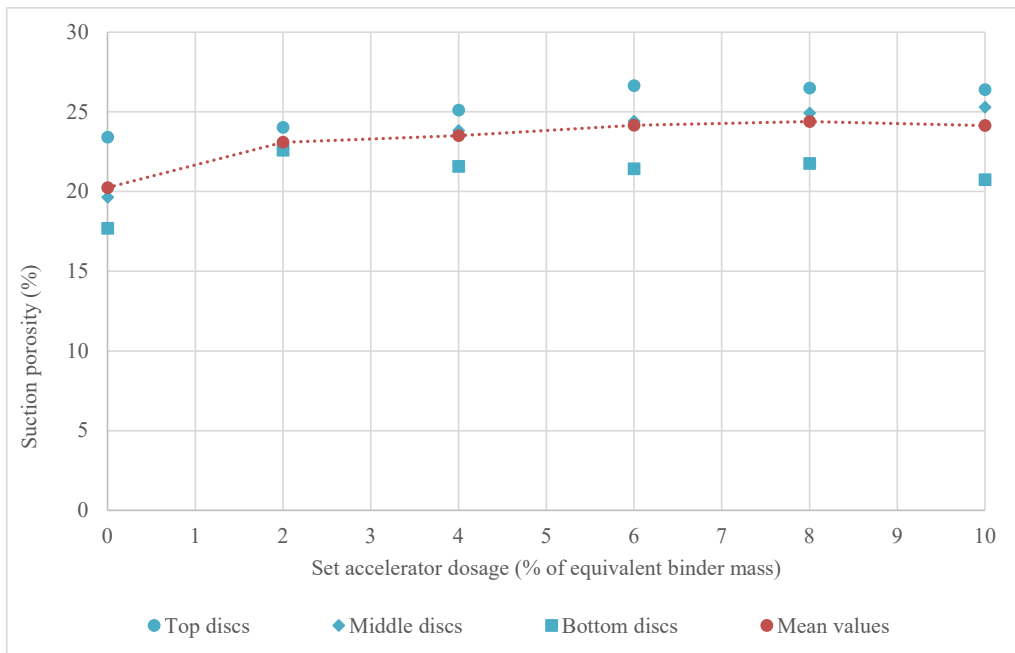


Figure 9 – Suction porosity against set accelerator dose

The capillary suction curves shown in Figures 6 and 7 show an increased rate of capillary suction in the discs with higher doses of set accelerator. This is confirmed by the plot of capillary number against set accelerator dose in Figure 5, though there is a degree of scatter in both graphs.

Figure 8 is a plot of the resistance numbers from the capillary suction curves against set accelerator dose. The graph shows that discs from the bottom of the cylinders have higher resistance numbers, especially for the 0 % set accelerator dose, so a longer time for the rising water front to reach the top of each disc. This is due to aggregate settlement in the cylinders, so the discs at the bottom have a higher proportion of aggregate and lower paste content. The cement paste content does not affect the resistance number but does affect the capillary number – therefore we see more variation in the capillary numbers compared to the resistance numbers. The mean values for each cylinder show a trend of decreasing resistance number with increasing set accelerator dose.

Figure 9 is a plot of suction porosity of the concrete against set accelerator dose and shows that suction porosity is increased from zero to 6 % set accelerator, albeit with similar suction porosity values for 6, 8 and 10 % set accelerator doses. The 4 volume % increase of mean suction porosity from zero % set accelerator to 6, 8 and 10 % set accelerator is even more marked when calculated as paste volume % – then the increase is 10 volume %. These porosity measurements in Figure 9 are consistent with the density measurements in Figure 4.

Despite the scatter, Figures 7 – 9 confirm previous findings from sprayed concrete specimens cored from panels after full-scale spraying with different accelerator doses [19] – the accelerator alters the pore structure of the sprayed concrete – increasing both suction porosity and the rate of capillary suction. The increase in suction porosity in accelerated sprayed concrete is due to both the additional water affect and the accelerator effect. This also agrees with findings from Salvador et al [16], that the “water accessible porosity” (which we interpret as suction porosity) increases in accelerated matrices.

The difference in suction porosity between top and bottom discs cut from the same cylinder indicates the degree of settlement, and resulting difference in paste content, between discs cut from the same cylinder. But the average values should meet the proportioned matrix volume and water/binder ratio. In general the cylinders with higher set accelerator doses show less difference in porosity between top and bottom disc, indicating less settlement of the aggregate. This is due to faster stiffening of the matrix with higher set accelerator doses.

The degree of hydration for each cast sample was calculated by rearranging a modified Powers equation. The modified Powers equation is given by Equation 8, based on [7, 9, 10, 11].

$$\varepsilon_{\text{suction}} = \frac{\frac{w}{c} - 0.172\alpha + 0.116 \frac{s}{c} \alpha_s}{\frac{w}{c} + 0.333 + \frac{1}{2.2} \frac{s}{c}} V_p \quad (8)$$

where	$\varepsilon_{\text{suction}}$	suction porosity
	w/c	mass of water / mass of cement
	α	degree of hydration of cement
	s/c	mass of microsilica / mass of cement
	α_s	degree of hydration of microsilica
	V_p	volume fraction of paste

Equation 8 can be rearranged to solve for degree of hydration, shown as Equation 9:

$$\alpha = \frac{1}{0.172} \frac{w}{c} + \frac{0.116\alpha_s s}{0.172} \frac{s}{c} - \frac{\varepsilon_{suc}}{0.172 V_p} \left(0.333 + \frac{w}{c} + \frac{1}{2.2} \frac{s}{c}\right) \quad (9)$$

The suction porosity, w/c and s/c ratios, paste volume fraction and calculated degree of hydration for each disc are shown in Table 4. The degree of hydration of the microsilica, α_s , is assumed to be 1.0. The paste volume has been calculated from the placed concrete composition [5], with the macro porosity measured by the PF equated to the air content of the placed concrete.

Table 4 – Suction porosity and solving for degree of hydration using modified Powers equation

Sample	Suction porosity $\varepsilon_{suction}$ Volume % From Table 3	Water/ cement mass ratio	Microsilica /cement mass ratio	Paste volume fraction V_p	Degree of hydration α Calculated with equation 9	Mean degree of hydration $\alpha_{average}$
0 % top	23.4	0.542	0.099	0.403	0.112	
0 % middle	19.6	0.542	0.099	0.404	0.623	
0 % bottom	17.7	0.542	0.099	0.405	0.880	0.539
2 % top	24.0	0.542	0.099	0.406	0.056	
2 % middle	22.7	0.542	0.099	0.406	0.227	
2 % bottom	22.6	0.542	0.099	0.406	0.240	0.175
4 % top	25.1	0.542	0.099	0.409	-0.065	
4 % middle	23.8	0.542	0.099	0.408	0.098	
4 % bottom	21.6	0.542	0.099	0.409	0.393	0.142
6 % top	26.6	0.542	0.099	0.414	-0.219	
6 % middle	24.4	0.542	0.099	0.413	0.058	
6 % bottom	21.4	0.542	0.099	0.413	0.446	0.095
8 % top	26.5	0.542	0.099	0.418	-0.173	
8 % middle	24.9	0.542	0.099	0.419	0.039	
8 % bottom	21.8	0.542	0.099	0.418	0.428	0.098
10 % top	26.4	0.542	0.099	0.426	-0.097	
10 % middle	25.3	0.542	0.099	0.426	0.041	
10 % bottom	20.7	0.542	0.099	0.427	0.625	0.190

The average degree of hydration value calculated for the discs with zero set accelerator is 0.54, which is a little lower than the expected value after three months of curing of the 150 mm diameter cylinders in water. The values for the discs cut from lower in the cylinder have higher degrees of hydration which are around the values we would expect, but the calculated degree of hydration for the disc cut from the top of the cylinder is only 0.11. This low value is due to aggregate

settlement, giving a higher actual paste volume fraction than the theoretical value used for the calculations. The higher paste volume fraction thus gives a higher suction porosity compared to lower in the unaccelerated cylinder, where the actual paste volume fraction is lower due to the aggregate settlement.

The calculated mean degree of hydration values for the samples cast containing set accelerator are very low – between 0.095 and 0.190. This is clearly not realistic given the three months of curing in water. Equation 9 is very sensitive to the paste volume fraction and a low V_p value gives an overly large negative part of the equation.

One uncertainty here is the interpretation of suction porosity in Equations 8 & 9 from the one sided capillary suction experiments and the fully submerged PF test, see Equations 3–6. The additional absorption from one sided to full submersion is in the order of 1–2 volume % of concrete according to our laboratory experience. For sprayed concrete we have previously proposed that this difference is entirely ascribed to filling of macro pores due to the special irregular and partly open macro pore structure in sprayed concrete, and hence not to be included as suction porosity in the cement paste [5]. However, in this work on laboratory cast accelerated concrete we observed that the difference in water absorption from one sided to fully submerged is similar to what we observed in sprayed concrete specimens [19]. Hence the mechanisms of filling open and closed macro pores as defined by Equations 4–6 are uncertain and it is not entirely clear whether the extra porosity filled from one-sided to submerged state should be ascribed to what we term suction porosity or macro porosity. In this study this difference makes up 0.1–1.0 volume % of concrete, so 0.25–2.5 volume % of paste, hence there is this volume % uncertainty in the calculated degrees of hydration.

We have corrected paste volume fractions for variations in macro porosity to avoid this problem. Furthermore the use of slices from top, middle and bottom of each cylinder will give average values representing the bulk of each cylinder so that effects of bleeding on effective water/binder variation over cylinder height are averaged out in the capillary transport and porosity measurements.

Overall we believe that the difference in calculated degree of hydration values between samples without and with accelerator demonstrate that the Powers porosity equation is invalid for concrete with set accelerators. This is due to different hydration products, other than the standard ordinary Portland cement with mainly CSH and calcium hydroxide, with phases containing more aluminate and sulphate [14, 16, 33, 34, 35]. The higher suction porosity in accelerated pastes increases the negative part of Equation 9, resulting in very low calculated degree of hydration values.

The use of set accelerators for permanent sprayed concrete tunnel linings is a compromise, in that the accelerator is essential for early strength development, enabling adhesion to the substrate and immediate ground support, but high accelerator doses give reduced long-term strength, increased porosity and increased water transport.

4. CONCLUSIONS

- In order to cast concrete with varying doses of set accelerator, the workability is a compromise between the different accelerator doses – a high slump was needed to give valuable seconds to mix in the higher doses of set accelerator before rapid stiffening occurred. Yet that high slump led to settlement of the aggregate in the cylinders, so the paste volume at

the top of the cylinder was higher than that at the bottom of the cylinder. Nevertheless a clear effect of accelerator dose could be deduced from these experiments.

- Whilst addition of set accelerator in wet sprayed concrete increases the water/binder ratio (due to the water content of the set accelerator), this experiment demonstrates that the increase in porosity is not only due to the additional water effect but also due to the effect of the accelerator on the hydration products. The porosity of the concrete increased by 4 volume % from zero set accelerator to set accelerator doses of 6, 8 and 10 % of effective binder mass. When considered as paste volume only this increase is in the order of 10 volume %.
- A clear effect of increased accelerator dose was seen on the rate of capillary suction. The mean capillary number increased by 84 % for the highest accelerator dose. This higher rate of water transport and higher suction porosity reduces the durability of the sprayed concrete.
- The degree of hydration values calculated with Powers' porosity equation demonstrate that this equation is invalid for concrete with set accelerators. This is due to higher suction porosity caused by addition of set accelerator leading to different hydration products compared to the hydration of standard Portland cement and microsilica. These results verify the findings from Trussell et al [19] from full scale spraying experiments.

5. ACKNOWLEDGEMENT

This paper is a part of the research project "Sprayed sUstainable PERmanent Robotized CONcrete tunnel lining (SUPERCON)" financed by the Research Council of Norway (project No. 294724), in cooperation with industrial partners Andersen Mek. Verksted, BASF, Bever Control, Bekaert, Elkem, Entreprenørservice, Norcem, SWECO Norge, Veidekke, Wacker Chemicals Norway. Research partners in SUPERCON are NGI, NTNU and SINTEF. The following project owners support the project; Bane NOR, Nye Veier and the Norwegian Public Roads Administration.

Thanks to Steinar Seehuus, Magne Stangeland Hårr and Per Øystein Nordtug of the Norwegian University of Science and Technology for help in developing the method and executing the experiments.

6. REFERENCES

1. Standard: EN 206:2013, Concrete – specification, performance, production and conformity.
2. Ginouse N & Jolin M: "Investigation of spray pattern in shotcrete applications". *Construction and Building Materials*, Vol. 93, 2015, pp. 966-972.
3. Banthia N: "Advances in sprayed concrete (shotcrete)", Chapter 12, "Developments in the Formulation and Reinforcement of Concrete" (edited by Mindess S), Woodhead Publishing Limited, Cambridge, UK, 2019, pp. 289-306.
4. Holter KG: "Properties of waterproof sprayed concrete tunnel linings". 197, PhD thesis, Norwegian University of Science and Technology, Department of Geology and Mineral Resources Engineering, Trondheim, Norway, 2015, 167 pp.
5. Trussell N & Jacobsen S: "Review of Sprayability of Wet Sprayed Concrete". *Nordic Concrete Research Journal*, Vol. 63, Issue 2, 2020, pp. 21-41.

6. Kauffman J, Frech K, Schuetz P & Münch: “Rebound and orientation of fibers in wet sprayed concrete applications”. *Construction and Building Materials*, Vol. 49, 2013, pp. 15-22.
7. Powers T C & Brownyard T L: “Studies of the hardened paste by means of specific volume measurements”. *Journal of the American Concrete Institute*, pp. 669-712 (1947).
8. Scrivener K, Muller A, Zalzal M, Do Q & McDonald P: “New insights on mechanics controlling kinetics and implications for pore structure”. *Proceedings*, Understanding the fundamental properties of concrete, Trondheim, Norway, 2013.
9. Sellevold E, Bager D, Klitgaard Jensen E & Knudsen T: “Condensed silica fume in concrete”. Report BML 82.610, Division of Building Materials, Norwegian Institute of Technology, 1982.
10. Muller A, Scrivener K, Gajewicz A & McDonald P: “Densification of C-S-H Measured by ¹H NMR Relaxometry”. *Journal of Physical Chemistry*, Vol. 117, No.1, 2013, pp. 403-412.
11. Nadelman E & Kurtis K: “Application of Powers’ model to modern portland and portland limestone cement pastes”. *Journal of the American Ceramic Society*, Vol. 100, Issue 9, 2017, pp. 4219–4231.
12. Salvador R, Cavalaro S, Monte R & de Figueiredo A: “Relation between chemical processes and mechanical properties of sprayed cementitious matrices containing accelerators”. *Cement and Concrete Composites*, Vol. 79, 2017, pp. 117-132.
13. Publication no. 7: “Sprayed Concrete for Rock Support”. Norwegian Concrete Association, Oslo, Norway, 2011.
14. Maltese C, Pistolesi C, Bravo A, Cella F, Cerulli T, Salvioni D & Dal Negro E: “Effects of alkali metal hydroxides on alkali-free accelerators”. *Advances in Cement Research*, Volume 23 Issue 6, 2011, pp. 277-288.
15. Myrdal R, Accelerating admixtures for concrete – state of the art, SINTEF report, Trondheim, Norway, 2007.
16. Salvador R, Cavalaro S, Cano M, de Figueiredo A: “Influence of spraying on the early hydration of accelerated cement pastes”. *Cement and Concrete Research*, Volume 88, 2016, pp. 7-19.
17. Taylor H: *Cement Chemistry*, 2nd edition, Thomas Telford, London, UK, 1997.
18. Sellevold E & Farstad T: “The PF-method – a simple way to estimate the w/c-ratio and air content of hardened concrete”. *Proceedings*, Construction materials: performance, innovations and structural implications, Vancouver, Canada, 2005, 10 pp.
19. Trussell N, Cepuritis R & Jacobsen S: “Effect of set accelerator on properties of wet sprayed concrete”. *Nordic Concrete Research Journal*, Vol. 66, Issue 1, 2022, pp. 19-39.
20. Hagelia P: “Deterioration mechanisms and durability of sprayed concrete for rock support in tunnels”. PhD thesis, Delft University of Technology, Delft, Netherlands, 2011, 320 pp.
21. Galan I, Baldermann A, Kusterle W, Dietzel M & Mittermayr F: “Durability of shotcrete for underground support – Review and update”. *Construction & Building Materials*, Vol. 202, 2019, pp. 465-493.
22. Glasser F, Marchand J & Samson E: “Durability of concrete — Degradation phenomena involving detrimental chemical reactions”. *Cement and Concrete Research*, Vol. 38, 2008, pp. 226-246.
23. Long G, Xie Y, Deng D & Li X: “Deterioration of concrete in railway tunnel suffering from sulfate attack”. *Journal of Central South University*, Vol. 18, 2011, pp. 881-888.
24. Lee S, Kim D & Jung H: “Sulfate Attack of Cement Matrix Containing Inorganic Alkali-free Accelerator”. *KSCE Journal of Civil Engineering*, Vol. 13, Issue 1, 2009, pp. 49-54.
25. Manquehual C, Jakobsen P, Holter KG, de Weerd K, Danner T & Bruland A: “Comparison of the condition of steel fiber-reinforced shotcrete with water-glass and alkali-free activators

- after more than 20 years of service in a subsea road tunnel”. *Construction and Building Materials*, Vol. 328, 2022, 127090.
26. Master Builders Solutions, SA 168 data sheet.
 27. Standard: EN 12350-1:2019, Testing fresh concrete – part 1: sampling and common apparatus.
 28. Standard: EN 12350-2:2019, Testing fresh concrete – part 2: slump test.
 29. Standard: EN 12350-6:2019, Testing fresh concrete – part 6: density.
 30. Standard: EN 12350-7:2019, Testing fresh concrete – part 7: air content – pressure methods.
 31. Punkki J & Sellevold E: “Capillary suction in concrete: effects of drying procedure”. *Nordic Concrete Research*, Vol. 15, 1994, pp. 59-74.
 32. Smeplass S: “Capillary absorption as a quality criterion”. SINTEF report, 1998, Trondheim, Norway.
 33. Maltese C, Pistolesi C, Bravo A, Cella F, Cerulli T & Salvioni D: “A case history: Effect of moisture on the setting behaviour of a Portland cement reacting with an alkali-free accelerator”. *Cement and Concrete Research*, Vol. 37, 2007, pp. 856-865.
 34. Salvador R, Cavalaro S, Cincotto M & de Figueiredo A: “Parameters controlling early age hydration of cement pastes containing accelerators for sprayed concrete”. *Cement and Concrete Research*, Vol. 89, 2016, pp. 230-248.
 35. Salvador R, Cavalaro S, Cano M & de Figueiredo A: “Influence of spraying on the early hydration of accelerated cement pastes”. *Cement and Concrete Research*, Vol. 88, 2016, pp. 7-19.

Paper IV

Anisotropy and macro porosity in wet sprayed concrete: laminations, fibre orientation and macro pore properties measured by image analysis, PF test, water penetration and CT scanning

Nicholas Trussell*, Magne Stangeland Hårr, Gaute Kjeka, Iman Asadi, Pål Erik Endrerud, Stefan Jacobsen

Department of Structural Engineering, Norwegian University of Science and Technology

* Corresponding author.

Email address: nicholas.h.trussell@ntnu.no

Abstract

Sprayed concrete typically contains large, irregular macro pores. These are a product of the spray application and are different to spherical pores formed by an air entrainment agent for frost protection. Image analysis, capillary suction and pressurised saturation (PF test) and CT scanning were used to measure and analyse the macro porosity in specimens taken from 20 different panels sprayed in four series with varying accelerator doses, varying spraying distances and angles and varying sprayed concrete mixes. Macro porosity measurements by image analysis (3.8–7.5 %) and CT scanning (4.7–10.1 % measured on five specimens only) were higher than measurements by pressure saturation (2.5–4.9 %). The macro porosity increased with increased set accelerator dose. 9–20 % of the of the PF macro pore volume filled with water when submerged at atmospheric pressure. The shape of the macro pores was measured to be non-spherical, with 50 % of length/width ratios greater than 1.5. The macro pores were measured to tend towards orientation parallel to the substrate. Likewise fibre orientation was measured by CT scanning to tend towards orientation towards parallel to the substrate. Water penetration tests were done on specimens with the water pressure applied parallel and perpendicular to the direction of sprayed concrete application. Water penetration was measured to be very low parallel to the direction of application, but much higher perpendicular to the direction of application, due to macro porosity and laminations in this direction, indicating the importance of execution in wet spraying of concrete.

Keywords: Sprayed concrete, shotcrete, porosity, voids, fibres, PF test, image analysis, CT scanning.

1. Introduction

Wet sprayed concrete is used for immediate tunnel support and increasingly for permanent linings [1]. Hence the durability of sprayed concrete tunnel linings is given increased attention [2]. Recent field studies have mapped long-term chemical changes indicating leaching after 25 years of service life [3], indicating the importance of pore structure and transport properties of sprayed concrete.

The wet spraying production method involves pumping a paste-rich fresh concrete with reduced coarse aggregate size to the nozzle, where a set accelerator is added and compressed air propels the concrete. The set accelerator causes rapid setting as the concrete impacts with the substrate. Sprayed concrete typically contains large, irregular macro pores that are a product of the spray application [4] [5]. These macro pores are different from the spherical pores formed by an air entrainment agent for frost protection in ordinary cast concrete. Figure 1 shows an example of a core from a sprayed concrete lining with macro pores larger than 1 mm visible.

Fibres are another important constituent of sprayed concrete and fibre orientation in hardened sprayed concrete has been measured to tend towards perpendicular to the spraying direction [6]. Segura-Castillo et al. [7] measured this anisotropy by double punch (Barcelona) tests and measured 3.5 times higher residual loading capacity in specimens loaded parallel to the spraying direction than in specimens loaded perpendicular. Perhaps the orientation of the macro pores may also tend towards the same orientation due to the impact of the sprayed concrete with the substrate causing anisotropic compaction? If so this anisotropy of the macro pores may also result in reduced mechanical properties such as stiffness and strength in the direction with the largest pore area.



Figure 1 Example of a core from sprayed concrete lining with macro pores larger than 1 mm

Video camera recordings of spray application show pulsation and uneven concrete flow during the spray application and two frames are given as an example in Figure 2. The constant flow of accelerator while concrete flow is pulsed may cause local overdoses of accelerator, leading to laminations in the hardened

sprayed concrete, even when sprayed during continuous application. Hence this gives an anisotropy which affects both mechanical properties and permeability.

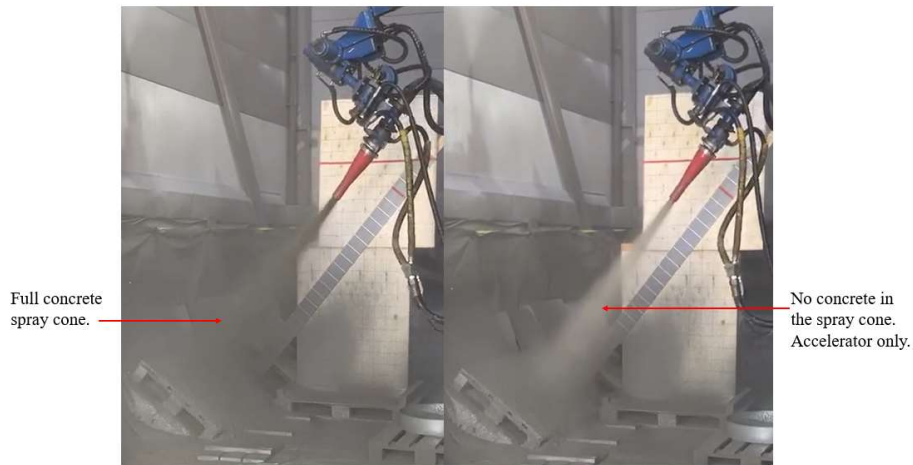


Figure 2 Left: sprayed concrete application with a full concrete spray cone. Right: sprayed concrete application with a pause in concrete flow, so pure accelerator is propelled through the nozzle to the substrate

1.1. Macro porosity in sprayed concrete

Increased macro pore content gives a reduction in strength [8], but the irregular macro pores in sprayed concrete [4] [5] further indicate that they can be partly open or form part of a continuous pore structure available for transport on a larger scale than capillary pores of 10–30 μm . The measured macro pore volume in hardened concrete depends, in addition to the concrete itself, on the measurement method. Gravimetric methods for measuring pore volume accessible to water include various drying, sorption, vacuum, boiling and pressure saturation methods on slices of concrete [9]. The macro pore content can be distinguished from the finer gel and capillary porosity in the hardened cement paste. The PF (pore fraction) is described by Sellevold & Farstad [10] and involves submerging the dried specimens in water, first at atmospheric and then at higher pressure. The mass increases following these steps are used to determine the suction and macro porosities. Furthermore we can differentiate between “open” and “closed” macro pores by defining the open macro pores as those that fill with water under atmospheric pressure, and defining the closed macro pores as those that only fill with water under subsequent pressurised saturation.

Optical 2D methods based on polished/impregnated surfaces and microscopy enable quantifying pore size distributions, shape and percolation using image analysis. The pore size that can be detected on polished sections prepared according to optic methods such as ASTM C457 [11] depends on the polishing and dye impregnation techniques and on the image resolution, but a minimum size of approximately 10–30 microns is typical. An image analysis method is described by Fonseca & Scherer

[12] and involves polishing the concrete surface, colouring it black, then filling the macro pores with a fine white powder. A Matlab script is used to analyse the scanned sample. The size distribution and total macro pore content can be computed.

The main 3D method is CT (computed tomography) scanning and uses x-ray measurements from different angles to produce tomographic images of a specimen [13]. Both macro pores and steel fibres can be differentiated from the aggregate and hydrated cement due to the high density of steel and the lower density of air/water in the macro pores. The two steps for CT scanning are image acquisition and reconstruction. In the first step 2D projections are acquired, and the second step involves the back-projection algorithm to reconstruct it as a 3D tomographic image [14].

Sellevoid & Farstad [10] compared macro porosity measurements by optical microscopy (ε_{IMA}) with PF method measurements ($\varepsilon_{\text{PF-cl}}$) on cast concrete. They found the macro porosity measured by optical microscopy to be lower than the equivalent values measured by the PF method by approximately 1 volume %.

Holter [4] used both the PF and image analysis methods to measure and compare the macro porosity content of sprayed concrete from four different tunnel linings. Holter measured macro pore volumes $\varepsilon_{\text{PF-cl}}$ of 4.0–6.0 % from 27 samples, with a mean of 4.5 %, using the PF method, while he measured a mean macro pore volume ε_{IMA} of 5.7 % using the image analysis method [12] on similar samples. Measurements of water permeability on 35 specimens taken from linings of three different wet sprayed concrete tunnels were done by Holter [4] showing that 89 % of the specimens had permeability coefficients less than 5×10^{-14} m/s.

Myren & Bjøntegaard [15] compared macro porosity in sprayed concrete. They measured an air content of 4.8–6.0 % in the fresh concrete, while they measured air content of 3.6–3.8 % by PF method and 2.9–3.1 % by image analysis in the hardened sprayed concrete. Yun et al. [16] used image analysis to measure macro porosity before and after spraying of concretes with and without an air entrainment agent. They found that the smallest entrained air pores (10–150 μm) were lost in mixes with an air entrainment agent after spraying, while concretes without an air entrainment agent had no difference in this pore size range before and after spraying.

1.2. Fibre content and orientation

The loss of fibres in sprayed concrete due to rebound is a well known phenomenon [6] [17]. Rebound is the mass of the concrete that does not adhere to the substrate, but instead bounces off. Rebound can be measured by placing a large tarpaulin on the floor prior to spraying to collect the rebound, weighing the collected rebound material and calculating this as a percentage of the mass of sprayed concrete [18]. The Norwegian Concrete Association publication no.7 [18] states that rebound is normally 5 % or less with modern wet spraying methods. But fibres are overrepresented in the rebound [6]. Given the

importance of fibres for the mechanical properties of the concrete (flexural and tensile strength, limiting crack widths), it is interesting to investigate in-situ fibre content and isotropic properties.

Kaufman et al. [6] measured the content and orientation of both steel and plastic fibres in sprayed concrete by CT scanning. He measured a reduction in the batched fibre content to the measured in-situ content of 25–44 %, due to rebound, with higher reduction in content for steel fibres compared to that of plastic fibres. He measured fibre orientation close to parallel to the substrate (i.e. perpendicular to the direction of spray application).

Žirgulis [19] used an orientation tensor to define the orientation of multiple fibres in cast concrete beams. He found that concrete with a fibre distribution closer to parallel (i.e. perpendicular to direction of load application) had a higher residual flexural strength [20], in line with the findings of Segura-Castillo [7].

1.3. Scope

The scope of this paper is to investigate anisotropy of macro pore shape and orientation, anisotropy of fibre orientation and anisotropy of permeability in wet sprayed concrete. The extent to which macro pores in sprayed concrete are partly open so can be filled with water under atmospheric pressure is also investigated. Anisotropy of macro pore shape and orientation is studied by image analysis of polished sections. Anisotropy of fibre orientation is studied by CT scanning and the fibre content measured by CT scanning is compared with measurements by crushing specimens, extracting the fibres using a magnet then weighing. Anisotropy of permeability is studied by water penetration followed by image analysis of the specimens after splitting and polishing. The fraction of closed and open macro porosity is studied by macro pores filled by pressure saturation compared to total macro porosity measured by PF test and by image analysis on polished sections. The macro porosity measurements by PF method, image analysis and CT scanning are compared.

2. Methods

The experimental programme consists of four series of full scale sprayed concrete experiments:

- Flekkefjord experiments with the set accelerator dose varied.
- Trondheim experiments with the set accelerator dose varied, with a reference mix (containing zero accelerator) pumped.
- Trondheim experiments with the spraying mechanics (spraying angle and distance) varied.
- Svorkmo experiments with the concrete proportioning varied.

Panels were sprayed for each experiment. Each panel was sprayed by a single application to a thickness of approximately 150 mm, from which cylinders were cored and specimens prepared for the laboratory tests.

2.1. Full scale spraying experiments

The details of the full scale wet sprayed concrete experiments are shown in Table 1.

Table 1 Summary of the full scale concrete spraying experiments

Series	Flekkefjord set accelerator experiments	Trondheim set accelerator experiments	Trondheim spraying mechanics experiments	Svorkmo mix proportioning experiments
Spraying machine	AMV 7450 shotcrete robot	Normet Spraymec NorRunner 140 DVC shotcrete robot	Normet Spraymec NorRunner 140 DVC shotcrete robot	Normet Spraymec NorRunner 140 DVC shotcrete robot
Concrete pump	Olin pump	Normet pump	Normet pump	Normet pump
Concrete flow rate	10 m ³ /hr	14 m ³ /hr	14 m ³ /hr	24 m ³ /hr
Accelerator type	MasterRoc SA 188	MasterRoc SA 168	MasterRoc SA 168	MasterRoc SA 188
Accelerator dose	Varied 0, 3, 6 and 10 % of effective binder mass	Varied 0, 3.5 and 7 % of effective binder mass	7 % of effective binder mass	7 % of effective binder mass
Distance and angle of nozzle to substrate	2.0 m Perpendicular to the panel	1.5 m Perpendicular to the panel	Varied	1.5 m Perpendicular to the panel

The concrete proportioning for the Flekkefjord and Trondheim spraying experiments, as well as the placed concrete compositions [5], were detailed in an earlier paper by Trussell et al. [21]. The concrete proportioning and the placed concrete composition for the spraying mechanics experiments is shown in Table 2, while the placed concrete proportioning for the Svorkmo spraying experiments is shown in Table 3.

2.2. Density and strength

Density was measured on cylinders of 75 mm diameter and 150 mm height by weighing in air and water. Strength was measured at ages 28–38 days by compressive strength tests.

Table 2 Fresh concrete composition and placed concrete composition (with 7 % accelerator added at the nozzle) for spraying mechanics experiment in Trondheim

Phase	Constituent	Mass [kg/m ³]	Volume [l/m ³]	Volume [l/m ³]	Placed concrete composition* [kg per m ³ concrete after spraying]
Matrix phase	Standard fly ash cement	433	145	437	417
	Water	214	214		223
	Microsilica	43	19.5		41.3
	Retarder	0.4	0.36		0.39
	Super plasticiser	3.7	3.5		3.56
	Air entrainment agent	0.6	0.6		0.58
	Set accelerator (dry)	-	-		18.5
	0 – 4 mm aggregate (<0.125 mm)	22	7.2		20.8
	0 – 8 mm aggregate (<0.125 mm)	128	47.3		123
	Air		(assumed) 40		Measured volume* = 59.7 litres
Particle phase	0 – 4 mm aggregate	152	50	523	147
	0 – 8 mm aggregate	1275	469		1228
	Steel fibres	30	4.2		28.9

* Air volume in hardened concrete measured by image analysis (Table 4)

Table 3 Placed concrete proportioning for eight mixes for sprayed concrete experiments at Svorkmo. Only mass is shown (for brevity) so air content is not shown

Phase	Constituent	Mass of constituents (kg/m ³) and air content (volume %)							
		Ref 1	Ref 2 Different fibre type	Ref 3 No SRA	Ref 4 No HA	Polymer mix	Fly ash mix	Lime filler mix	Low matrix
Matrix phase	Std fly ash cement	447	452	459	453	432	356	384	366
	Silica fume	18.6	18.8	19.1	18.8	18.1	18.7	20.2	15.1
	Fly ash	-	-	-	-	-	92.7	-	-
	Limestone powder	-	-	-	-	-	-	98.6	-
	Added water (including water part of accelerator)	211	215	219	223	204	203	199	181
	Superplasticiser	4.0	4.1	4.1	4.1	3.9	4.0	4.8	6.7
	Air entrainment agent	0.6	0.6	0.6	0.6	0.6	0.6	0.6	0.5
	Retarder	1.0	1.0	1.0	1.0	0.5	0.8	0.4	0.4
	Shrinkage reducing agent (SRA)	2.3	2.4	-	2.4	2.3	2.3	2.5	1.9
	Hardening accelerator (HA)	7.6	7.7	7.8	-	7.8	7.6	7.7	7.5
	Polymer powder	-	-	-	-	19.3	-	-	-
	Set accelerator	16.9	17.1	17.4	17.1	16.3	13.4	14.5	13.8
	Air content (volume %)	7.3	5.7	5.2	5.9	5.8	7.0	6.2	7.1
Aggregate <0.125 mm	140	143	143	142	143	141	142	156	
Particle phase	Aggregate >0.125 mm	1343	1366	1368	1357	1364	1345	1359	1491
	Steel fibres	38.0	48.5	38.9	38.5	38.7	38.0	38.7	37.3
SUM (kg/m ³)		2230	2266	2278	2258	2250	2222	2272	2277
Matrix volume fraction (excluding air)		434	441	445	443	441	436	439	383
Effective water/binder ratio		0.457	0.462	0.462	0.465	0.459	0.466	0.494	0.488

2.3. Capillary suction and PF (pore fraction) test

The capillary suction and PF tests were undertaken on specimens following Smeplass [22] and Sellevold & Farstad [10]. Samples were 100–120 days old at the start of the test. Discs of 98 mm diameter and 25 mm thickness were dried at 105 °C for 72 hours before testing. The mass after drying was recorded as w_1 . The discs were then placed on a perforated metal tray with a depth of 1 mm of the disc immersed in water. The increase of mass with time was measured. The mass after four days of capillary suction was recorded as $w_{1.5}$. Samples were then completely submerged under water at atmospheric pressure for four days. The additional uptake from unilateral to complete submersion is considered to fill the open macro pores. The mass after atmospheric (unpressurised) submersion is recorded as w_2 . The samples were then submerged under a pressure of 5 MPa for 48 hours to fill the closed macro pores. The mass after pressurised submersion is recorded as w_3 .

The total porosity is calculated by:

$$\varepsilon_{\text{total}} = \frac{w_3 - w_1}{v} \quad (4)$$

The open macro porosity (ε_{OP}) is calculated by:

$$\varepsilon_{\text{cap abs open macro}} = \frac{w_2 - w_{1.5}}{v} \quad (5)$$

The closed macro porosity (ε_{CP}) is calculated by:

$$\varepsilon_{\text{PF closed macro}} = \frac{w_3 - w_2}{v} \quad (6)$$

According to Sellevold & Farstad [6] the standard deviation of macro pore content measured by pressure saturation varies in the range 0.2–1.0 volume % based on 8 different concrete qualities, each with 6 parallel specimens.

2.4. Image analysis

Macro porosity was measured by black and white image analysis [12]. A core from each sprayed panel was cut in half lengthways to make two specimens and the flat surface of each was polished. A Tegramin 30 apparatus was used and the samples were polished using resin bonded, diamond surfaced discs of:

1. Vickers hardness 220, grain size 75 μm ,
2. Vickers hardness 600, grain size 30 μm ,
3. Vickers hardness 1200, grain size 15 μm .

The polished surface was coloured black and the macro pores were filled with white barium sulphate powder of particle size 1–4 μm . An example is shown in Figure 3a. The samples were then scanned at a resolution of 2400 pixels per inch. A Matlab script [12] was used to calculate the ratio of white and hence the macro porosity of each specimen. The accuracy of this method is given in [12], suggesting a log-normal distribution of frequency as a function of size for conventional, air entrained concrete. We have not computed distribution functions for sprayed concrete due to the content of large macro pores causing steps in the distributions in Figure 10 and Figure 11. We consider the accuracy of sample preparation, scanning and analysis in this study to be equivalent to that in [12] but with different

distribution functions. One potential source of error in this study, though, is the polishing of specimens containing steel fibres, as the polishing may cause movement of the fibres resulting in damage to the surrounding hardened paste. This would manifest as macro pore so may lead to an overestimate of macro porosity with this method.

Major imperfections were cropped out of the image analysis. For example the concrete sprayed with 10 % set accelerator in Flekkefjord contained a major lamination normal to the spraying direction, several tens of millimetres wide, due to pulsation of the concrete flow while accelerator was added at a steady flow, as shown in Figure 2. This lamination is omitted from the image analysis, as shown in Figure 3b.

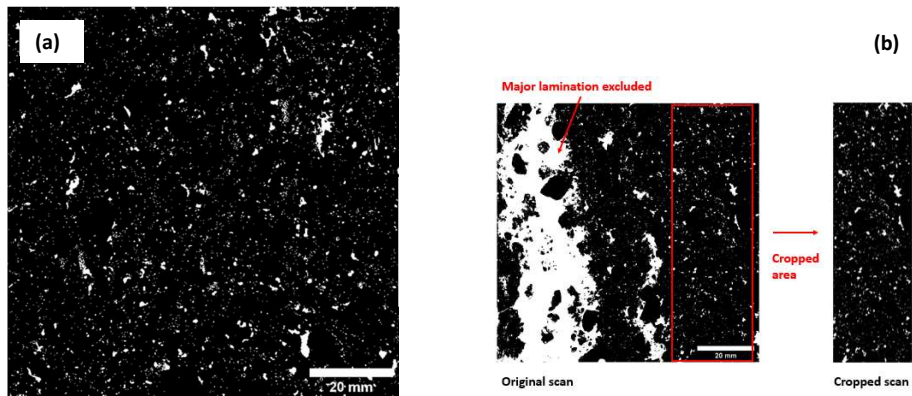


Figure 3 Example of polished concrete surface coloured black and white for image analysis

The shape and orientation of the macro pores were analysed using JMicroVision v1.3.4 software [23]. The length was measured as the longest dimension of a pore and the width as the dimension perpendicular to the length, while the length/width ratio was calculated for each pore. An example is shown in Figure 4. The orientation of the macro pores to the direction of spraying was also analysed by measuring the angle between the length and the orientation of the substrate. The orientation of macro pores is described by Figure 5 and is grouped by 0–30°, which we define as parallel to the substrate, 30–60°, which we define as having no orientation, and 60–90°, which we define as perpendicular to the substrate.

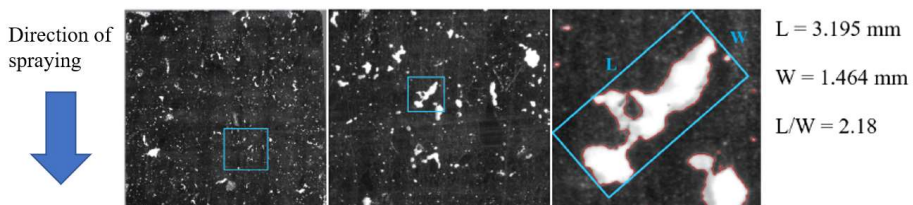


Figure 4 Example for measuring length/width ratio of macro pores using image analysis

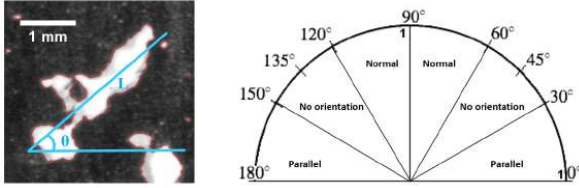


Figure 5 Definition of macro pores orientation

2.5. Water penetration

Water penetration is a test of water permeability [24]. Water permeability of concrete is a material parameter that takes a long time to measure under steady state. Permeability is very sensitive to curing, ageing, drying and wetting in addition to concrete composition because it depends on pore structure [25] [26]. Here a comparative study was made on cubes sawn from panels with the water pressure applied either parallel or perpendicular to the direction of spraying. The water pressure and exposure time was varied and applied to the cube face of dimensions 125×125 mm. The concrete was from the Flekkefjord experiments sprayed with 3 % or 10 % set accelerator. These samples were 2 years and 1 month old and the panels had been stored in air before sawing into cubes a few days before water penetration tests.

The cubes were split immediately after water penetration testing to mark the water front within the concrete. After marking and photographing, the split surface was sawn, ground and polished following the method described in section 2.4 to identify any laminations in the sprayed concrete that may have affected the water penetration. The equivalent permeability values, $K_{Valenta}$ (m/s) were calculated according to a simplified solution of non-steady-state pressurised flow, which is defined in Equation 8 [8]:

$$K_{Valenta} = \frac{e^2 v}{2ht} \quad (8)$$

Where e (m) is the observed maximum water penetration depth in m, v is the volumetric fraction of macro pores that fill by water under pressure, t is the duration in seconds, and h is the pressure expressed as an equivalent hydraulic height, $h = p/\rho g$.

The accuracy of the calculated value depends on the simplification that Equation 8 represents and the accuracy of the measured penetration depth. Given that a penetration depth of 1 mm can be measured, for a water pressure of 0.1 MPa applied for 72 hours with a macro pore content of 4.1 % (average of all specimens in this study), we calculate the minimum $K_{Valenta}$ value that could be determined to be 7.8×10^{-15} m/s with this experimental set up.

2.6. CT scanning for porosity measurements and fibre orientation

A METROTOM 1500 G2 scanner with the acquisition software METROTOM OS 3.6.2.19227 [27] was used. A voltage of 190 kV and a current of 440 μ A was used to scan cored cylinders of 98 mm

diameter and variable height. Postprocessing of the 3D images included segmentation to distinguish between the pores, steel fibres and solid matrix/aggregate. The histogram option in the VG Studio max software was used to analyse the images, as shown in Figure 6. The lower density parts of materials, such as air voids, are presented as dark points, and the higher density materials, like steel fibres, are brighter. The voxel size was 74–118 μm .

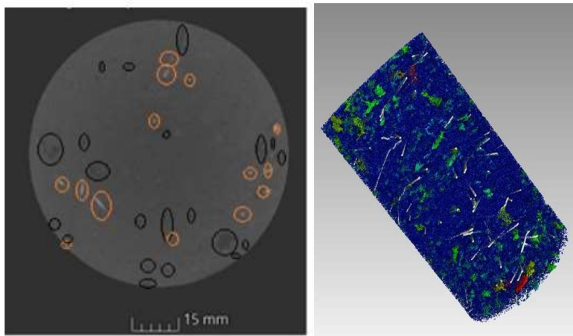


Figure 6 (a) Identification of steel fibres and macro pores by different grey values in 2D slice, and (b) image of 3D scanned cylinder with steel fibres visible as white

An artefact effect was produced due to high density contrast between the steel fibres and the other materials and pores. Therefore, the “VGDefX” algorithm [27] was selected when applying the “noise reduction” filter. The “medium adaptive” noise reduction, a Gauss filter algorithm, was applied.

Figure 7 shows grey histograms for segmentation of surfaces of pores and steel fibres based on the local grey value. The iso value applies a grey value to the data set. We used iso 50 (red line), which is the mean of material and the background (Figure 7a – pores), and the mean of the first material and the second material (Figure 7b – steel fibres).

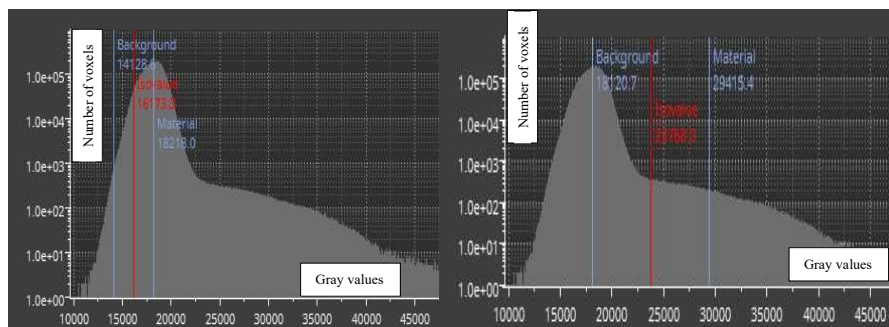


Figure 7 (a) Histogram for CT scan of sample with surface threshold and iso value (red) for macro pores shown, and (b) with the surface threshold and iso value (red) for steel fibres shown

2.7. Fibre content

The fibre content of the hardened sprayed concrete specimens was also measured manually by crushing cored cylinders and extracting the fibres with a magnet from the crushed concrete. The fibres were

weighed and fibre volume calculated, then divided by the volume of the core, which had been measured by weighing in air and water before crushing.

3. Results and Discussion

3.1. Porosity measurements

Porosity measurements measured by capillary suction and PF method, and by image analysis for all the samples are shown in Table 4. Ratios between the porosity measured by PF method and image analysis are also shown in the right two columns. The fact that the measured capillary suction increased with increased set accelerator dose has been explored in another paper [21]. There is a correlation between increased set accelerator dose and increased macro porosity in the Flekkefjord experiments, whereas the opposite trend was measured in the Trondheim experiments (though the sample with zero accelerator was cast by pumping the ready-mixed concrete from the hopper of the spraying machine through the nozzle and into moulds, thus retaining a higher content of the entrained air in the fresh concrete). The macro porosity measured by image analysis was higher than that measured by PF method, by a mean of 0.94 volume %. The porosity values measured by CT scanning are closer to those measured by image analysis than those measured by the PF method.

Figure 8 shows the ratio of macro porosity measured by PF method (both open and open + closed) over that measured by image analysis for the Flekkefjord and Svorkmo series. All the ratios determined for $\epsilon_{CP}/\epsilon_{IMA}$ are less than 1.0, while the ratios for $(\epsilon_{CP} + \epsilon_{OP})/\epsilon_{IMA}$ are higher but 19 of the 20 are still lower than 1.0. This demonstrates that image analysis measures a higher macro porosity than PF method. This disagrees with the results of Sellevold & Farstad [10], who measured higher macro porosity with PF method than with image analysis on conventional concrete with and without air entrainment. The implication of this is that macro pores in conventional concrete are less likely filled by water under (atmospheric) capillary suction than macro pores in wet sprayed concrete. However, Sellevold & Farstad [10] used 10 MPa water pressure and fluorescent impregnated polished sections so the results are not entirely comparable.

3.2. Density and strength

Mean values for measured density and strength are included in Table 4. The results for the two experiments in which the accelerator dose was varied gave good correlation between density, total porosity (measured by PF method) and strength.

$$\text{Strength (MPa)} = 0.395 \times \text{density (kg/m}^3) - 864$$

with an R^2 value of 0.89 for density between 2250–2350 kg/m³, and

$$\text{Strength (MPa)} = 139 - 4.11 \times \text{total porosity (volume \%)}$$

with an R^2 value of 0.78 for total porosity between 17–26 volume %.

Table 4 Porosity measurements by PF method, image analysis and CT scanning (individual specimens) and density and strength (mean values)

Sample		Strength (MPa)	Density (kg/m ³)	Capillary suction and PF method (volume %)			CT scanning	Image analysis	$\epsilon_{CP}/\epsilon_{BMA}$	$(\epsilon_{CP} + \epsilon_{OP})/\epsilon_{I,MA}$
				Suction porosity	Open macro porosity	Closed macro porosity	(volume %)	(volume %)		
1	0 % accelerator	59.9	2345	14.6	0.4	3.7		4.4	0.90	0.99
				14.5	0.4	3.7		3.8		
2	3 % accelerator	54.5	2303	16.4	0.7	4.1		4.7	0.93	1.05
				15.8	0.5	4.7		4.8		
3	6 % accelerator	65.1	2357	15.4	0.4	3.8		4.4	0.87	0.95
				14.7	0.3	3.4		4.0		
4	10 % accelerator	24.4	2265	22.7	0.6	3.8		5.4	0.64	0.75
				22.1	0.7	3.7		6.2		
5	0 % accelerator (cast)	50.2	2316	17.9	0.3	4.3		6.3	0.71	0.76
				18.2	0.3	4.5		6.1		
6	3.5 % accelerator	37.8	2279	18.1	0.5	3.7		5.1	0.88	0.99
				17.7	0.6	4.9		4.7		
7	7 % accelerator	46.1	2307	20.5	0.5	4.0		4.4	0.86	0.98
				20.1	0.6	3.8		4.7		
8	1.5 m spraying distance	35.3	2287	23.6	0.8	4.1	8.1	5.5	0.69	0.81
				18.6	0.7	4.2		6.6		
9	2.5 m spraying distance	39.3	2287	20.1	0.5	4.5	4.7	5.1	0.76	0.86
				18.5	0.6	3.8		5.9		
10	3.5 m spraying distance	39.2	2285	24.1	0.6	3.6	7.4	5.9	0.59	0.70
				23.6	0.9	3.8		6.7		
11	23° from perpendicular	29.3	2234	25.3	1.0	4.2	10.1	5.5	0.57	0.71
				26.4	0.6	2.4		6.1		
12	45° from perpendicular	Not measured – insufficient well compacted concrete for extracting cylinders		20.1	0.6	3.9	7.3	6.6	0.63	0.74
				22.4	0.7	4.0		5.9		
13	Reference mix 1	36.0	2303	19.7	1.0	4.1		7.5	0.58	0.71
				19.0	0.8	4.4		7.1		
14	Reference mix 2	38.7	2306	18.6	0.7	4.2		5.9	0.74	0.85
				20.1	0.6	4.2		5.4		
15	Reference mix no SRA	38.9	2321	20.9	0.8	4.4		5.1	0.84	0.99
				19.9	0.8	4.3		5.3		
16	Reference mix no HA	38.9	2292	18.9	0.8	4.7		6.0	0.75	0.90
				19.0	0.9	4.1		5.7		
17	Mix with fly ash	42.8	2274	21.0	0.9	4.5		6.7	0.59	0.72
				23.7	0.9	3.8		7.3		
18	Mix with limestone filler	45.8	2287	19.1	0.8	4.5		5.9	0.73	0.85
				18.8	0.7	4.5		6.4		
19	Mix with polymer powder	36.6	2286	19.6	0.9	4.5		5.9	0.81	0.93
				17.2	0.9	5.0		5.8		
20	Low matrix mix	41.0	2323	18.9	0.8	4.7		6.7	0.63	0.75
				17.8	0.9	4.3		7.5		

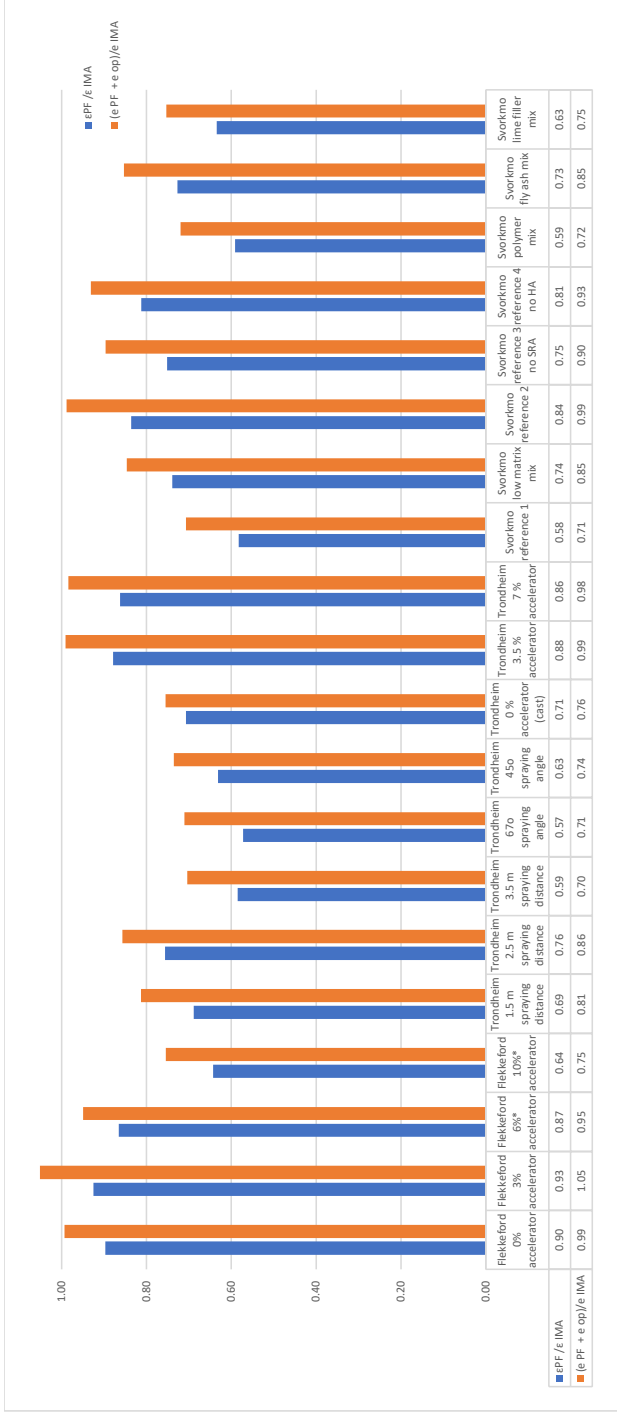


Figure 8 e_{CP}/e_{IMA} and $(e_{CP} + e_{op})/e_{IMA}$ for Flekkeford and Svorkmo series

Figure 9 shows fractions of open macro pore content measured by PF method (y axis) and by pressure saturation as a fraction of image analysis (x axis) for all the sprayed concrete mixes investigated in this study. Figure 9 shows that the fraction of open macro pores detected going from one sided capillary suction to full submersion in water varies from 0.09–0.2 of the total macro pores measured by water suction and pressure saturation (y-axis). The fraction of open macro pores relative to the total macro porosity measured by image analysis (x-axis) varies more, from 0.04–0.43. The one series that was not sprayed but pumped through the nozzle gave an average value of 0.29 on the x-axis which is not in line with the conventional concretes studied by Sellevold and Farstad [10], whereas the value on the y-axis was only 0.06. These results indicate that the two methods of measuring fraction open macro porosity (x axis and y axis) correlate to some extent. Hence the simpler and less laborious PF test can probably be used alone as an indication of open macro porosity in sprayed concrete.

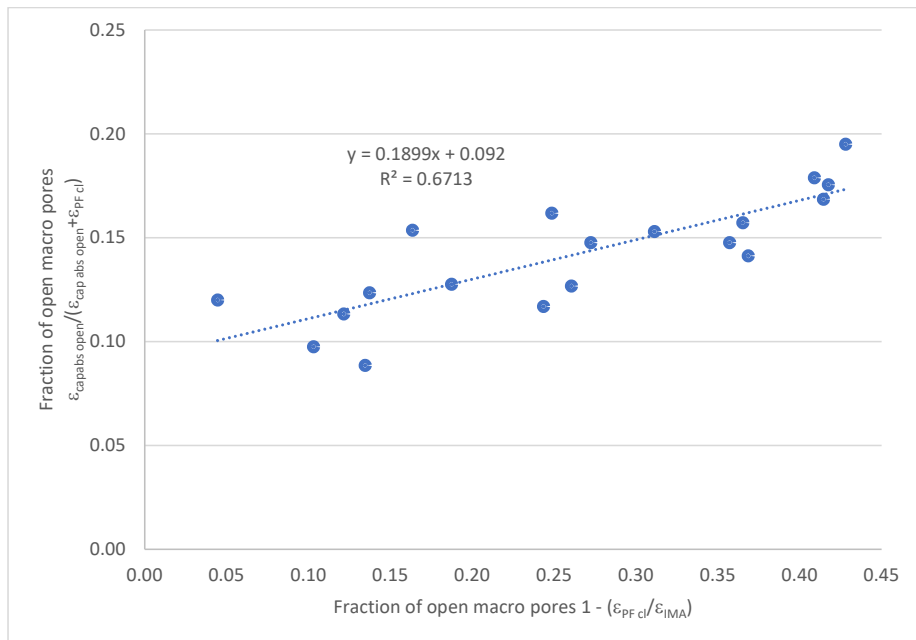


Figure 9 Open/total macro porosity in all sprayed concrete specimens measured by PF method and image analysis

Cumulative macro pore size distribution measured by image analysis are shown in Figure 10 for Flekkefjord and Figure 11 for Trondheim set accelerator experiments. Figure 11 shows that the cast specimens containing zero set accelerator have a higher total macro porosity, with most of the macro pores up to a size of 800 μm. This is due to the air entrainment agent in the concrete mix which forms spherical air bubbles in the fresh concrete. Most of the entrained air content is lost during the spraying process and/or upon impact with the substrate, whereas this air content is retained in the cast concrete. Figure 11 shows that the cumulative macro pore content in the cast concrete diverges from the sprayed at around 150 microns. These results agree with findings from Yun et al. [16] and Beaupré [29]. Figure

10 and Figure 11 show that the samples with lower doses of set accelerator (0–7 %) have similar cumulative macro pore size distributions, whereas the samples containing 10 % set accelerator have a higher content of larger macro pores.

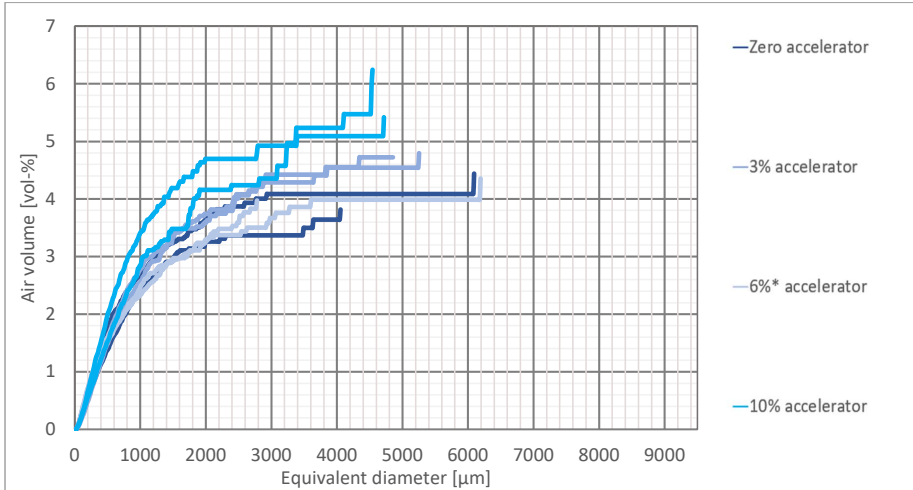


Figure 10 Cumulative macro pore size distribution for the Flekkefjord set accelerator experiments

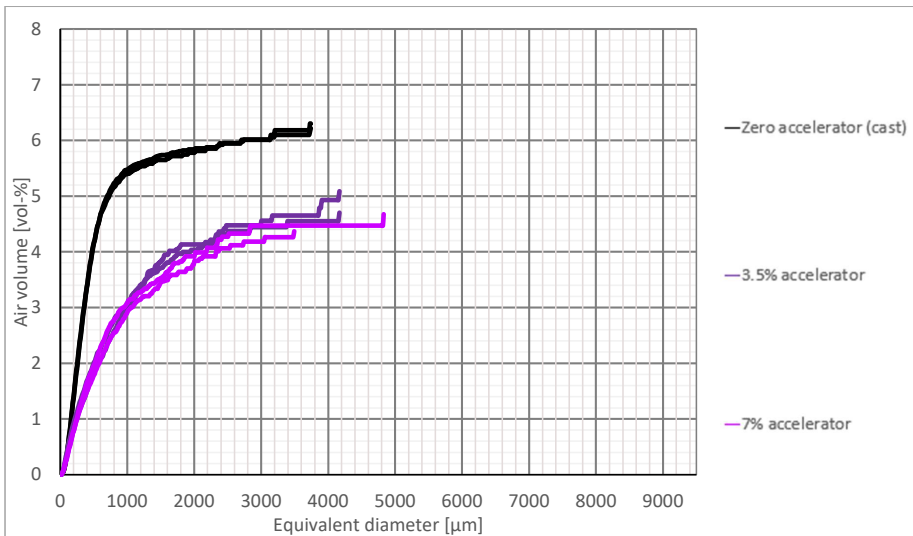


Figure 11 Cumulative macro pore size distribution for the Trondheim set accelerator experiments

3.3. Shape analysis

Cumulative length/width distributions for macro porosity measured by image analysis are shown in Figure 12 for Flekkefjord and Figure 13 for Trondheim set accelerator experiments.

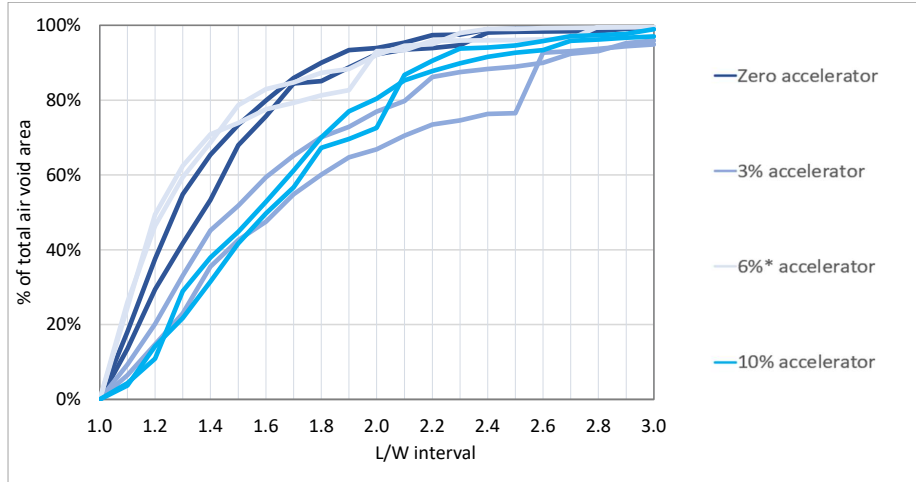


Figure 12 Cumulative length/width distribution for the Flekkefjord set accelerator experiments

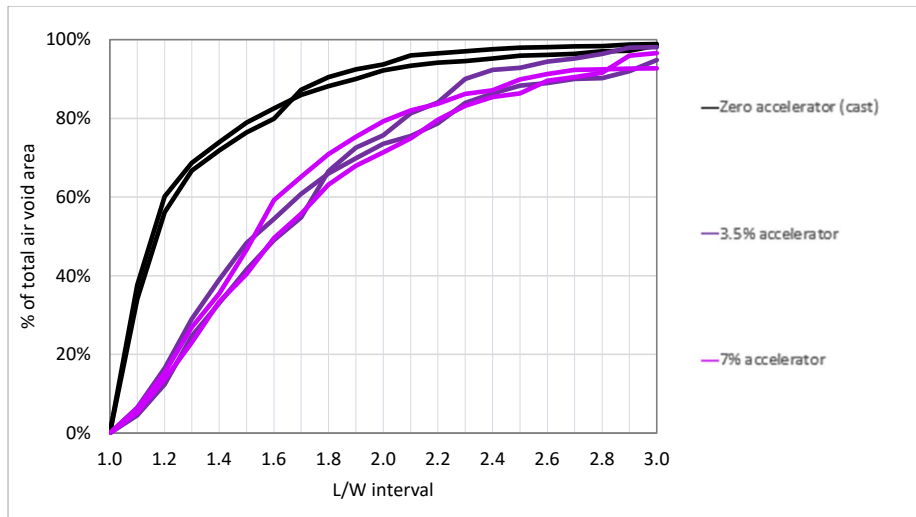


Figure 13 Cumulative length/width distribution for the Trondheim set accelerator experiments

Figure 13 shows a far higher content of spherical macro pores, with length/width ratio close to 1.0, in the cast concrete than in the sprayed concrete samples. The length/width ratio distributions are similar among the sprayed samples with different accelerator doses. Figure 12 shows a slightly lower length/width ratio distribution with increasing set accelerator dose for the Flekkefjord series, suggesting that the sphericity of the macro pores reduces with increasing set accelerator dose. Hence we can infer

that the flash set due to the accelerator affects the formation of the macro pores. All the mixes in this study included an air entrainment agent, which improves the workability of fresh concrete due to the spherical air bubbles [29], though a high proportion of these are lost through the spraying process (Figure 11). We have not investigated the macro porosity in sprayed concrete without an air entrainment agent, though that has been investigated elsewhere [16].

3.4. Orientation analysis and macroscopic effects

The orientation of the macro pores is plotted in Figure 14, Figure 15, Figure 16 and Figure 17 for the Flekkefjord set accelerator experiments, the Trondheim set accelerator experiments, the Trondheim spraying mechanics experiments and the Svorkmo proportioning experiments respectively. Each vector length is the mean of two parallel specimens. Amongst all the series there is a trend of orientation of macro pores towards parallel to the substrate, with 35–50 % of macro pores orientated in this direction, while 20–30 % are orientated normal to the substrate, although there is a degree of scatter in the data. This data demonstrates that sprayed concrete is not an isotropic material. Based on the measurements of elongated, irregularly shaped macro pores (Figure 4–5, Figure 12–13) and the orientations in Figure 14–17, there are possible implications for the concrete properties. The key properties of strength and permeability are affected differently in the directions normal and parallel to the direction of spray application by the elongated macro pores and steel fibres, both tending towards orientation perpendicular to the direction of spray application. Furthermore there is the effect of pulsation of concrete from the nozzle, which may result in a concentration of set accelerator and laminations in the hardened sprayed concrete. So we may expect reduced strength in the direction parallel to the direction of spray application and increased permeability in the perpendicular direction. Hence careful attention to execution is needed during wet spraying.

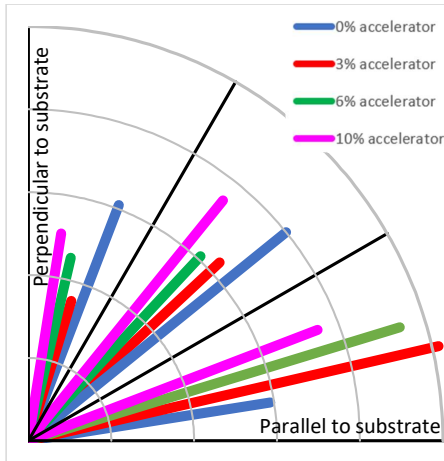


Figure 14 Macro porosity orientation for the Flekkefjord set accelerator experiments

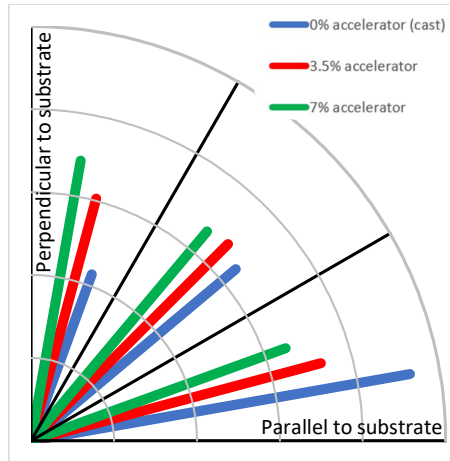


Figure 15 Macro porosity orientation for the Trondheim set accelerator experiments

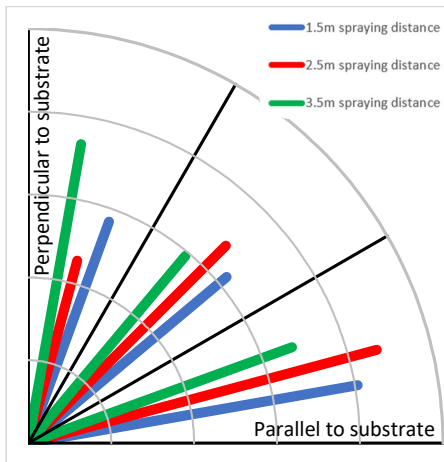


Figure 16 Macro porosity orientation for the Trondheim spraying mechanics experiments

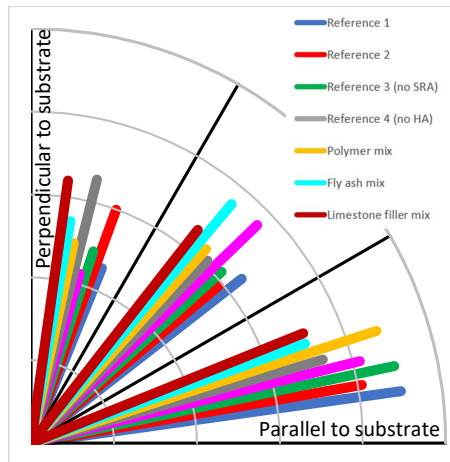


Figure 17 Macro porosity orientation for the Svorkno proportioning experiments

3.5. Water penetration

Examples of measured water penetration fronts for faces of split cubes sprayed with 10 % set accelerator (Figure 18) and 3 % set accelerator (Figure 19) are presented. Table 5 gives all individual measurements and equivalent permeabilities calculated according to Equation 8. Table 5 shows that the sprayed concrete specimens with 3 % accelerator have very low water penetration values. The lowest single values are three specimens with zero water penetration observed with water pressure parallel to the spraying direction though there is a degree of scatter as one specimen has a permeability of $2 \times 10^{-11} \text{ ms}^{-1}$. For the specimens sprayed with 10 % accelerator the water penetration is much higher.

Table 5 Water penetration results, and corresponding permeability coefficients calculated with Equation 8

Sample and orientation	Pressure (MPa)	Duration (hours)	Maximum water penetration depth (mm)	K_{vakuta} (m/s)
3 % normal	0.3	72	31	2.7×10^{-12}
3 % normal	0.1	48	16	3.2×10^{-12}
3 % normal	0.3	72	13	4.7×10^{-13}
3 % normal	0.3	72	41	4.7×10^{-12}
3 % parallel	0.5 (70 hours) and 0.7 (24 hours)	94	10	1.2×10^{-13}
3 % parallel	0.3	72	0	–
3 % parallel	0.5	3	23	2.1×10^{-11}
3 % parallel	0.1	48	14	2.4×10^{-12}
3 % parallel	0.3	72	0	–
3 % parallel	0.3	72	0	–
3 % parallel	0.5	70	6	6.1×10^{-14}
3 % parallel	0.5 (70 hours) and 0.7 (24 hours)	94	11	1.4×10^{-13}
10 % normal	0.1	1.75	84	2.0×10^{-9}
10 % normal	0.1	1.75	67	1.4×10^{-9}
10 % normal	0.1	24	>100	$>2.1 \times 10^{-10}$
10 % normal	0.1	1.75	96	3.1×10^{-9}
10 % parallel	0.3	6.33	70	1.3×10^{-10}
10 % parallel	0.3	6.33	80	1.7×10^{-10}
10 % parallel	0.1	1.75	19	1.0×10^{-10}
10 % parallel	0.1	24	26	1.4×10^{-11}
10 % parallel	0.1	1.75	5	6.6×10^{-12}
10 % parallel	0.1	1.75	14	5.3×10^{-11}

Simultaneously looking at water penetration profiles and polished sections visualizing laminations and macro pores we can observe very low or even zero (Figure 19) water penetration where the water pressure is applied in the same direction as the direction of spraying. In this case the laminations, identifiable in the polished black and white image analysis, are normal to the direction of water pressure, so the water front would have to penetrate layers of properly compacted sprayed concrete before reaching the laminations. Where the water pressure is applied perpendicular to the direction of spraying we can see local areas of higher water penetration. These areas coincide with the laminations, which are again identifiable in the polished black and white image analysis, whereas they are not always identifiable in the unpolished and uncoloured concrete. Applying Equation 8, the results indicate low permeability parallel to the direction of spraying, which is equivalent to water pressure applied to the extrados of a tunnel lining permeating towards the intrados.

Permeability through sprayed concrete linings can be much higher perpendicular to the direction of spraying, which would be in the circumferential (or hoop) direction in a tunnel lining, where layering or laminations in the sprayed concrete occur. These can be caused by pulsation during spraying giving

layers of increased concentration of accelerator, high macro pore content orientated perpendicular to the spraying direction and/or spraying fresh concrete onto hardened concrete. The results demonstrate that the kind of pulsation execution seen in Figure 2 and local variations in accelerator dose may cause large variations in permeability of wet sprayed concrete.

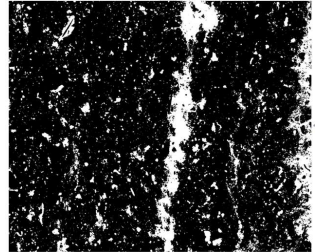
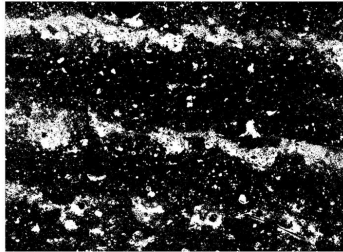
3.6. Fibre content and orientation

The fibre content of the hardened sprayed concrete, as volume %, was measured by crushing hardened specimens, extracting the fibres by hand and with a magnet and weighing the fibres, which was then compared to the volume which had been measured by weighing the sample in air and water. The fibre content measured by this method and that measured by CT scanning on adjacent cores from the same panel, is shown in Table 6, along with a measure of fibre orientation. The proportioned fibre content of the fresh concrete was 0.42 volume % and the theoretical volume for the placed concrete should be 0.37 volume % after correction for addition of accelerator and measured macro porosity. We see a little fibre loss in the samples, though the fibre content in the concrete sprayed perpendicular at a distance of 1.5 m has a slightly higher fibre content than the proportioned value. There is scatter in the fibre content of the different samples, but a slight trend of decreasing fibre content with increasing spraying distance / spraying angle from perpendicular. Any fibre loss would be due to rebound.

Examples of the fibre orientation measurements are shown in Figure 20, with the direction of sprayed concrete application perpendicular to the substrate for Figure 20 (a) and at 45° for Figure 20 (b). Figure 20 (a) shows that the orientation of the fibres tends towards perpendicular to the direction of spraying, so parallel to the substrate. Figure 20 (b) shows that at the bottom of the core, where the concrete was sprayed directly onto the substrate, the fibres tend to align parallel to the substrate, whereas as the thickness was built up this alignment changes to orientation at 45° to the substrate, so still perpendicular to the direction of spray application.

Table 6 Fibre content and orientation

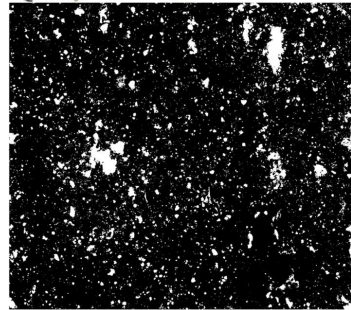
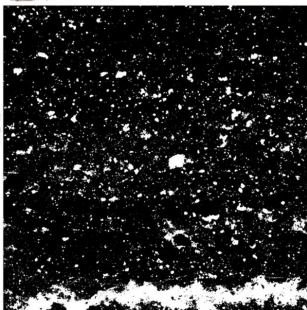
	Fibre content measured manually (volume %)	Fibre content measured by CT scan (volume %)	Median fibre orientation from substrate (degrees)
1.5 m spraying distance	0.42	0.66	30.8
2.5 m spraying distance	0.38	0.31	30.3
3.5 m spraying distance	0.27	0.40	31.3
67° spraying angle	0.35	0.31	28.9
45° spraying angle	Not measured	0.34	31.8



10% accelerator, water pressure applied parallel
 $e_{\max} = 5 \text{ mm}$, 0.1 MPa, 1.75 hr
 $K_{\text{Valenta}} = 6.6 \times 10^{-12} \text{ m/s}$

10% accelerator, water pressure applied normal
 $e_{\max} = 96 \text{ mm}$, 0.1 MPa, 1.75 hr
 $K_{\text{Valenta}} = 3.1 \times 10^{-9} \text{ m/s}$

Figure 18 Water penetration front (top) for adjacent cubes sprayed with 10 % set accelerator with the water applied parallel to the direction of spraying (left) and perpendicular to the direction of spraying (right).



3% accelerator, water pressure applied parallel
 $e_{\max} = 0 \text{ mm}$, 0.3 MPa, 72 hr
 $K_{\text{Valenta}} < 3 \times 10^{-15} \text{ m/s}$

3% accelerator, water pressure applied normal
 $e_{\max} = 41 \text{ mm}$, 0.3 MPa, 72 hr
 $K_{\text{Valenta}} < 4.7 \times 10^{-12} \text{ m/s}$

Figure 19 Water penetration front (top) for adjacent cubes sprayed with 3 % set accelerator with the water applied parallel to the direction of spraying (left) and perpendicular to the direction of spraying (right)

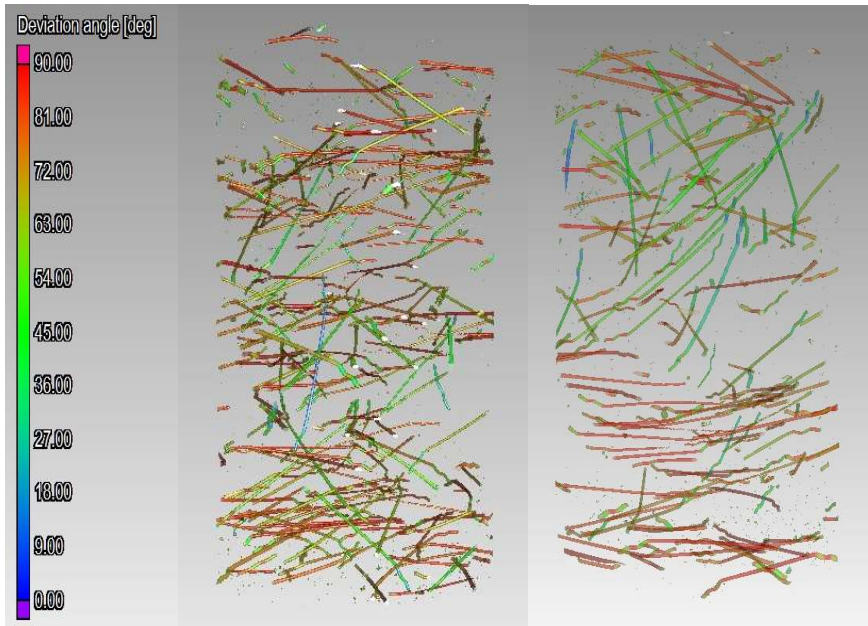


Figure 20 Fibre orientation measurements by CT scanning for cores from panel sprayed with (a) nozzle perpendicular to and at a distance of 1.5 m from substrate and (b) nozzle at 45° to substrate at a distance of 1.5 m. Scale is deviation from the z-axis (vertical).

4. Conclusions

- Macro pores are ubiquitous in sprayed concrete and are non-spherical in shape. These irregular macro pores due to the spraying process are different to the spherical pores caused by use of an air entrainment agent in the fresh concrete. The spray application causes most of the spherical entrained air bubbles due to use of an air entrainment agent to be lost.
- There is a trend of increased macro porosity with increasing set accelerator dose.
- The image analysis method measured higher macro pore content than the PF method and this excess macro pore content can be interpreted as open macro pores, made up of 7–43 % of the macro porosity measured by image analysis.
- Macro porosity measured by CT scanning was higher than that measured by PF method.
- CT scanning gives us a new, quick and non-destructive laboratory method to measure porosity. It can also be used to give information on the shape and size distribution of macro pores. It is quicker than the PF and image analysis methods, though post-processing can take some time.
- The orientation of macro pores (i.e. the longest internal dimension of the macro pore) tends to orientate perpendicular to the direction of spraying.

- Laminations can occur in sprayed concrete. One cause of laminations is that this is a part of the material that has received a higher accelerator dose due to pulsation in the concrete flow. Another would be spraying fresh concrete onto hardened concrete. Water penetration tests indicated that these laminations cause the permeability perpendicular to the direction of spraying to be far higher than parallel to the direction of spraying. Hence careful attention to execution is needed during wet spraying.
- Fibres in sprayed concrete align towards parallel to the substrate. Where the direction of application is not perpendicular to the substrate, the fibres orientate towards parallel in the initial sprayed thickness before tending towards perpendicular to the direction of spraying in subsequent thickness.
- Due to the tendency for the fibres and macro pores to be orientated perpendicular to the direction of spraying, as well as the presence of laminations with lower permeability normal to spraying than parallel to spraying, sprayed concrete is an anisotropic material.

5. Acknowledgement

This paper is a part of the research project “Sprayed sUustainable Permanent Robotized CONcrete tunnel lining (SUPERCON)” financed by the Research Council of Norway (project no. 294724), in cooperation with industrial partners AMV, BASF, Bever Control, Bekaert, Elkem, Entreprenørservice, NORCEM, SWECO Norge, Veidekke, Wacker Chemicals Norway and Unicon AS. Research partners in SUPERCON are NGI, NTNU and SINTEF. The following project owners support the project; Bane NOR, Nye Veier and the Norwegian Public Roads Administration.

Thanks to Karl Gunnar Holter from the Norwegian Geotechnical Institute for leading most of the full-scale spraying experiments, and to Erik Johansen from SINTEF and Per Øystein Nordtug from NTNU for help with preparation of specimens.

6. References

- [1] W. Aldrian, A. Thomas and K. G. Holter, “Permanent Sprayed Concrete Linings – an international update,” *Spritzbeton-Tagung 2021*, pp. 1-15, 2021.
- [2] I. Galan, A. Baldermann, W. Kusterle, M. Dietzel and F. Mittermayr, “Durability of shotcrete for underground support - review and update,” *Construction and Building Materials*, vol. 202, pp. 465-493, 2019.

- [3] C. J. Manquehual, P. D. Jakobsen, K. G. Holter, K. D. Weerd and A. Bruland, "Investigation of leaching in steel fiber-reinforced shotcrete exposed to fresh and saline groundwater in a subsea road tunnel," *Cement and Concrete Research*, vol. 163, no. 107011, p. 21, 2023.
- [4] K. G. Holter, PhD thesis: Properties of waterproof sprayed concrete tunnel linings, Trondheim: Norwegian University of Science and Technology, 2015.
- [5] T. N and S. Jacobsen, "Review of Sprayability of Wet Sprayed Concrete," *Nordic Concrete Research*, vol. 63, no. 2, pp. 21-41, 2020.
- [6] J. Kaufmann, K. Frech, P. Schuetz and B. Münch, "Rebound and orientation of fibers in wet sprayed concrete applications," *Construction and Building Materials*, vol. 49, pp. 15-22, 2013.
- [7] L. Segura-Castillo, S. H. P. Cavalaro, C. Goodier, A. Aguado and S. Austin, "Fibre distribution and tensile response anisotropy in sprayed fibre reinforced concrete," *Materials and Structures*, vol. 51, no. 29, p. 12, 2018.
- [8] A. M. Neville, *Properties of Concrete*, Harlow, England: Pearson, 2011.
- [9] Y. Bu, R. Spragg and J. Weiss, "Comparison of the Pore Volume in Concrete as Determined Using ASTM C642 and Vacuum Saturation," *Advances in Civil Engineering Materials (ASTM)*, vol. 3, no. 2, pp. 1-9, 2014.
- [10] E. J. Sellevold and T. Farstad, "The PF-method – a simple way to estimate the w/c-ratio and air content of hardened concrete," in *Construction materials: performance, innovations and structural implications*, Vancouver, Canada, 2005.
- [11] Standard, "ASTM C457: Standard Test Method for Microscopical Determination of Parameters of the Air-Void System in Hardened Concrete," ASTM International, 2016.
- [12] P. C. Fonseca and G. W. Scherer, "An image analysis procedure to quantify the air void system of mortar and concrete," *Materials and Structures*, vol. 48, pp. 3087-3098, 2015.
- [13] S. R. Stock, "Recent advances in X-ray microtomography applied to materials," *International materials reviews*, vol. 53, pp. 129-181, 2008.
- [14] I. Asadi, N. Trussell, M. S. Hårr, G. Kjekka, P. E. Endrerud, E. Grøv and S. Jacobsen, "Macro pore content in wet-sprayed concrete characterized by CT scanning," in *fib International Congress*, Oslo, 2022.
- [15] S. A. Myren and Ø. Bjøntegaard, "Fibre reinforced sprayed concrete (FRSC): mechanical properties and pore structure characteristics," in *7th International Symposium on Sprayed Concrete*, Sandefjord, 2014.
- [16] K.-K. Yun, S.-Y. Choi, B.-S. Seo, B.-S. Jung and C.-K. Jeon, "Air void structures in blended-cement wet-mix shotcrete," in *Shotcrete: Elements of a System*, London, Taylor & Francis Group, 2010, pp. 291-298.

- [17] H. S. Armelin and N. Banthia, "Mechanics of aggregate rebound in shotcrete - Part I," *Materials and Structures*, vol. 31, no. March, pp. 91-98, 1998.
- [18] Norwegian Concrete Association, "Publication no.7: Sprayed concrete for rock support," Oslo, 2011.
- [19] G. Zirgulis, Fibre orientation quantification methods and influence of formwork surface and reinforcement bars in structural elements, PhD thesis, Trondheim: Norwegian University of Science and Technology, 2015.
- [20] Standard, "EN 14651: Test method for metallic fibre concrete - measuring the flexural tensile strength (limit of proportionality (LOP), residual)," 2005.
- [21] N. Trussell, R. Cepuritis and S. Jacobsen, "Effect of Set Accelerator on Properties of Wet Sprayed Concrete," *Nordic Concrete Research*, vol. 66, no. 1, pp. 21-41, 2022.
- [22] S. Smeplass, "Capillary absorption as a quality criterion (in Norwegian)," SINTEF, Trondheim, Norway, 1988.
- [23] "JMicroVision," [Online]. Available: <https://jmicrovision.github.io/>. [Accessed August 2021].
- [24] Standard, "EN 12390-8: Testing hardened concrete part 8: depth of penetration of water under pressure," 2019.
- [25] T. C. Powers, L. E. Copeland, J. C. Hayes and H. M. Mann, "Permeability of hardened Portland cement paste," *Journal of the American Concrete Institute*, vol. 26, no. 3, pp. 285-298, 1954.
- [26] R. D. Hooton, "Concrete permeability and the search for the Holy Grail," in *The first Canadian symposium on cement and concrete*, Quebec, 1989.
- [27] Volume Graphics, VGStudio MAX 3.4, 2021.
- [28] S. U. Lee, S. Y. Chung and R. H. Park, "A comparative performance study of several global thresholding techniques for segmentation," *Computer vision, graphics and image processing*, vol. 52, no. 2, pp. 171-190, 1990.
- [29] D. Beaupre, Rheology of high performance shotcrete, PhD thesis, Vancouver: University of British Columbia, 1994.

Paper V

Water transport in cracks controlled by digital image correlation in wet sprayed concrete with and without an EVA based co-polymer admixture

Nicholas Trussell*, Per Øystein Nordtug, Iman Asadi, Martin Kristoffersen, Stefan Jacobsen

Department of Structural Engineering, Norwegian University of Science and Technology

Abstract

Experiments were undertaken on wet sprayed concrete discs to investigate the effect of cracking on capillary suction and permeation through sprayed concrete for tunnel linings. The 98 mm diameter, 50 mm thick discs were cracked by tensile splitting, with the crack widths controlled and measured by digital image correlation and also checked by microscope measurements. Both a standard sprayed concrete mix and a mix containing an EVA (ethylene-vinyl-acetate) based co-polymer powder were tested. Cracks increased the rate of capillary suction compared to uncracked samples, due to rapid rise of water in the crack and absorption occurring over the surface area of the crack in addition to the area of the base of the disc. Discs with wider crack widths exhibited a higher rate of water permeation per area of crack. Inclusion of the EVA based co-polymer reduced the rate of capillary suction and the permeation flow rate coefficient (measured flow / theoretical viscous laminar flow) for a given crack width compared to the standard mix. Self-healing occurred both during water permeation and water storage of cracked discs. The use of CT scanning to measure the crack through the full thickness of a disc was explored and compared to crack width measurements made at one surface of the disc only.

Keywords: Sprayed concrete, shotcrete, cracking, permeation, capillary suction, polymer, healing

1. Introduction

Sprayed concrete tunnel linings in contact with water-bearing ground are subjected to water transport. The pathways for groundwater and deleterious substances through the sprayed concrete tunnel lining are the capillary pore system or cracks in the lining. Water transport through tunnel linings is undesirable due to visible water ingress within the tunnel, durability of the fixings and fittings within the tunnel and for the durability of the concrete lining itself. Water transport underlies most degradation

* Corresponding author.

E-mail address: nicholas.h.trussell@ntnu.no (Nicholas Trussell)

Submitted to *Construction and Building Materials*

phenomena in concrete [1]. Water transport through the lining and evaporation at the intrados leads to an accumulation of deleterious substances, yielding higher concentrations in the concrete and this can be detrimental to the durability. Transport of water through the concrete linings also leads to leaching [2]. The durability of sprayed concrete tunnel linings can be improved by improving the water tightness of the linings. Hence the sustainability can be improved, given that increased service life leads to reduced environmental impact. Durability of sprayed concrete linings is important with increased use of wet sprayed concrete worldwide due to the global need for underground infrastructure [3]. So limiting water transport through the concrete is vital to achieve durable, permanent, sprayed concrete linings. It is also important to increase our understanding and knowledge of the sprayed concrete material, given that we only have approximately 50 years' experience with wet sprayed concrete and only around 25 years' experience with alkali-free set accelerators for sprayed concrete [4].

Sprayed concrete typically has a water/effective binder ratio of 0.45 or less, including the water content of the set accelerator added at the nozzle [5]. But the capillary porosity is higher due to the effect of the set accelerator on the hydration products [6] [7]. The capillary porosity is the path for water transport in bulk concrete. Holter [8] performed water permeability measurements with 0.5 MPa water pressure on 35 sprayed concrete specimens without imperfections (i.e. without cracks and large macro pores) from three different tunnels in Norway. He measured permeability between 3.3×10^{-11} and $9.6 \times 10^{-12} \text{ ms}^{-1}$ in four of the specimens, whilst measuring zero water flow through the remaining specimens. With the sensitivity of the equipment being $5 \times 10^{-14} \text{ ms}^{-1}$, we can conclude from Holter's results that crack free and well compacted sprayed concrete can have a very low water permeability of less than $5 \times 10^{-14} \text{ ms}^{-1}$.

But cracking is inevitable in sprayed concrete linings. Linings experience cracks at joints between consecutive applications of sprayed concrete and due to shrinkage [8] [9]. Shrinkage cracking can occur in sprayed concrete as it is restrained when sprayed onto the rock surface or previous layer. Furthermore the initial temperature rise due to the cement hydration precedes cooling, which also may induce tensile strains and hence cracks, as concrete has a thermal expansion and shrinkage coefficient in the order of 10^{-5} K^{-1} [10]. Such cracks present paths for water transport [8], which is higher than through the capillary porosity by orders of magnitude.

In the following sections we review the transport mechanisms, factors and methods for the study of transport through cracks in sprayed concrete tunnel linings. Capillary suction, diffusion and permeation are the three main transport mechanisms for flow through concrete tunnel linings. In cracks, however, diffusion is less significant than permeation and capillary suction because the increase of flow is only proportional to crack cross sectional area as a fraction of the exposed concrete surface area [11]. So we consider capillary suction and permeation as the most important transport mechanisms.

1.1 Capillary suction

We can consider the rise y (m) at time t (s) of a liquid in an ideal crack given by Equation (1), which is derived from the LaPlace equation [12],

$$y(t) = \sqrt{\frac{w \sigma_{lg}}{4\eta}} \cdot \sqrt{t} \quad (1)$$

where w (m) is the crack width, σ_{lg} (N/m) is the surface tension at the air-water meniscus, and η (Pa.s) is the dynamic fluid viscosity. Considering concrete discs of height of 50 mm (0.05 m), the water rise calculated from Equation (1) is shown in Figure 1 using crack widths $w \in \{0.05, 0.10, 0.20, 0.30\}$ in mm, with $\sigma_{lg} = 0.073$ N/m and $\eta = 0.001$ Pa.s. The water under suction in these cracks should theoretically rise to the top the disc in a few seconds, whereas the rise in the bulk concrete with a resistance number of 10^8 (typical value[13]) is far slower. So we can expect capillary suction to be faster in cracked concrete.

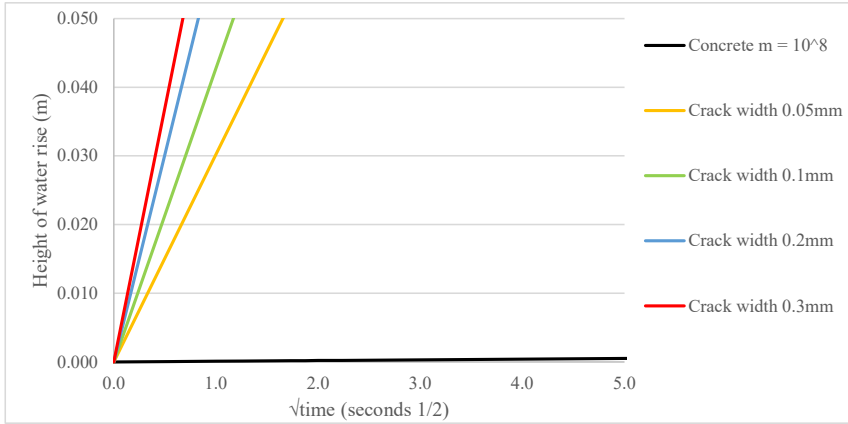


Figure 1 Expected rise of water in cracks calculated from Equation (1) compared with the rise in bulk uncracked concrete due to capillary suction

1.2 Permeation

Equation (2) [14] defines the flow rate Q (in m³/s) of a liquid permeating through a crack, excluding any flow in the bulk, uncracked material.

$$Q = \frac{\zeta w^3 b \Delta P}{12\eta L} \quad (2)$$

Here, ΔP is the pressure difference (in Pa), while L is the length (in m) over which the pressure difference acts and b is the length of the crack (in m). The tortuosity, roughness and discontinuity of the crack is accounted for by the flow rate coefficient, ζ . Equation (2) states that flow rate Q is proportional to w^3 , so crack width is the key criterium for flow through cracks.

Alternatively, we can consider the flow velocity (m/s) of a liquid permeating through a crack with Equation (3):

$$v = \frac{\zeta w^2 \Delta P}{12\eta L} \quad (3)$$

Here, the expression $\frac{\zeta w^2}{12\eta}$ can be considered the Darcian permeability coefficient for steady state flow velocity in the crack. The flow rate coefficient, ζ is equal to the measured flow rate divided by the theoretical, as defined in Equation (4). For viscous laminar flow through an ideal crack, $\zeta = 1$.

$$\zeta = \frac{Q_{measured}}{Q_{theoretical}} \quad (4)$$

Hence the flow rate coefficient can be calculated from flow rate measurements by rearranging Equation (2) to form Equation (5),

$$\zeta = \frac{12Q_{measured}\eta L}{w^3 b \Delta P} \quad (5)$$

1.3 Cracking and water transport

There are several methods to obtain controlled crack widths for laboratory experiments. Recent studies have used tensile splitting given it can give a constant tension over the centreline of the specimen and given the simple experimental set-up. Rapoport et al [15] carried out tensile splitting (Brazilian) tests on fibre reinforced concrete discs and the samples were cracked to specific crack widths. After cracking, the discs were tested for permeability. They found a linear relationship between the crack width and the logarithm of the permeability of the cracks.

Akhavan et al [16] measured water permeation through cracks with increasing crack width. The cracks were formed by tensile splitting, with the crack width measured indirectly using linear variable differential transformers (LVDTs) at the sides of the samples. They measured increasing crack permeability with increasing crack width and determined that crack permeability, represented by $\zeta w^2/12\eta$ in equation (2), is a function of the crack width squared. They calculated Reynolds numbers lower than 118, confirming the flow to be laminar. They investigated crack tortuosity and modified the Louis equation [16] with a tortuosity factor to calculate crack permeability as a function of crack geometry.

Rastiello et al [17] also measured water permeation through cracks. The cracks were formed by tensile splitting, with the crack width again measured indirectly using LVDTs at the sides of the samples. Rastiello et al measured water permeation through the crack simultaneously to tensile splitting. Separate tests, without water permeation through the crack, used digital image correlation to validate the crack measurements from the LVDTs. They measured increasing crack permeability with increasing crack width, with permeability values from 10^{-12} m/s for crack widths of 0.02 mm to 10^{-9} m/s for crack widths of 0.14 mm. They calculated Reynolds numbers to confirm the flow to be laminar.

Ripphausen [14] performed water permeation tests through cracks in reinforced concrete slabs

and determined flow rate coefficients between 0.005 and 0.17, though with a larger, more traditional set-up to form the cracks. Clear [18], also with a different set-up to form the cracks, used equation (2) but without the flow rate coefficient ζ . Instead he solved for crack width and used the measured flow rate to calculate the “effective crack width”, which he used to describe the cracks. In this work we choose to use the factor ζ to quantify how the measured flow deviates from theoretical laminar flow.

1.4 Crack healing

Edvarsen [19] stated that precipitation of calcium carbonate in the crack is the primary cause of autogenous healing and is initially faster and slows significantly over time. Clear [18] determined that initial autogenous healing is due to mechanical blocking before precipitation of calcium carbonate. Crack width is the most significant factor that influences the rate of crack healing [19], with the water pressure the second most significant factor [19]. White precipitate at the surface of concrete members indicates calcite formation [19] [20].

Reinhardt & Jooss [21] tested water permeation through cracks formed by tensile splitting and studied self-healing. They measured a 55 % reduction in flow rate through a crack of 0.05 mm width after 25 hours. They measured just 2 % of the initial flow rate after 336 hours in this sample and 14 % of the initial flow rate through a crack of width 0.15 mm. Akhavan et al [16] also measured crack healing, with up to an 85 % reduction in crack permeability after 24 hours of water permeation, with the permeability of narrower cracks reducing more than wider cracks.

1.5 Sprayed concrete with set accelerator

In sprayed concrete set accelerators based on aluminium sulphates [22] are added at the nozzle to give rapid set as the concrete hits the substrate. These accelerators affect the hydration and give different hydration products [6] [23] [24] [25]. Therefore it is important to investigate whether sprayed concrete with set accelerator has self-healing properties. Study of crack healing of sprayed concrete with set accelerator is of interest given the waterproofing function of tunnel linings and the limited knowledge of self-healing in sprayed concrete with set accelerators. We have not found any laboratory studies of self-healing of sprayed concrete, but evidence of crack healing, by precipitation of white calcium carbonate, can often be seen in sprayed concrete tunnel linings, as recorded by Aldrian et al [26].

1.6 Polymer admixtures

The effect of polymers on transport in bulk concrete, i.e. transport through the capillary pores, has been investigated previously but (to our knowledge) not for transport through cracks. Ohana [27] reported that upon hardening, the polymer particles form a film of polymer, or a co-matrix, around aggregates. Ohana reported that polymer modified concrete has a lower water permeability and water absorption [27]. Øye [28] reported a strong decrease in the rate of capillary suction in polymer modified mortars.

Justnes et al [29] measured capillary suction and vapour diffusion in mortars with various redispersible polymer powders. They determined reduced diffusion coefficients and reduced rates of capillary suction with increased polymer content in mortars.

Ethylene-vinyl-acetate (EVA) co-polymer based waterproofing membranes are commonly used between layers of sprayed concrete tunnel linings [8]. But inclusion of EVA co-polymers may be used in the concrete itself to modify the properties of the concrete with respect to water transport properties. Bonin [30] reported visual assessment of water permeation through sprayed concrete containing different dosages of ethylene-vinyl-acetate (EVA) co-polymer. With application of firstly 0.15 then 0.6 MPa water pressure on one side of the concrete he reported damp patches on the other side of the sprayed concrete with zero co-polymer. He observed the surface of the sprayed concrete containing 7.5 % co-polymer by binder mass to be dry after 0.15 MPa water pressure while that containing 10 % of co-polymer was observed to be dry after both 0.15 and 0.6 MPa water pressure application.

Lee et al [31] studied the effect of polyacrylate based superabsorbent polymers included as admixtures on crack healing in concrete. They found peak flow decreased to negligible flow rates after around 10 hours, faster than in the reference concrete without the polymer admixture. While polymers are a wide group of materials with different properties as admixtures, reviews [32] [33] have summarised the effect of various polymers on self-healing of cracks, indicating that polymers can have a positive effect on healing of cracks.

1.7 CT scanning

X-ray computed tomography (CT scanning) is a non-destructive test for visualizing the microstructure of concrete [34]. This technique provides a three-dimensional image of the specimen and can be used to measure crack volume, geometry and continuity. This may help study cracks through the full thickness of specimens, whereas otherwise cracks can only be measured at the surfaces. In this study we explore measuring cracks by CT scanning and present the results on a single specimen, comparing the crack measurements with those by digital image correlation on the surface only.

1.8 Scope

From the reviewed literature it seems that research is needed in the field of flow through cracks in sprayed concrete tunnel linings. The spraying production technique with the addition of set accelerator at the nozzle causes a distinct material with a different pore structure and hydration products compared with conventional concrete [9]. Hence there is a need to investigate aspects such as the water transport in the cracks and how it is affected by varying crack widths, use of a polymer admixture and the self-healing potential of sprayed concrete.

This paper investigates the effect of cracking in sprayed concrete on two water transport mechanisms: capillary suction and permeation. An ordinary sprayed concrete mix is compared to one containing an ethylene-vinyl-acetate (EVA) based dispersible co-polymer powder to investigate the

effect of this co-polymer on water transport in the cracked concrete. The fresh concrete was mixed at a commercial plant and panels were sprayed in full scale experiments with wet spraying equipment. The placed composition [9] was corrected for the macro pore content in the hardened sprayed concrete, measured optically on cored specimens, and the effective water/binder ratio was calculated including the water content of the accelerator added at the nozzle.

Cracks were formed by tensile splitting of the steel fibre reinforced sprayed concrete discs and the crack widths were controlled and measured by digital image correlation (DIC) using the in-house developed code eCorr [35]. The crack widths were also measured with an optic microscope to check the validity of the DIC measurements. Capillary suction testing was then performed on both cracked and uncracked discs to determine the effect of the cracking on the rate of capillary suction. Water permeation tests were performed on cracked specimens. Both a standard sprayed concrete mix and a mix containing an ethylene-vinyl-acetate (EVA) based dispersible co-polymer powder were tested, to investigate the effect of the co-polymer on water transport in the sprayed concrete. A single cracked disc was retested after storage in water to investigate the effect of crack healing. CT scanning was used to measure the crack through the full thickness of the disc, to explore the potential of this method.

2. Experimental work

2.1 Spraying of samples

The samples were produced by full-scale concrete wet spraying equipment in an access tunnel in Svorkmo, near Orkanger in Norway. The concrete spraying machine was a Normet Spraymec NorRunner 140 DVC shotcrete robot. The concrete was sprayed onto panels orientated at 75° to the horizontal, with the nozzle perpendicular and 1.5 m from the panels whilst spraying at a concrete flow rate of 15–20 m³/hour. 7 % set accelerator (MasterRoc SA 188) of cement mass was added at the nozzle.

2.2 Proportioning of sprayed concrete and fresh concrete properties

Three mixes were tested for this study – the first two mixes are standard sprayed concrete mixes, the difference between them being the type of steel fibre. The third mix contains an ethyl-vinyl-acetate (EVA) co-polymer – Etonis 3500 W. The placed concrete compositions were calculated following the method outlined by Trussell & Jacobsen [9] and are shown in Table 1. The placed compositions are corrected for the measured air content of the fresh concrete, the addition of the set accelerator at the nozzle and the measured air content of the hardened sprayed concrete measured by image analysis following [36]. The mixes contained super-plasticiser (MasterEase 1020, a polycarboxylate based solution), air entrainment agent (MasterAir 11, tenside based surfactant), retarder (MasterRoc HCA 20), a prototype shrinkage reducing agent (from Master Builders Solutions) and a hardening accelerator based on seeding (Master X-Seed 100). The 0–4 mm aggregate was crushed gabbro rock with a particle

density of 3030 kg/m³ and a water absorption of 0.5 % by mass. The 0–8 mm sand was natural fluvial glacial deposits with mainly granitic gneiss and some sandstone and mafic rock with a particle density of 2720 kg/m³ and 0.7 % water absorption by mass. The cement was Norcem standard fly ash cement (CEM II/B-M 42.5 R).

2.3 Preparation of specimens

The sprayed concrete panels were stored in the tunnel wrapped in plastic at 10–15 °C for three weeks before being transported to the lab. Cores of 98 mm diameter were taken from the panels and these were stored in water for 70 days at room temperature. 50 mm discs were cut from these cores. The discs were sprayed with a solid white background paint and a black speckled pattern to aid use of DIC, as shown in Figure 2.

Table 1 Placed concrete compositions for the full-scale spraying experiments

Phase	Constituent	Standard mix 1			Standard mix 2			Mix with Etonis		
		Mass [kg/m ³]	Volume [l/m ³]	Volume [l/m ³]	Mass [kg/m ³]	Volume [l/m ³]	Volume [l/m ³]	Mass [kg/m ³]	Volume [l/m ³]	Volume [l/m ³]
Matrix phase	Standard fly ash cement	447	149	507	452	151	498	432	151	499
	Water	211	211		215	215		204	204	
	Silica fume	18.6	8.4		18.8	8.5		18.1	8.2	
	Super plasticiser	4.0	3.8		4.1	3.9		3.9	3.7	
	Air entrainment agent	0.62	0.61		0.63	0.61		0.59	0.58	
	Retarder	1.0	0.89		1.0	0.90		0.46	0.42	
	Shrinkage reducing agent	2.3	2.5		2.4	2.5		2.3	2.4	
	Hardening accelerator	7.6	6.7		7.7	6.8		7.8	6.8	
	Etonis 3500 W	-	-		-	-		19.3	18.0	
	Set accelerator (solids)	16.9			17.1			16.3		
	Aggregate (<0.125 mm)	140	50.8		143	51.7		143	52	
Air (measured)		73.0		56.8		58.5				
Particle phase	0 – 4 mm aggregate (> 0.125 mm)	1343	488	493	1366	497	502	1364	496	501
	Steel fibres	38.0	4.8		38.5	4.9		38.7	4.9	
SUM		2230	1000	2266	1000	2250	1000			
Effective water/binder ratio		0.457		0.462		0.459				

2.4 Tensile splitting

Two points were marked at 20 mm on each side of the vertical diameter of the disc before applying the tensile splitting load to the top and bottom of the disc. These points were used for the digital extensometer; the length extension between these two points was monitored in real-time, as indicated in Figure 2, to measure an extension equivalent to the target crack widths of 0.2–0.4 mm, after which the load application was stopped. The compressive force was applied by increasing vertical displacement at the top of the disc of 1.0 mm/minute. The experimental set-up is shown in Figure 3.

The compressive force was applied in the direction perpendicular to the orientation of spraying,

and in the same plane as dominant fibre orientation (given that the fibres orientate perpendicular to the direction of spray application [37]). Thus this compressive force is applied in the same direction as a hoop compressive force in a tunnel lining, so can be considered to simulate such a force. A typical single crack is shown in Figure 4 – Figure 7.

2.5 Digital image correlation for crack measurement

DIC analyses based on finite elements (FE) were run to measure the global displacement field [35]. The nodal displacements are found by iteratively building and solving a linear system of equations [38]. The displacements are constrained to being continuous and are optimised to minimise the grayscale residuals for the part of the image covered by the mesh. The finite element solution is thus not ideal after cracks appear, although some accommodations can be made for the crack path in the FE mesh. Still, it is possible to estimate the location of a crack by a localised spike in grayscale residuals as illustrated in Figure 4. Thus, the crack widths were rather measured by the subset tracking option in the DIC code.

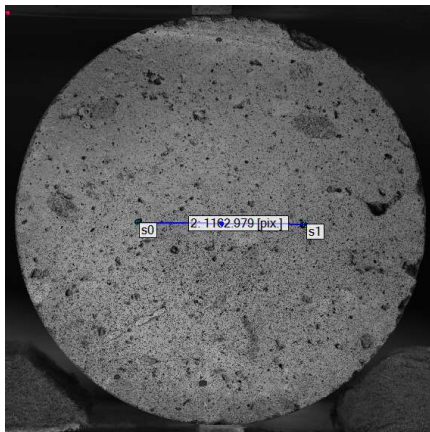


Figure 2 A specimen with the positions for the subsets used for crack measurement, also acting as a digital extensometer.

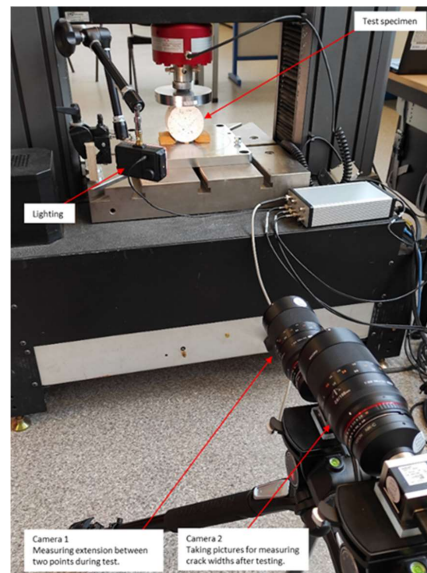


Figure 3 Experimental set-up of tensile splitting test.

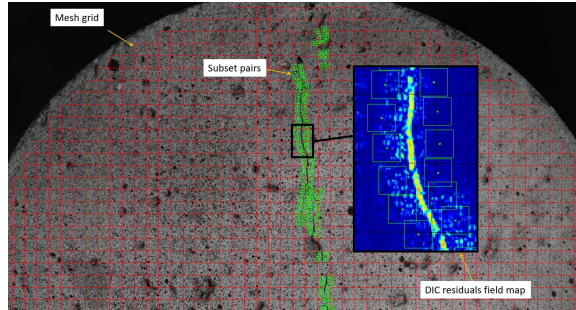


Figure 4 Example of a specimen with subset pairs placed along a crack represented by the grayscale residuals.

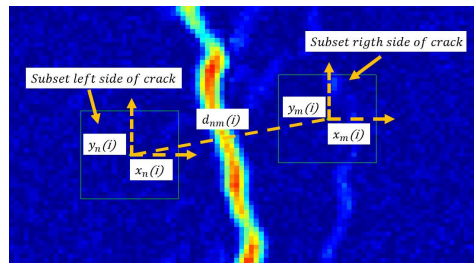


Figure 5 Diagram showing measurement of displacement in x and y directions to measure the change in distance between subset pairs.

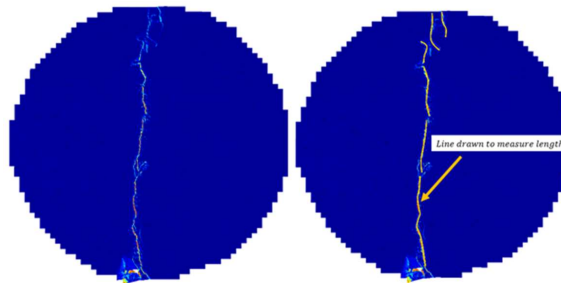


Figure 6 Diagram of cracks on specimen S11, with yellow lines drawn in software to measure crack length.

Using the DIC residual field map to determine where the cracks appeared on the surface of each sample, subset pairs were placed on opposing sides normal to the crack along the length of the crack. The crack widths were found by measuring the relative rigid body pixel displacement between the subsets in each pair as shown in Figure 5. The average crack width is then the average relative displacement over all subset pairs. In addition, the crack length in pixels was measured using the residual field map as exemplified in Figure 6. Knowing the diameter of the cylinder gives the pixel to millimetre ratio.

2.6 Measurement of crack widths by microscope

To verify the crack widths measured by the DIC, crack widths were manually measured using a digital calliper and microscope and compared with the DIC measurements. An example of microscope crack width measurements is shown in Figure 7.



Figure 7 Example of microscope measurements of crack width for sample P11, with measurements shown in red.

2.7 Capillary suction

Cracked and uncracked samples were placed in the oven at 105 °C for 5 days to remove the moisture. Then capillary suction was undertaken following [39]. The samples were placed on a perforated metal tray with a depth of 1 mm of the disc immersed in water as shown in Figure 8. The samples were weighed at time intervals to measure the rate of water absorption over time. The capillary number K_{cap} and the resistance number m were calculated according to Equations (6) and (7) respectively,

$$K_{cap} = \frac{G(t)}{\sqrt{t}} \quad (6)$$

$$m = \frac{t_{cap}}{h^2} \quad (7)$$

in which $G(t)$ is the water absorption (kg/m^2) at time t (seconds), h is the height (m) of the disc and t_{cap} is the time (seconds) it takes for the rising water to reach the top of the disc, which occurs at the inflection point on the capillary suction curve.

After capillary suction, the specimens were submerged in water until constant mass was reached. The volume was determined by weighing the specimens in air and water. The suction porosity $\epsilon_{suction}$ of the samples was then calculated by Equation (8), following [40],

$$\epsilon_{suction} = \frac{w_{submerged} - w_{dry}}{\text{volume}} \quad (8)$$

where $w_{submerged}$ is the constant mass after submersion in water and w_{dry} is the weight in air. The

volume is the weight in air minus the weight in water.



Figure 8 Capillary suction test for cracked and uncracked discs

2.8 *Water permeation*

Different cracked specimens were used for water permeation tests, given that the harsh drying prior to capillary suction changes the porosity. The specimens used for permeation testing were stored in air between tensile splitting and permeation testing rather than water to prevent crack healing. Butyl tape was wrapped around the circumference of each disc and onto the top and bottom to seal and prevent water outflow from the circumference of the disc. During trials this butyl tape failed under the water pressure so, to prevent this, each specimen was wrapped with a steel sleeve to provide restraint. An example of the wrapped discs is shown in Figure 9. Rubber rings of diameter 145 mm with a hole of diameter 70 mm were placed above and below the samples to seal the water flow. Water pressure was applied and measured at the top of the sample. The water flowing through the sample was collected in a measuring cylinder with the mass measured and logged every second. The experimental set-up is shown in Figure 10.



Figure 9 Cracked sprayed concrete disc wrapped in butyl tape and steel sleeve.

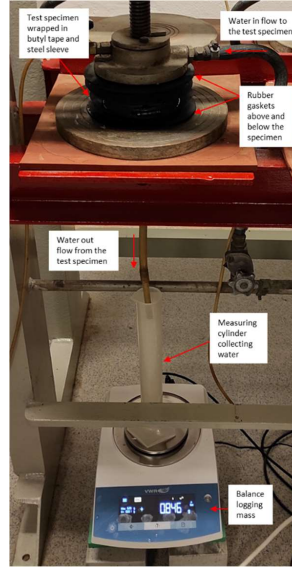


Figure 10 Experimental set-up for measuring water permeation through cracked discs

2.9 Crack healing

A single specimen was stored in water after initial testing and the water permeation was retested at time intervals.

2.10 CT scanning of cracked disc

The CT scanner METROTOM 1500 was used to scan a single specimen, which was the same specimen used for crack healing measurements. The sample was scanned in the CT scanner with a tube voltage of 150 kV and a current of 360 μ A, respectively. The software VGStudio Max 3.5.2 was applied to analyse the obtained image.

3. Results and Discussion

3.1 Tensile splitting and crack measurement

A graph showing the tensile splitting stress against the strain measured by the digital extensometer is shown in Figure 11. The tensile splitting stress f_{ct} was calculated using Equation (9) [41]

$$f_{ct} = \frac{2F}{\pi Ld} \quad (9)$$

where F is the force applied, L is the thickness of the disc, and d is the diameter of the disc. The peak tensile splitting stress occurs at fracture of the disc and decreases during further widening of the crack in our experiments. The peak tensile splitting stress was slightly lower in the mix containing the EVA-

based co-polymer compared with the standard mix. The displacement between the two points closes during unloading by between 0.05 and 0.15 mm. So, whilst the peak crack width during tensile splitting can be accurately controlled, the displacement between the two points after unloading is lower.

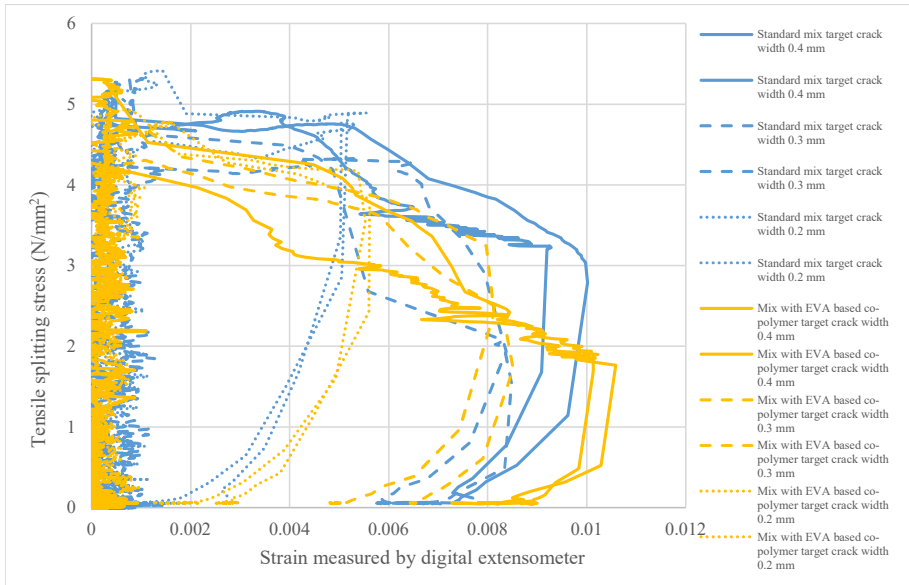


Figure 11 Tensile splitting stress against strain measured by the digital extensometer.

The tensile splitting stress against crack width measured by subset tracking is plotted in Figure 12. The graph shows that the maximum average crack width is lower than both the target crack width and the displacements between the points measured by the digital extensometer. This is because the digital extensometer is positioned at the centre of the disc, so only measures the crack at this location, and crack widths may vary above or below. This is illustrated by Figure 13, which describes the variation in crack width along the crack length for a single sample, with the crack width varying from 0.12 mm to 0.39 mm. Microscope measurements of the crack widths were done on all specimens and confirmed the DIC measurements.

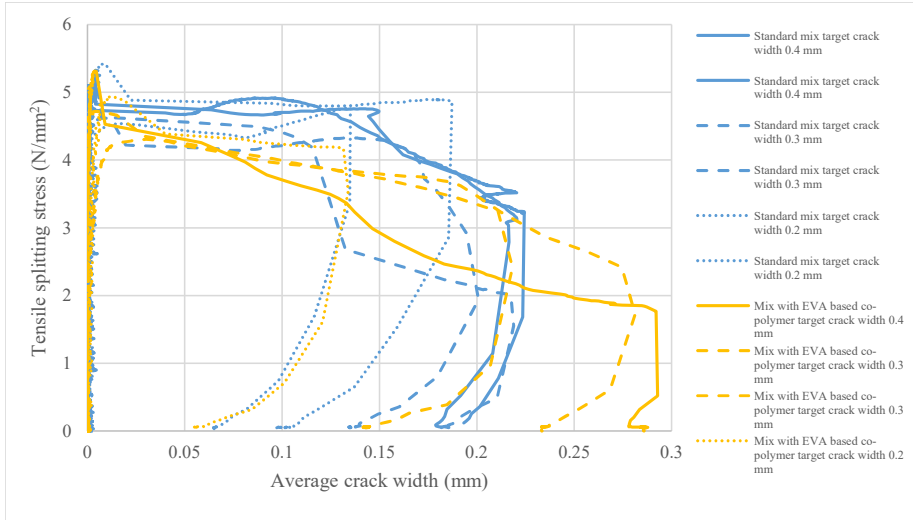


Figure 12 Tensile splitting stress against average crack width measured over the length of the crack by digital image correlation (DIC).

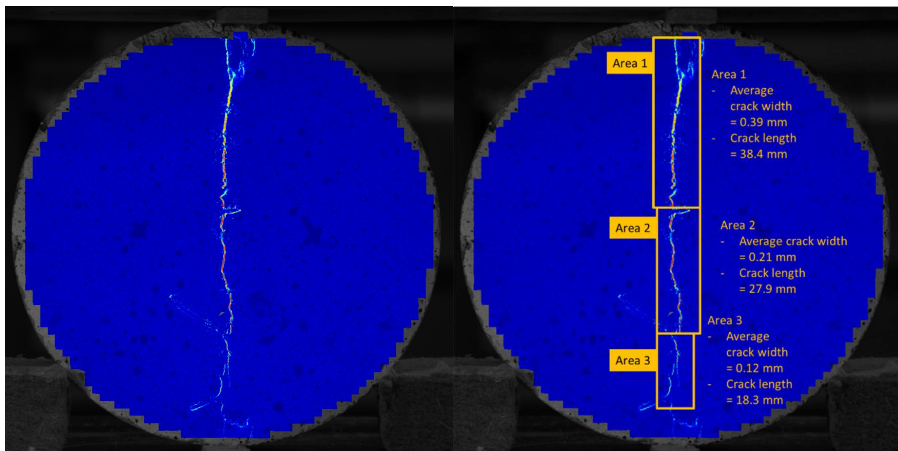


Figure 13 DIC measurements of crack widths on specimen P9, with measured crack widths annotated in right diagram.

Figure 14 shows the major principal strain field as calculated by the FE-based DIC. The figure shows the progressing major principal strain fields for a disc with a target crack width of 0.3 mm. The top image of part (a) shows the disc at peak load. The strain field below shows a clear indication of a crack before it is visible to the naked eye. The same is true for part (b), which shows the disc just after reaching the peak load. Part (c) shows that the strain clearly localises in a band across the diameter of the disc, while part (d) shows the disc at maximum crack width. Finally, part (e) shows the force vs. the average crack width as measured by subset tracking. Here we observe that the crack width closes by approximately 0.06 mm after unloading.

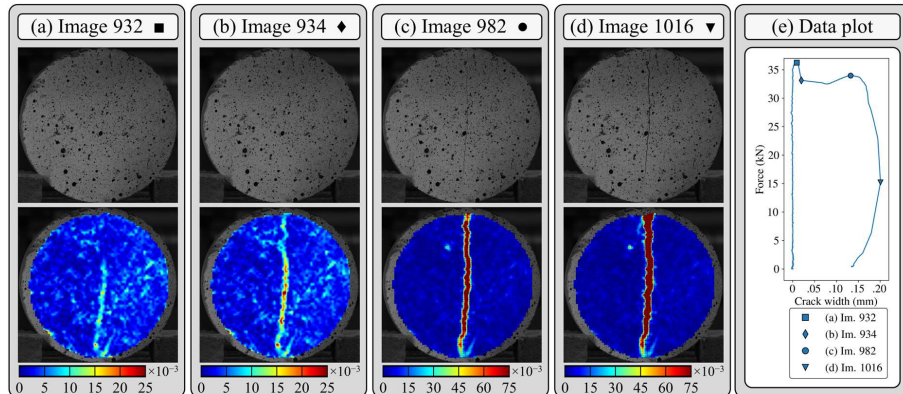


Figure 14 Strain field diagrams of tensile splitting showing development of the crack for sample S12

3.2 Capillary suction

Figure 15 shows the difference in water rise between a cracked (left) and uncracked specimen (right). The capillary suction curves for both cracked and uncracked discs are shown in Figure 16. The graphs show that cracked discs have a faster rate of water absorption than uncracked. Further, the rate of water absorption is slower in the discs from the mix containing the co-polymer than in the standard mix.

The calculated capillary and resistance numbers for each disc tested are shown in Table 2. The capillary numbers are calculated as the gradient of the first part of the capillary suction curve to the knee point and are plotted against crack width in Figure 17. The resistance numbers are the time to reach the knee point and are plotted against crack width in Figure 18. The tested discs were 50 mm thick, so the capillary suction curves do not feature the sharp “knee points” of curves for 20 mm thick discs as described by [39], and especially for the co-polymer mix. The crack widths, crack areas and suction porosity values for the discs are also included in Table 2.



Figure 15 Left: example of capillary suction in a cracked sample. The water rise in the crack is visible compared to the lower level of capillary rise in the remainder of the specimen. Right: capillary suction in uncracked sample.

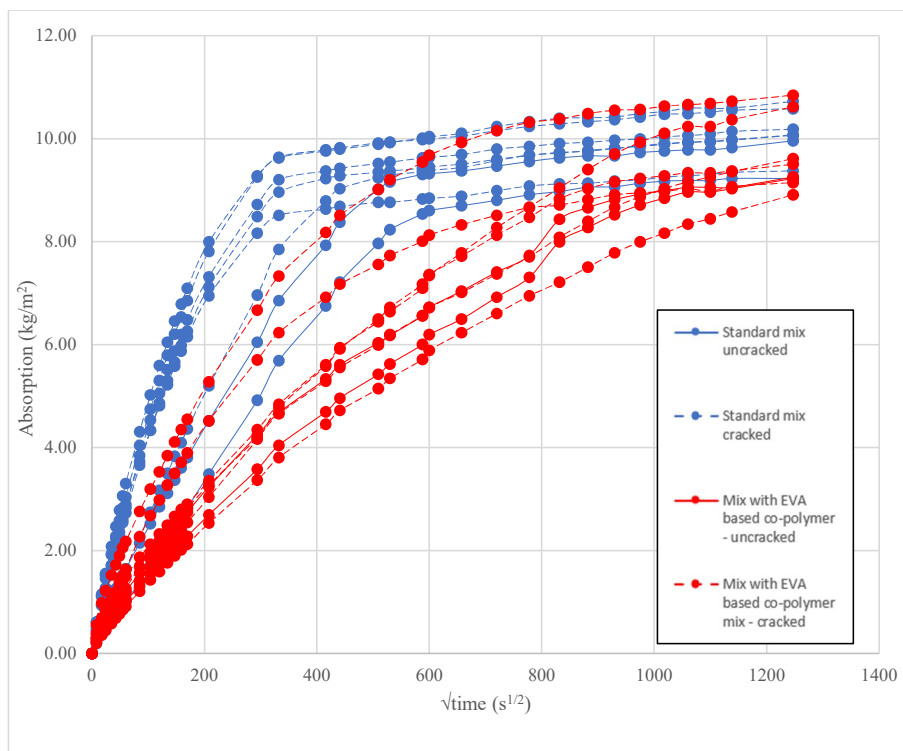


Figure 16 Capillary suction curves for cracked and uncracked discs from both a standard sprayed concrete mix and a mix containing polymer

Table 2 Crack widths measured by DIC, crack areas, crack volumes, suction porosity, capillary number, and resistance numbers for cracked and uncracked discs from capillary suction test

Sample	Mean crack width (mm)	Crack area (mm ²)	Suction porosity (%)	Capillary number (kg/m ² √s)	Resistance number (s/m ²)
Standard mix					
S1	Uncracked		20.3	0.0193	1.1 x 10 ⁸
S2	Uncracked		19.0	0.0167	1.1 x 10 ⁸
S3	0.05	4.15	20.3	0.0257	7.8 x 10 ⁷
S4	0.05	5.42	21.2	0.0493	4.4 x 10 ⁷
S5	0.20	20.10	20.1	0.0436	4.4 x 10 ⁷
S6	0.12	14.96	20.5	0.0452	4.4 x 10 ⁷
S7	0.12	16.63	21.7	0.0450	4.4 x 10 ⁷
S8	0.18	27.13	19.1	0.0350	4.4 x 10 ⁷
Mix containing EVA based co-polymer					
P1	Uncracked		19.6	0.0127	4.5 x 10 ⁸
P2	Uncracked		19.1	0.0148	4.1 x 10 ⁸
P3	0.07	6.73	19.1	0.0149	3.5 x 10 ⁸
P4	0.06	6.54	21.2	0.0161	4.5 x 10 ⁸
P5	0.09	12.01	21.7	0.0280	2.4 x 10 ⁸
P6	0.09	10.20	18.5	0.0130	4.8 x 10 ⁸
P7	0.17	20.68	19.8	0.0169	4.8 x 10 ⁸
P8	0.15	15.16	18.4	0.0249	2.4 x 10 ⁸

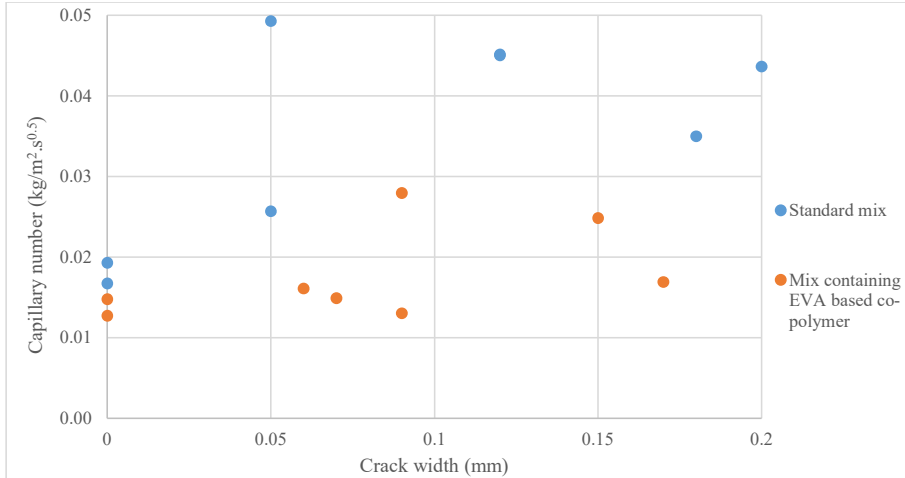


Figure 17 Capillary number against crack width.

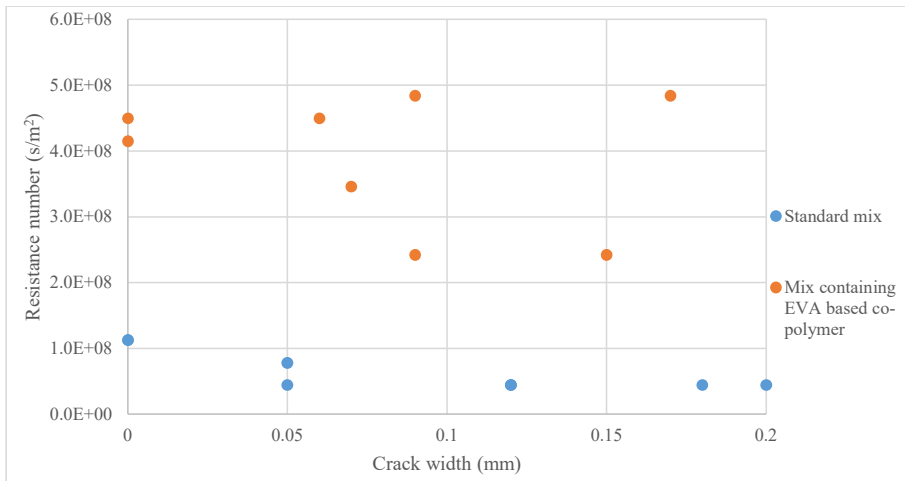


Figure 18 Resistance number against crack width.

Figure 17 and Figure 18 show that the rate of capillary suction (capillary number) is increased and resistance number decreased by cracking. They also show that the rate of capillary suction is reduced and resistance number increased for the mix containing the EVA based co-polymer compared to the standard mix. Figure 17 shows that the rate of water absorption in the capillary suction experiment is independent of the crack width, while Figure 18 shows that for the full range of the crack widths the time to reach the top of the disc is equal, and greater than for the uncracked discs.

We can investigate further the effect of the cracks on the rate of capillary suction. Figure 1 states that suction to a height of 50 mm occurs in an ideal crack of 0.05–0.4 mm in only 0–3 seconds. If this crack quickly becomes full of water then the surface of the crack will provide additional surface

area for absorption. The surface area of the crack can be estimated as,

$$A_{\text{crack surface}} = 2L_e h \quad (10)$$

with L_e being the effective length of the crack, and h is the height of the disc.

Replotting the capillary suction curves, for the standard mix only, with the absorption area equal to the area of the base of the disc plus the surface area of the crack, we find that the initial rates for capillary suction for the cracked and uncracked discs are in the same range, shown in Figure 19. The rate of capillary absorption per total area in contact with water (base of disc plus crack surface area) for all but one of the cracked samples (disc S3) lies between the capillary suction lines for the uncracked discs, which are unchanged from Figure 17. The modified capillary suction curves support the hypothesis that the water rise in the crack is rapid (Figure 1), after which the crack provides additional surface area for water absorption and increases the rate of capillary absorption. The rate of water absorption through the surface area of the crack is demonstrated to be equal to that through the base of the disc in the first part of the capillary suction curve, until approximately 6 hours ($\sqrt{t} = 147 \text{ s}^{1/2}$). After that the rate of water absorption over the crack surface area plus the area of the base of the disc reduces compared with the uncracked specimens (water absorption through base of the disc only), presumably due to overlap between the capillary water rise from the different surfaces – rising capillary level in the intact concrete overlaps with horizontal capillary water absorbed from the crack surface.

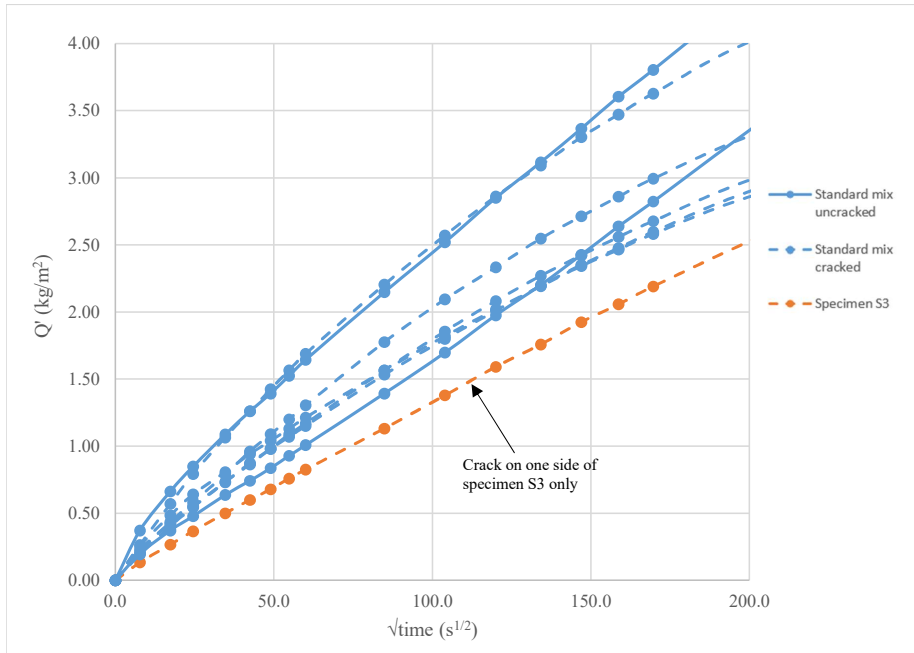


Figure 19 Capillary absorption per area of base of disc plus surface area of the crack against square root of time.

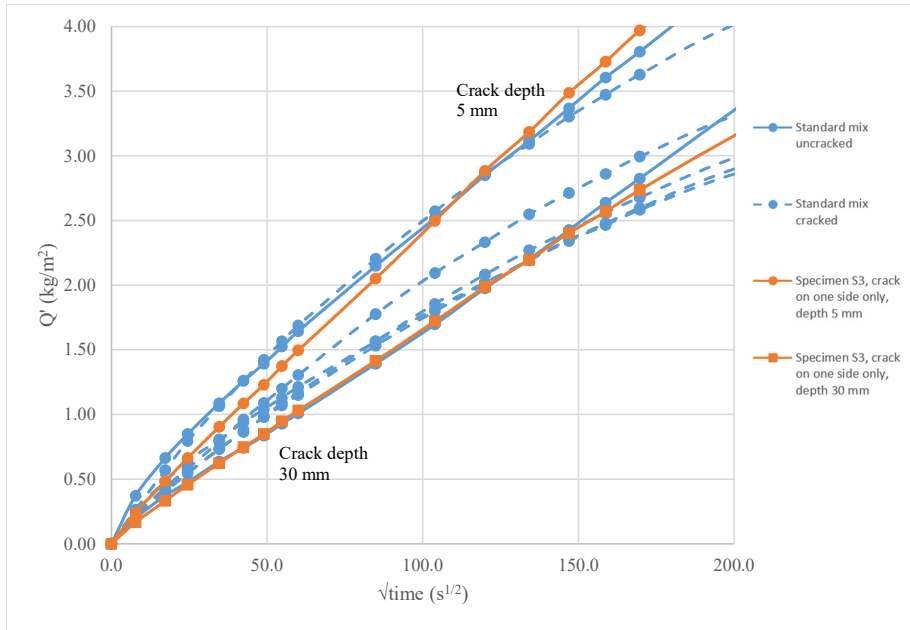


Figure 20 Capillary absorption per area of base of disc plus surface area of the crack against square root of time modified to solve for crack depth of partially cracked disc S3

In disc S3, with a crack width of 0.05 mm and resistance number of $7.8 \times 10^7 \text{ m/s}^2$, the crack is only identifiable on the painted side (used for DIC measurements) and not on the opposite side, indicating that the crack is not continuous. The other cracked discs have equal resistance numbers ($4.4 \times 10^7 \text{ m/s}^2$). Hence the time is lower for the water to rise to the top of the disc with a discontinuous crack than for the other cracked discs. This indicates the time for water rise in the disc is decreased by the crack but independent of crack width, in line with the theoretical rise described in Figure 1. By considering the maximum and minimum of the other capillary suction lines in Figure 19 as upper and lower bounds, we can solve to determine the depth of the crack through disc S3. The total capillary absorption area for the sample with the discontinuous crack is the area of the base of the disc plus the crack surface area multiplied by a fraction representing the crack depth. Two lines are replotted in orange in the adjusted capillary suction curves presented in Figure 20 – the upper line represents a crack depth of 5 mm and the lower a crack depth of 30 mm in the 50 mm thick disc. These two lines fit within the upper and lower bounds of the data so we can deduce that the depth of the crack is between 5 and 30 mm in disc S3.

These results are important with respect to the effect of cracking on transport in concrete tunnel linings. While the capillary suction is not a realistic experiment, due to the harsh drying beforehand, the effect of cracking clearly gives access to a much larger surface area of bulk concrete, considering the substantial crack patterns observed and recorded by Holter [8] in tunnel linings.

The concept for increased rate of capillary suction in cracked discs due to rapid rise of water in the crack, which provides a larger area for absorption, is less applicable for the mix containing the EVA based co-polymer. This is because the water rise in the crack is slower than for the standard mix. While the rise of water in the cracks results in additional absorption surface for capillary suction in the discs containing the EVA based co-polymer, the rise in the crack is slower. So, the increase in capillary suction due to cracking is less for the discs containing the co-polymer. These results agree with those of [28] and [29], who reported decreased rates of capillary suction in concretes containing polymers.

3.3 Water permeation through cracks

A summary of the specimens, the crack widths, the measured flow rates and the calculated flow rate coefficients is given in Table 3. A graph of the mass of water flow through the cracked discs is shown in Figure 21 and Figure 22. Both graphs capture the same data with different scales on the horizontal axis due to the very different rates of water permeation through the cracked discs. The water permeation through specimens with wider crack widths, around 0.15 mm or greater, filled the measuring cylinder of 250 ml in a time of 20–30 seconds but the volume of water that flowed through narrower crack widths, of less than 0.1 mm, in a period of 3–4 hours was less than the 250 ml capacity of the measuring cylinder. Reynolds numbers were calculated between 0.09 (lower flow rates) and 10.7 (higher flow rates), confirming the flow to be laminar.

The rates of water permeation shown in Figure 21 and Figure 22 are not constant – the rate of water permeation is initially higher and decreases over time. This is illustrated in Figure 23, which plots the rate of water flow against time. This agrees with results from [21], who reported a reduction of initial flow rate of 55 % after 25 hours. This is not due to water absorption into non-saturated concrete adjacent to the crack, as that would give the opposite trend. Instead this must be due to clogging of the crack or self-healing of the crack.

The rate of water flow through the discs in mass per second against mean crack width is plotted in Figure 24, showing a tendency of increased flow with increasing mean crack width, though with some scatter. For the faster rates of water permeation, those that are near linear in Figure 21 with a duration of typically 20–30 seconds, a mean value for the duration of the experiment was plotted. Where the rate of water permeation can be seen to decrease over time, both an initial rate and a rate once flow becomes linear, representing steady state flow, were plotted based on Figure 22.

Figure 25 plots the flow rate of water, Q , against mean crack width, while Figure 26 plots the flow rate coefficient, calculated with Equation (5) against mean crack width. Both Figure 25 and Figure 26 show far lower flows through cracks of average crack width less than 0.1 mm for both the standard mix and for the mix containing the EVA based co-polymer. For cracks above 0.1 mm mean width, the mix containing the co-polymer shows a clear trend of gradually increasing flow and flow rate coefficient with increasing crack width. However, for the standard mix there is no clear trend above crack widths of 0.1 mm. A lack of a clear trend suggests that the data could be analysed in a different manner.

Table 3 Crack widths measured by DIC, crack areas, measured flow rates and calculated flow rate coefficients for water permeation tests.

Sample	Mean crack width (mm)	Maximum crack width (mm)	Crack area (mm ²)	Mean flow rate (m ³ /s)		Mean flow rate coefficient ζ	
				Initial flow rate (m ³ /s)	Steady state flow rate (m ³ /s)	Initial flow	Steady state flow
Standard mix							
S9	0.19	0.19	14.4	1.9×10 ⁻⁵		0.0763	
S10	0.18	0.22	11.4	1.3×10 ⁻⁵		0.0769	
S11	0.18	0.21	11.0	1.8×10 ⁻⁵		0.109	
S12	0.14	0.25	7.15	1.2×10 ⁻⁵		0.180	
S13	0.23	0.21	18.0	1.2×10 ⁻⁵		0.0246	
S14	0.11	0.28	7.01	1.6×10 ⁻⁵		0.377	
S15	0.10	0.17	6.70	1.0×10 ⁻⁴		0.0309	
S16	0.07	0.07	2.81	6.5×10 ⁻⁸	1.0×10 ⁻⁹	0.00354	0.00021
S17	0.07	0.08	4.52	2.3×10 ⁻⁸	1.4×10 ⁻⁹	0.00865	0.00013
Mix containing EVA based co-polymer							
P9	0.29	0.39	15.8	2.1×10 ⁻⁵		0.0315	
P10	0.23	0.46	16.8	1.7×10 ⁻⁵		0.0392	
P11	0.23	0.23	13.9	4.8×10 ⁻⁶		0.0131	
P12	0.14	0.18	8.30	5.0×10 ⁻⁷		0.00295	
P13	0.07	0.07	3.74	1.9×10 ⁻⁷	1.0×10 ⁻⁹	0.0207	0.00011
P14	0.05	0.06	2.77	3.8×10 ⁻⁸	1.3×10 ⁻⁹	0.0102	0.00035

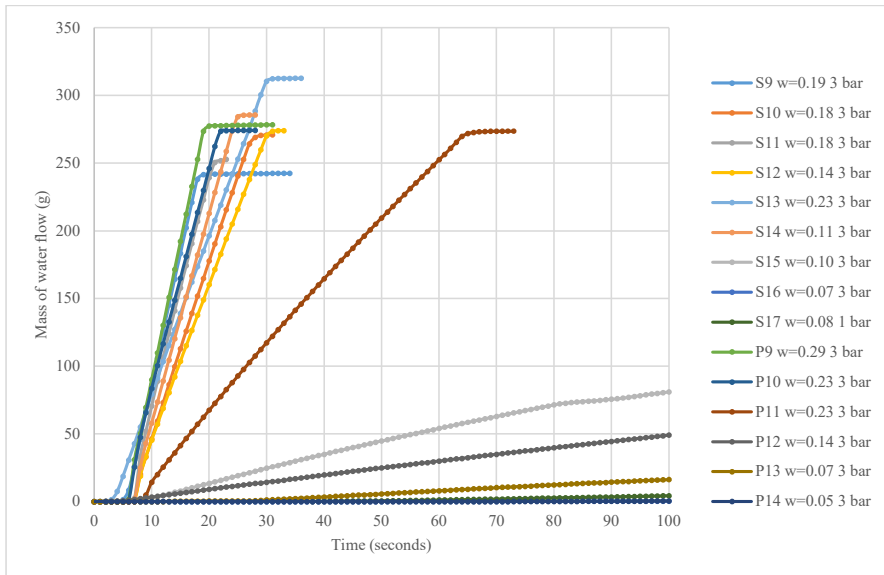


Figure 21 Mass of water flow through discs against time (0 – 100 seconds).

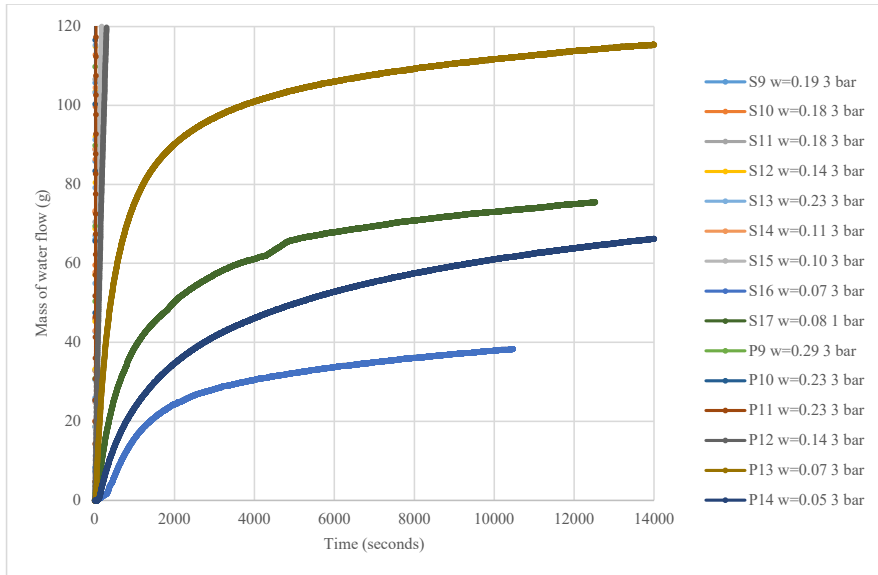


Figure 22 Mass of water flow through discs against time (0 – 14000 seconds).

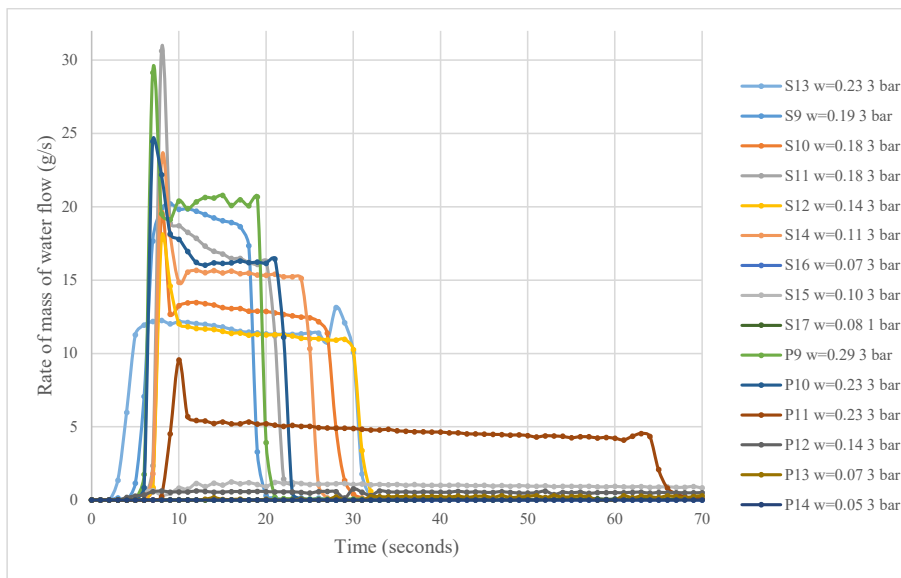


Figure 23 Rate of water flow through discs against time.

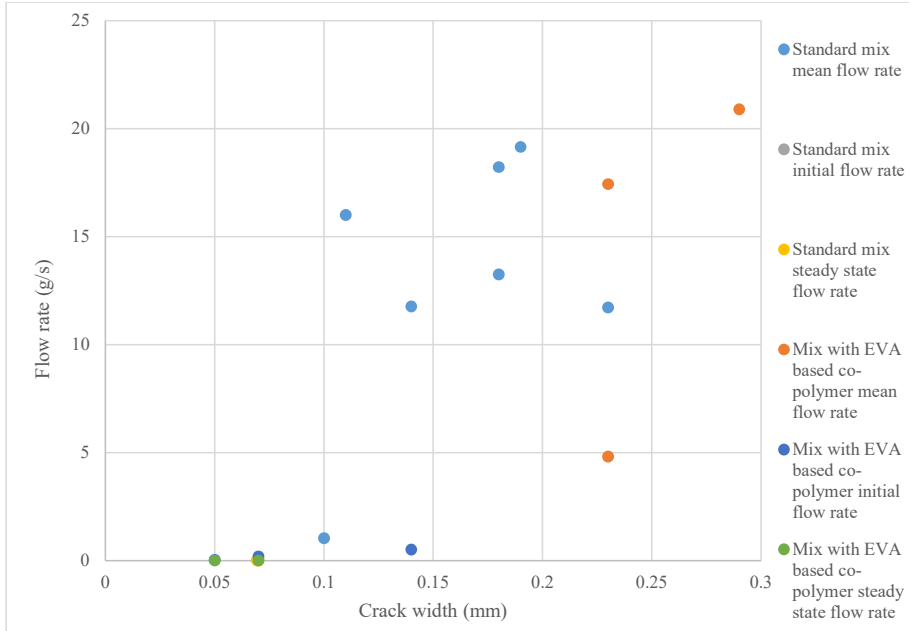


Figure 24 Rate of water flow through discs against mean crack width.

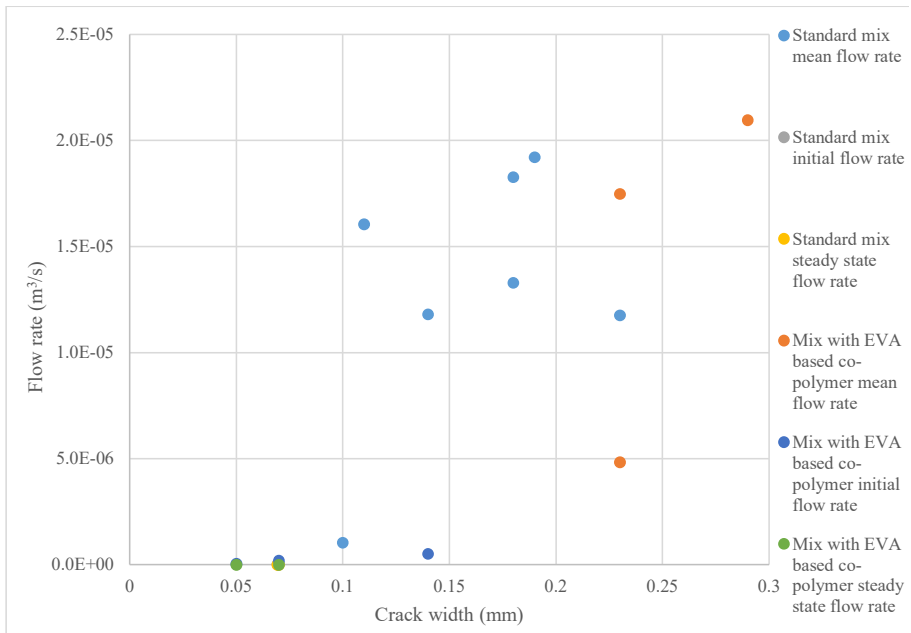


Figure 25 Rate of water flow through discs against mean crack width.

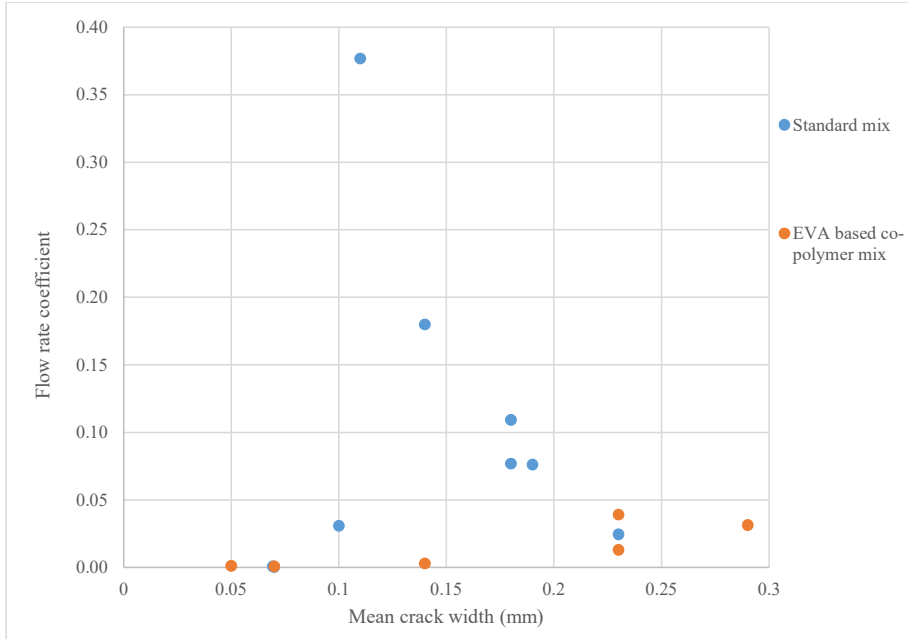


Figure 26 Flow rate coefficient against mean crack width.

We know from Figure 24 that the water flow through narrower cracks (less than 0.1 mm) is much lower than that through wider cracks. And we also know that the crack width along the length of the crack is not constant, instead it can vary, as demonstrated by the example shown in Figure 13. So perhaps describing the crack by the mean width is inadequate.

Instead, we can plot the flow rate coefficient against the maximum crack width, which is presented as Figure 27. For this relationship there is a clear trend of increasing flow rate coefficient with increasing maximum crack width. The data points indicate that the flow rate coefficient increases in an exponential manner with increasing crack width for the standard sprayed concrete mix. The improved correlation by plotting maximum instead of mean crack width is in line with the effect of crack width cubed on total flow through a crack (Equation 2). We expect that the actual flow rate varies along the length of the crack due to the variation in crack width. The rate of water permeation is likely highest through the widest part of the crack and lower through narrower parts. The deviation from the theoretical crack flow (described by ζ) increases with narrower crack width, likely because a large fraction of the flowing water is affected by the surface roughness. We think the narrower cracks are also likely to be less continuous through the thickness of the disc. The flow rate coefficients values plotted in Figure 26 and Figure 27 range from 0.00057 (for a narrow crack) to 0.38 (for a wider crack). These compare well with the values of 0.005 and 0.17 measured by Ripphausen in cracks in reinforced concrete slabs [14].

The plotted points suggest that the trend for the mix containing the EVA based co-polymer is a

more linear increase of flow rate coefficient with increasing crack width. Figure 27 demonstrates that addition of the EVA based co-polymer reduces the flow rate coefficient for cracks wider than 0.1 mm compared to the standard mix. Hence the EVA based co-polymer reduces viscous flow through a crack with a given crack width and pressure gradient.

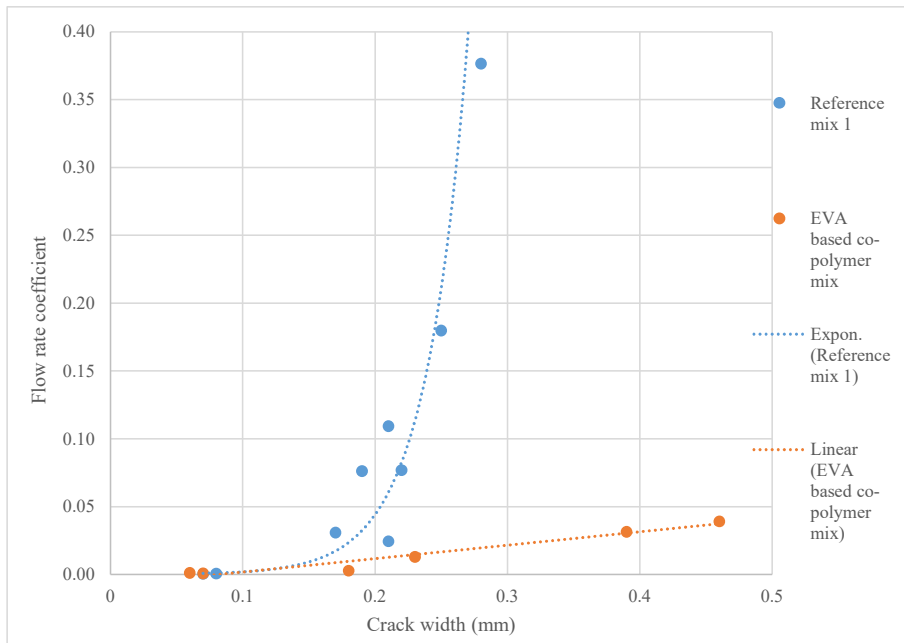


Figure 27 Flow rate coefficient against maximum crack width.

3.4 Crack healing

A graph showing the mass of water flow through specimen S9 (standard mix with mean crack width of 0.19 mm) re-tested at time intervals after storage in water is shown in Figure 28. The rate of water permeation through the crack decreases after time stored in water. The reduction of flow rate coefficient after water storage is due to crack healing.

The flow rate coefficient against time that the sample had been stored in water is plotted in Figure 29. The flow rate coefficient decreases to 12 % of the initial value after 32 days stored in water, and 7 % after further storage in water. These results indicate that crack healing does indeed occur in sprayed concrete containing aluminium sulphate based set accelerators.

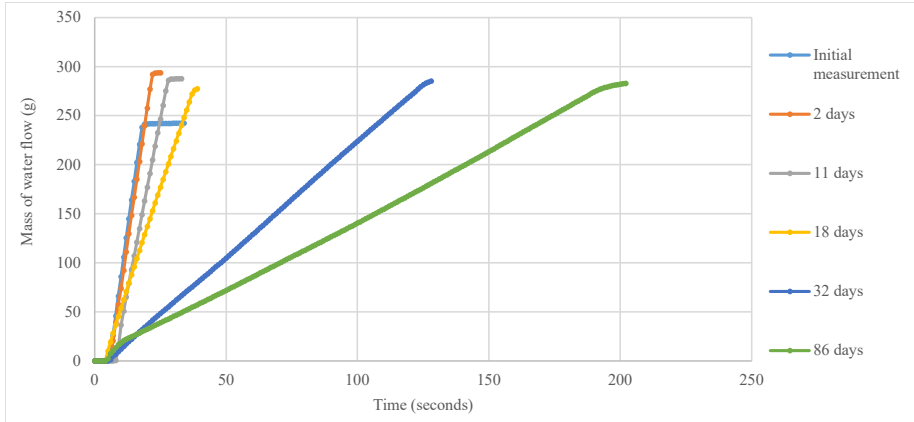


Figure 28 Mass of water flow through disc against time for sample S9 with a crack width 0.19 mm

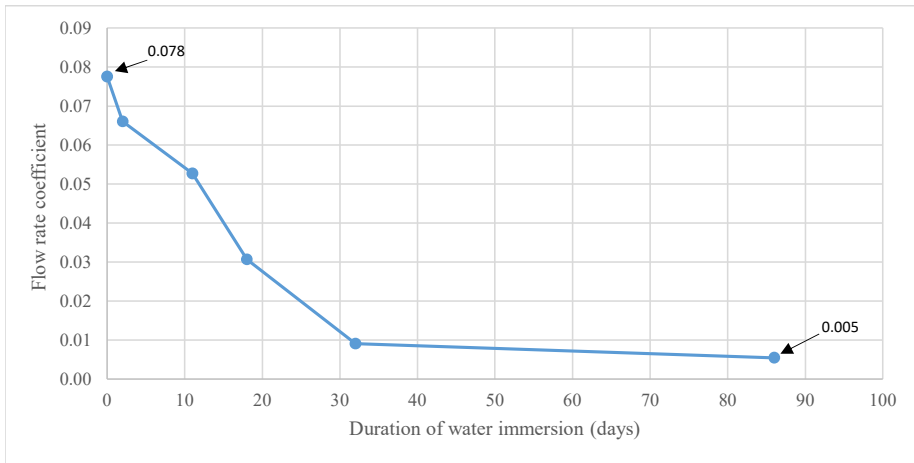


Figure 29 Flow rate coefficient against duration of water immersion for sample S9 with a crack width 0.19 mm

3.5 CT scan of cracked disc

Figure 30 shows the crack distribution in sample S9 from above (a) and side view (b) visualised by CT scanning. The crack volume was calculated by refining the region of interest (ROI) around the crack to remove the measurement of macro pores, which would otherwise lead us to overestimate the crack volume. Furthermore during tensile splitting partial pull-out of the fibres occurred, as indicated by the voids around the fibres shown in Figure 31. These voids are connected to the crack in some instances, so this is another reason to refine the ROI around the crack to avoid overestimating the crack volume.

The centre of the sample contained many ring artefacts. Therefore, making a binary image made many errors in segmentation between the crack and matrix. Thus the sample was divided into 23

different slices with a thickness of 2 mm (the total height of ROI was selected as 46 mm to avoid errors at the surfaces). The crack volume for each slice was calculated by applying the “only threshold” algorithm in the VG studio software porosity/inclusion analysis. In this algorithm, each group of defect candidates is considered a defect if the grey value is below the specified threshold. The voxel size was 0.000300763 mm^3 with resolution length of 0.067 mm in x, y, and z dimensions. The crack volume in each 2 mm thick slice is reported in Figure 32, which also shows images at six different heights through the thickness of the disc. Figure 32 shows that the crack length varies through the thickness of the disc, hence demonstrating how useful CT scanning could be for measuring cracks through the full thickness of specimens. The total volume of the crack in the sample is the sum of these individual volumes and is 1565 mm^3 . This is 1.65 times the crack volume estimated using the crack width at the surface measured by DIC ($0.19 \text{ mm crack width} \times 100 \text{ mm crack length} \times 50 \text{ mm specimen thickness} = 950 \text{ mm}^3$). Given that the crack width and length varies through the thickness of the specimen, flow rates will also vary along the length of the crack and through the thickness of the specimen following equation (2).

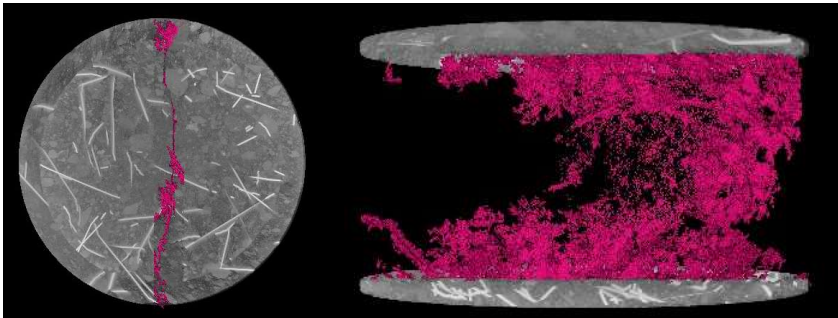


Figure 30 Visualisation of the crack (a) from top and (b) from the side by CT scanning in specimen S9. The crack is shown in dark pink.

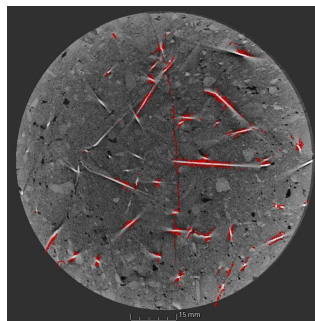


Figure 31 CT scan of specimen S9 showing void around fibres, indicating pull-out of the fibres during tensile splitting

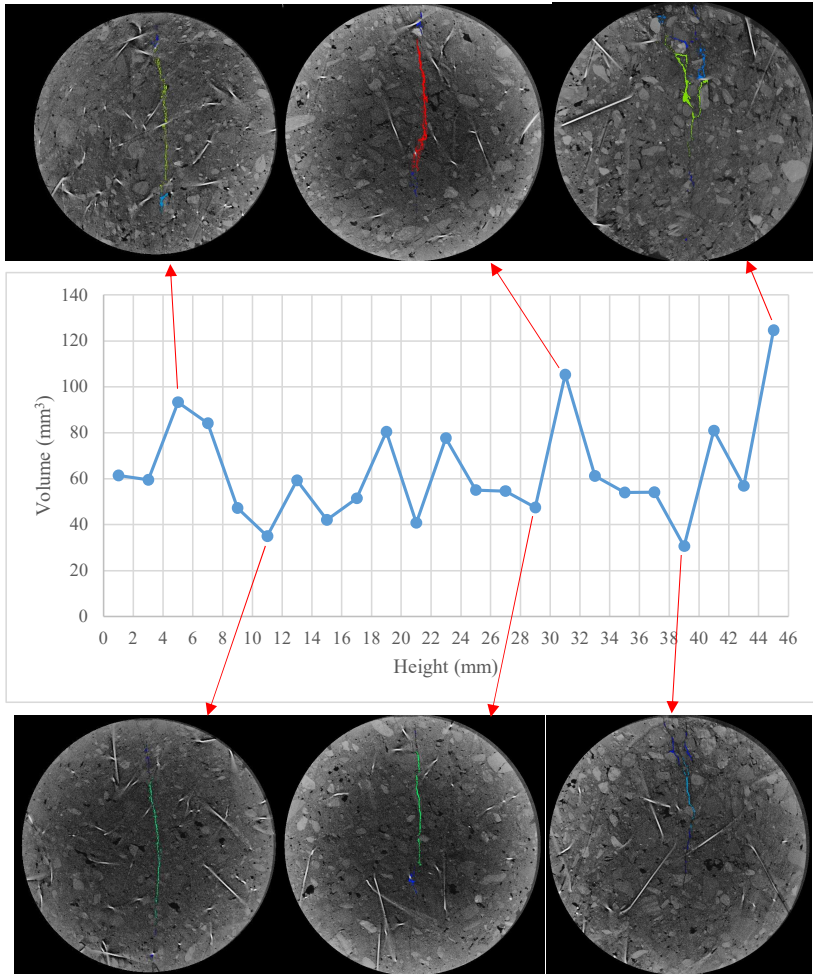


Figure 32 Calculated volume of crack for each 2 mm thick slice, and images for at six different locations through the thickness of specimen S9

4. Conclusions

- A series of DIC-controlled tensile splitting tests were conducted on sprayed concrete specimens, drilled from panels from full-scale spraying of standard mixes and a mix containing an EVA based co-polymer. The objective was to investigate the effect of cracks on water transport in sprayed concrete. The peak crack width was controlled accurately during tensile splitting, but the crack closed by between 0.05 and 0.15 mm after unloading, so the final crack width was always less than the target crack width. The crack widths measured by digital image correlation subset tracking

concluded with the values obtained by microscope measurement to a tenth of a millimetre.

- The peak tensile splitting stress, i.e. the peak stress before cracking, for the discs containing the EVA based dispersible co-polymer powder was slightly lower than that for the standard mix. This was contrary to expected results – Ohana [27] stated that matrices containing polymer have a higher tensile strength and fracture toughness.
- The rate of capillary suction was higher in the cracked discs than in the uncracked discs. This is due to rapid rise of water in the crack, and the crack surface providing additional area for absorption.
- The rate of capillary suction was lower in the mix containing the EVA based co-polymer for both cracked and uncracked discs. The water rise in the crack was slower, so the crack surface provided less additional area for absorption, and water suction through the capillary pores was slower. These results agree with those of Øye [28] and Justnes et al [29], who reported decreased rates of capillary suction in concretes containing polymer.
- The flow rate of permeating water increased with increasing crack widths. Flow rates of less than $1 \times 10^{-6} \text{ m}^3/\text{s}$ were measured for crack widths of 0.1 mm and lower while, above this threshold crack width, flow rates of up to $2 \times 10^{-5} \text{ m}^3/\text{s}$ were measured.
- Describing each crack simply by a mean crack width is insufficient. The width varied along the length of the crack and permeation through cracks is higher by an order of magnitude in wider cracks. Describing the crack by the maximum width rather than mean gave clearer trends.
- The inclusion of the ethylene-vinyl-acetate (EVA) based dispersible co-polymer powder had no effect on water permeation in cracks less than 0.1 mm width but reduced the flow rate coefficient in wider cracks. Above 0.1 mm width the flow rate coefficient increases exponentially with increasing crack width in the standard sprayed concrete discs, whereas with inclusion of the EVA based co-polymer, flow rate coefficient increases far less with increasing crack width.
- Water permeation through the cracked specimens is not constant, rather it decreases over the duration of a single test, due to clogging of the cracks, swelling of the concrete or crack healing. Water permeation reduced after water storage due to crack healing.
- Inclusion of the EVA (ethylene-vinyl-acetate) based co-polymer in sprayed concrete reduces water transport in sprayed concrete linings, both through the capillary pore network and through cracks. Thus this admixture improves durability and can help to achieve durable, permanent, sprayed concrete linings.
- The X-ray computer tomography scanner was applied to visualise a crack through the whole thickness of a specimen and accurately measure the volume. The macro porosity appeared as void, as did the partial fibre pull-out that occurred during tensile splitting. It is necessary to refine the region of interest to remove these voids around the fibres and avoid over-estimating the crack volume. CT scanning is a promising method for measuring cracks and we recommend use for future studies on cracks.

5. Acknowledgement

This paper is a part of the research project “Sprayed sUustainable Permanent Robotized CONcrete tunnel lining (SUPERCON)” financed by the Research Council of Norway (project no. 294724), in cooperation with industrial partners AMV, BASF, Bever Control, Bekaert, Elkem, Entreprenørservice, NORCEM, SWECO Norge, Veidekke, Wacker Chemicals Norway and Unicon AS. Research partners in SUPERCON are NGI, NTNU and SINTEF. The following project owners support the project; Bane NOR, Nye Veier and the Norwegian Public Roads Administration.

Thanks to Karl Gunnar Holter from the Norwegian Geotechnical Institute for leading the full-scale spraying experiments, to Trond Auestad from NTNU for his work controlling the crack widths by digital image correlation during the tensile splitting, to Rolands Cepuritis for help with concrete proportioning, to Erik Johansen from SINTEF for assistance with the water permeation testing, and to Pål Erik Endrerud from NTNU for operating the CT scanner.

6. References

- [1] Scrivener, Muller, Zalzale, Do and McDonald, “New insights on mechanics controlling kinetics and implications for pore structure,” in *Understanding the fundamental properties of concrete*, Trondheim, Norway, 2013.
- [2] Manquehual, Jakobsen, Holter, D. Weerdt and Bruland, “Investigation of leaching in steel fiber-reinforced shotcrete exposed to fresh and saline groundwater in a subsea road tunnel,” *Cement and Concrete Research*, vol. 163, no. 107011, p. 21, 2023.
- [3] Broere, “Urban underground space: Solving the problems of today’s cities,” *Tunnelling and Underground Space Technology*, vol. 55, pp. 245-248, 2016.
- [4] Manquehual, Jakobsen, Holter, D. Weerdt, Danner and Bruland, “Comparison of the condition of steel fiber-reinforced shotcrete with water-glass and alkali-free activators after more than 20 years of service in a subsea road tunnel,” *Construction and Building Materials*, vol. 328, no. 127090, 2022.
- [5] Norwegian Concrete Association, “Publication no.7: Sprayed concrete for rock support,” Oslo, 2011.
- [6] Salvador, Cavalaro, Segura, Figueiredo and Perez, “Early age hydration of cement pastes with alkaline and alkaline-free accelerators for sprayed concrete,” *Construction and Building Materials*, vol. 111, pp. 386-398, 2016.
- [7] Trussell, Cepuritis and Jacobsen, “Effect of Set Accelerator on Properties of Wet Sprayed Concrete,” *Nordic Concrete Research*, vol. 66, no. 1, pp. 21-41, 2022.

- [8] Holter, Properties of waterproof sprayed concrete tunnel linings - a study of EVA-based sprayed membranes for waterproofing of rail and road tunnels in hard rock and cold climate, PhD thesis, Trondheim, Norway: Norwegian University of Science and Technology, 2015.
- [9] Trussell and Jacobsen, "Review of Sprayability of Wet Sprayed Concrete," *Nordic Concrete Research*, vol. 63, no. 2, pp. 21-41, 2020.
- [10] Neville, Properties of Concrete, Harlow, England: Pearson, 2011.
- [11] Jacobsen, Gerard and Marchand, "Concrete cracks: observation, self-healing, permeability and durability - a review," Norwegian Building Research Institute, Oslo, 1998.
- [12] Nguyen, Water and heat transfer in cement based materials, PhD thesis, Tromsø, Norway: University of Tromsø, 2011.
- [13] Smeplass, "Capillary absorption as a quality criterion (in Norwegian)," SINTEF, Trondheim, Norway, 1988.
- [14] Ripphausen, Zur Wasserdurchlässigkeit von Stahlbetonbauteilen mit Trennrissen (Water permeability of concrete structures with separation cracks) PhD thesis, in German, Aachen: Rheinisch-Westfälische Technische Hochschule Aachen, 1989.
- [15] Rapoport, Aldea, Shah, Ankenman and Karr, "Permeability of Cracked Steel Fiber-Reinforced Concrete," *Journal of Materials in Civil Engineering*, vol. 14, no. 4, pp. 355-358, 2002.
- [16] Akhavan, Shafaatian and Rajabipour, "Quantifying the effects of crack width, tortuosity, and roughness on water permeability of cracked mortars," *Cement and Concrete Research*, vol. 42, pp. 313-320, 2012.
- [17] Rastiello, Boulay, D. Pont, Tailhan and Rossi, "Real-time water permeability evolution of a localized crack in concrete under loading," *Cement and Concrete Research*, vol. 56, pp. 20-28, 2014.
- [18] Clear, "Technical report 559: The effects of autogenous healing upon the leakage of water through cracks in concrete," Cement and Concrete Association, Slough, 1985.
- [19] Edvardsen, "Water permeability and autogenous healing of cracks in concrete," *ACI Materials Journal*, Vols. 96-M56, no. July-August, pp. 448-454, 1999.
- [20] Hearn, "Self-healing, autogenous healing and continued hydration: what is the difference?," *Materials and Structures*, vol. 31, no. October, pp. 563-567, 1998.
- [21] Jooss and Reinhardt, "Permeability and diffusivity of concrete as function of temperature," *Cement and Concrete Research*, vol. 32, no. 9, pp. 1497-1504, 2002.
- [22] Myrdal, "Accelerating admixtures for concrete – state of the art," SINTEF, Trondheim, Norway, 2007.

- [23] Salvador, Cavalaro, Cano and Figueiredo, "Influence of spraying on the early hydration of accelerated cement pastes," *Cement and Concrete Research*, vol. 88, pp. 7-19, 2016.
- [24] Salvador, Cavalaro, Cincotto and Figueiredo, "Parameters controlling early age hydration of cement pastes containing accelerators for sprayed concrete," *Cement and Concrete Research*, vol. 89, pp. 230-248, 2016.
- [25] Salvador, Cavalaro, Monte and Figueiredo, "Relation between chemical processes and mechanical properties of sprayed cementitious matrices containing accelerators," *Cement and Concrete Composites*, vol. 79, pp. 117-132, 2017.
- [26] Aldrian, Thomas and Holter, "Permanent Sprayed Concrete Linings – an international update," *Spritzbeton-Tagung 2021*, pp. 1-15, 2021.
- [27] Ohana, "Polymer-based admixtures," *Cement and concrete composites*, vol. 20, pp. 189-212, 1998.
- [28] Øye, Repair systems for concrete – polymer cement mortars, Trondheim, Norway: Norwegian Technical College, 1989.
- [29] Justnes, Reynaers and VanZundert, "Moisture transport in polymer cement mortars based on latices and redispersible polymer powders," in *International Congress on Polymers in Concrete*, Bologna, 1998.
- [30] Bonin, "Performance improvement of shotcrete by polymer binder modification," in *Shotcrete for underground support XIV*, Thailand, 2019.
- [31] Lee, Wong and Buenfeld, "Self-sealing of cracks in concrete using superabsorbent polymers," *Cement and Concrete Research*, vol. 79, p. 194–208, 2016.
- [32] V. Tittelboom and D. Belie, "Self-Healing in Cementitious Materials - A Review," *Materials*, vol. 6, pp. 2182-2217, 2013.
- [33] Reddy, Ramesh and Macrin, "Effect of crystalline admixtures, polymers and fibers on self healing concrete - a review," *Materials Today: Proceedings*, vol. 33, p. 763–770, 2020.
- [34] Brisard, Serdar and Monteiro, "Multi-scale X-ray tomography of cementitious materials: a review," *Cement and Concrete Research*, vol. 128, no. 105824, 2020.
- [35] Fagerholt, "eCorr – Digital Image Correlation Tool," Norwegian University of Science and Technology, 13 December 2014. [Online]. Available: <https://www.ntnu.edu/kt/ecorr>. [Accessed 28 April 2021].
- [36] Fonseca and Scherer, "An image analysis procedure to quantify the air void system of mortar and concrete," *Materials and Structures*, vol. 48, pp. 3087-3098, 2015.
- [37] Kaufmann, Frech, Schuetz and Munch, "Rebound and orientation of fibers in wet sprayed concrete applications," *Construction and Building Materials*, vol. 49, pp. 15-22, 2013.

- [38] Fagerholt, Børvik and Hopperstad, "Measuring discontinuous displacement fields in cracked specimens using digital image correlation with mesh adaptation and crack-path optimization," *Optics and Lasers in Engineering*, vol. 51, no. 3, pp. 299-310, 2013.
- [39] Punkki and Sellevold, "Capillary suction in concrete: effects of drying procedure," *Nordic Concrete Research*, vol. 15, pp. 59-74, 1994.
- [40] Sellevold and Farstad, "The PF-method – a simple way to estimate the w/c-ratio and air content of hardened concrete," in *Construction materials: performance, innovations and structural implications*, Vancouver, Canada, 2005.
- [41] Standard, "EN 12390-6: Testing hardened concrete – Part 6: Tensile splitting strength of test specimens," 2009.
- [42] Hearn, "Self-sealing, autogenous healing and continued hydration: What is the difference?," *Materials and Structures*, vol. 31, no. October 1998, pp. 563-567, 1998.
- [43] Jacobsen, Marchand and Hornain, "SEM observations of the microstructure of frost deteriorated and self-healed concretes," *Cement and Concrete Research*, vol. 25, no. 8, pp. 1781-1790, 1995.
- [44] Araujo, V. Tittelboom, Dubruel, V. Vlierberghe and D. Belie, "Acrylate-encapped polymer precursors: effect of chemical composition on the healing efficiency of active concrete cracks," *Smart Materials and Structures*, vol. 26, 2017.
- [45] Gruyaert, Debbaut, Snoeck, Diaz, Arizo, Tziviloglou, Schlangen and D. Belie, "Self-healing mortar with pH-sensitive superabsorbent polymers: testing of the sealing efficiency by water flow tests," *Smart Materials and Structures*, vol. 25, 2016.

Trussell, Nicholas Henry; Holter, Karl Gunnar; Klausen, Anja Birgitta Estensen; Cepuritis, Rolands; Skjølvold, Ola; Hammer, Tor Arne. More sustainable sprayed concrete tunnel linings with reduced cement content and reduced water transport properties. This paper is submitted for publication and is therefore not included.

Paper VI

ISBN 978-82-326-5331-7 (printed ver.)
ISBN 978-82-326-6882-3 (electronic ver.)
ISSN 1503-8181 (printed ver.)
ISSN 2703-8084 (online ver.)



NTNU

Norwegian University of
Science and Technology